EMERGENT IMPACTS OF RAPIDLY CHANGING CLIMATE EXTREMES IN ALASKA

By

Rick T. Lader, M.S.

A Dissertation Submitted in Partial Fulfillment of the Requirements

for the Degree of Doctor of Philosophy

in

Atmospheric Sciences

University of Alaska Fairbanks

August 2018

APPROVED:

Dr. John E. Walsh, Committee Chair

Dr. Uma S. Bhatt, Committee Member

Dr. T. S. Rupp, Committee Member

Dr. Xiangdong Zhang, Committee Member

Dr. Uma S. Bhatt, Chair,
Department of Atmospheric Sciences

Dr. Anupma Prakash, Interim Dean,
College of Natural Science & Mathematics

Dr. Michael Castellini, Dean of the Graduate School

ABSTRACT

The frequency and intensity of certain extreme weather events in Alaska are increasing, largely due to climate warming from greenhouse gas emissions. Future projections indicate that these trends will continue, potentially leading to billions of dollars in climate-related damages this century. Expected damages arise from increases in extreme precipitation, severe wildfire, altered ocean chemistry, land subsidence from permafrost thaw, and coastal erosion. This dissertation applies new downscaled reanalysis and climate model simulations from the fifth phase of the Coupled Model Intercomparison Project to enhance current understanding of climate extremes in Alaska. Model output is analyzed for a historical period (1981-2010) and three projected periods (2011-2040, 2041-2070, 2071-2100) using representative concentration pathway 8.5. Unprecedented heat and precipitation are expected to occur when compared to the historical period. Maximum 1-day and consecutive 5-day precipitation amounts are expected to increase by 53% and 50%, respectively, and the number of summer days per year (T_{max} > 25˚C) increases from a statewide average of 1.5 from 1981-2010 to 29.7 for 2071-2100. Major alterations to the landscape of Alaska are anticipated due to a decreasing frequency of freezing temperatures. Growing season length extends by 48-87 days by 2071-2100 with the largest changes in northern Alaska. In contrast, projections indicate a reduced snow season length statewide and many locations in southwest Alaska no longer have continuous winter snow cover. Changes to these metrics indicate that a climate-warming signal emerges from the historical inter-annual variability, meaning that future distributions are entirely outside of those previously observed. The largest changes

to extremes may be avoided by following a lower emissions trajectory, which would reduce the impacts and associated costs to maintain infrastructure and human health.

TABLE OF CONTENTS

LIST OF FIGURES

Page

LIST OF TABLES

Page

ACKNOWLEDGEMENTS

This dissertation is the product of many contributions beyond my personal efforts, none of which are greater than those from my Ph.D. advisor, Dr. John Walsh. His knowledge and expertise in the atmospheric sciences field enabled me to contribute to many projects outside of my core PhD research, broadening my perspective, and ultimately improving the manuscripts that follow. Perhaps more importantly, however, was his willingness to provide timely guidance, seemingly regardless of how busy his schedule was.

Thank you to Dr. Uma Bhatt, who served as my MS advisor in addition to being a member of my PhD committee, for her willingness to take me on as her graduate student in Fall 2011. Upon arriving in Fairbanks with just a suitcase and without knowing anyone, she made the transition to life in Alaska as seamless as possible. Her skills as a researcher and instructor have steadily built my capabilities as a research scientist.

Thank you to Dr. Scott Rupp for always being an advocate for me as I have navigated the graduate school experience. He has continually found means for me to travel to conferences to present research and highlight the work that is being conducted by the University of Alaska. Thank you to Dr. Xiangdong Zhang for his guidance as a member of my PhD committee and as an instructor, particularly for his enthusiasm teaching Synoptic Analysis and Atmospheric Radiation.

This dissertation would not have been possible without my funding sponsors. The Alaska Center for Climate Assessment and Policy (ACCAP) enabled me to conduct my research and afforded me the opportunity to present at many conferences. The manuscripts in this dissertation (Chapters 2-4) investigated observed and projected

changes to extreme climate in Alaska, supporting ACCAP's mission to strengthen the resilience of Alaskans against anticipated changes. I also thank the Alaska Climate Adaptation Science Center for supporting my MS research and providing funding immediately afterward for my work as a research technician.

Dr. John Walsh's prior experience with climate extremes indices served as a basis for Chapter 2, "Projections of twenty-first-century climate extremes for Alaska via dynamical downscaling and quantile mapping". This study demonstrated how newly developed downscaled climate model data could add value to existing climate information in Alaska. I calculated the extremes indices and wrote the manuscript. Each of the co-authors discussed the results and provided recommendations before and throughout the peer-review process.

An objective of Chapter 3, "Agro-climate projections for a warming Alaska", was to relate changing extremes to a particular impact (e.g., growing season length). This study discussed connections with earlier research by Dr. Uma Bhatt that examined changing biomass characteristics in Alaska. The analysis in Chapter 3 includes data from an additional downscaled climate model simulation, the CCSM4, largely due to Dr. Peter Bieniek's efforts. Rick Thoman of the National Weather Service provided the observed green-up time series. I conducted the analysis and wrote the first draft of Chapter 3, while each of the co-authors provided weekly comments to help improve the final version.

Chapter 4, "Anticipated changes to the snow season in Alaska: Elevation dependency, timing and extremes" studied some of the impacts that could result from a reduced frequency of freezing temperatures. I conducted the analysis and wrote the initial draft of this paper, while receiving weekly advice from the co-authors. Dr. Uma Bhatt

provided suggestions for many of the literature references found in the Introduction of Chapter 4, while Dr. John Walsh's recommendations substantially improved the figure set. Dr. Scott Rupp provided ideas that enhanced the Discussion section of Chapter 4.

Many thanks go to those that I have worked with on various other publications. In particular, I thank Rick Thoman for his willingness to discuss weather and climate issues, and for his monthly climate forecast outlook briefings. Dr. Peter Bieniek has been a fixture in my graduate studies and has repeatedly helped me with coding and modeling issues. I could always count on Peter to stop by my desk and see how the research was progressing, too.

My day-to-day experience while conducting these studies was enriched by friends inside and outside of the Department of Atmospheric Sciences. Barbara Day has always reminded me of important dates and deadlines to keep me on track. I have been able to commiserate with Greg Deemer, a long-suffering Cleveland Browns fan, because he understands where I am coming from as a similarly long-suffering Buffalo Bills fan. Thank you to Erin Gleason, Paul Leonard, Claire Stuyck, the 'Mikes' – Pirhalla and Madden, Derek Starkenburg, Katia Kontar and Becca Rolph.

Thank you to my parents in New York State for regular phone calls and updates of goings-on back home. Thank you to John Burr and Ruth Gronquist for taking me in as part of the family for the past five years. Finally, thank you to Erika Burr for being there every day along the journey.

1 INTRODUCTION

1.1 General Introduction

Eight of the top-ten warmest years of record (1880-present), globally, have occurred within the last decade (NOAA 2018a) and it is extremely likely that human activities are the primary cause (IPCC 2014). This warmth reflects a change in mean temperature, but also characterizes a shift of the entire temperature distribution, such that extreme cold has become less frequent and record high temperatures more routine (IPCC 2012). According to the Clausius-Clapeyron relationship, warmer temperatures have a higher capacity to hold water vapor, and thus it is expected that extreme precipitation will also increase (Donat et al. 2016). Indeed, the frequency of weather and climate disasters in the United States that have resulted in one billion dollars or greater in losses has shown significant increases since 1980 (Smith and Katz 2013). These costs stem from not only altered climate dynamics, but heightened exposure and vulnerability, too.

The rate of warming in the Arctic, including much of Alaska, is nearly twice the global average (AMAP, 2017; Overland et al. 2016). This discrepancy is especially apparent during Northern Hemisphere winter (Figure 1.1), largely due to amplifying processes such as the sea ice- and snow-albedo feedbacks (Pithan and Mauritsen 2014). Much of the excess heat has been absorbed by the ocean, which has contributed to significant ($p < 0.01$) losses of global sea ice (Parkinson 2014). The combination of increasing heat and an amplified hydrologic cycle (i.e., a tendency for enhanced precipitation and drought) has already been associated with an increased likelihood of certain extreme weather events in the Alaska region. Extreme events here generally refer

to the exceedance of a threshold at the tails of a meteorological variable's distribution that produces a relatively rare (and often problematic or dangerous) outcome.

Extreme event attribution studies use a combination of observations and modeling to assess the likelihood of a particular hazard occurring in the current climate as opposed to an earlier period without climate change (National Academies of Sciences 2016). A typical metric used in this assessment is the fraction of attributable risk (i.e., the risk attributable to human-caused climate change), calculated as $1-P_0/P_1$, where P_0 (P_1) represents the probability of occurrence in the earlier (current) period (Stott et al. 2016). The 2015 wildfire season, which burned more than five million acres throughout Alaska, was found to be 34-60% more likely due to anthropogenic warming when compared to pre-industrial times (Partain et al. 2016). The record-breaking upper oceanic heat content in the Gulf of Alaska and Bering Sea during 2016, which was attributed to devastating marine ecosystem impacts, had no analogs in the modern period (Walsh et al. 2017).

Another tool to measure changes to extremes was developed by the Expert Team on Climate Change Detection and Indices (ETCCDI; http://www.climdex.org/indices.html; Klein Tank et al. 2009). This is a set of 27 indices that are based on observed surface temperature and precipitation. These indices are used to examine changes to extreme event frequencies, and percentile and threshold exceedances. Changes to these indices were evaluated globally using 31 members of the Coupled Model Intercomparison Project phase 5 (CMIP5; Taylor et al. 2012) during historical (Sillmann et al. 2013a) and future periods (Sillmann et al. 2013b). Over the Alaska region, this evaluation indicated strong asymmetric warming of extremes, such that extreme cold became much less frequent while extreme heat more so.

Several of the ETCCDI indices relate to metrics such as the number of frost days per year, or the annual growing season length. These are of particular relevance for Alaska because the statewide average temperature is below, but close to, freezing (Figure 1.2). The warmest year of record (1925-2017) in Alaska occurred in 2016 when the average temperature was -0.1˚C; however, with warming expected to continue, it is feasible that future years could be above freezing. Approximately 38% of mainland Alaska contains near-surface permafrost (Pastick et al. 2015), and this frozen soil is susceptible to thaw when mean temperatures rise above 0˚C. When permafrost thaws, it causes subsidence of the land and markedly changes surface hydrology. Projections of unmitigated 21st-century warming suggest that climate-related change in Alaska will lead to $5.5 billion in damages, and the second highest contribution to this figure is associated with permafrost thaw and structural costs (Melvin et al. 2016).

Associated with extreme event assessment and attribution is the question of when, and if, a climate change signal will emerge from the inter-annual natural variability. Such emergent behavior means that the new distribution of a meteorological variable is outside of the historically observed one. Figure 1.3 shows an example of this for the distribution of snow season length at Barrow, Alaska from 1958-2017. The snow season length is defined as the continuous number of days with snow cover each cold season, which in this case is measured by a minimum depth of 2.54 cm (1.0 in.). Observations are from the Global Historical Climatology Network Daily Database (Menne et al. 2012; https://www.ncdc.noaa.gov/ghcn-daily-references). The gray shaded area represents one standard deviation above and below the mean snow season length for the period from 1958-1987. These 30 years are used as the 'historical' period and are compared to the

next 30 years from 1988-2017. It is standard convention to use 30-year periods for climate monitoring (WMO 2011), which is why the most recent 60 years are used (i.e., two 30-year periods). Notice that after 2010 every point in Figure 1.3 falls outside of the shaded area, indicating that the snow season length index for Barrow can no longer be characterized by historical conditions. A more robust measure would use two standard deviations.

Despite the magnitude of change that is occurring, observations for Alaska remain relatively limited, particularly with respect to high-resolution long-term climate records. There is an increasing number of cooperative weather stations in Alaska, but these often do not meet the 30-year standard for climate studies or they contain too many missing values for adequate coverage. Global reanalyses, which assimilate *in situ* and satellite observations into a forecast model and produce physically-consistent gridded meteorological fields, help to alleviate the large data problems facing Alaska (Lader et al. 2016). However, these frequently have a coarse spatial resolution (e.g., 2.0° latitude × 2.5° longitude), which produces overly smoothed data and do not resolve the state's varying topography. The same limitations exist for studies that examine future scenarios that are based on global climate models (GCMs). Changing data assimilation in the reanalyses can also produce artificial boundaries in time and space.

Regional downscaling of reanalyses and GCMs offers an attempt to further improve the quality of climate data for Alaska. The North American Regional Climate Change Assessment Program (NARCCAP) produced dynamical-forced reanalysis and GCM simulations at 50-km resolution; however, the project's domain did not include any of northwest Alaska (Mearns et al. 2009). More recently, Monaghan et al. (2017) produced

a 4-km resolution dataset that covers Alaska using the Weather Research and Forecasting (WRF) Model (Skamarock et al. 2008) from 2002-2016. While they found that their downscaled product showed suitably high correlations between observed temperature and precipitation, the short time period precludes its use in many climate studies. The Scenarios Network for Alaska and Arctic Planning (SNAP) produced a 2-km dataset using a delta downscaling methodology (Hayhoe 2010) that covers historical and future periods (https://www.snap.uaf.edu/). These data take modeled differences between two periods (e.g., future and present) and superimpose these changes to a known historical distribution, producing monthly gridded information. These projects have vastly improved data quality in Alaska, but they often have significant limitations in space and time that make it difficult to investigate how climate extremes have changed and are projected to change.

1.2 Objectives

The purpose of this research is to increase understanding of how certain extreme climate events are projected to change in the 21st century for the state of Alaska. One source of the current knowledge gap stems from a lack of high-resolution gridded climate data. The research described here utilizes newly developed dynamical downscaled reanalysis and climate model simulations that produce information on 20-km grids with daily time resolution. The downscaled simulations include the ERA-Interim reanalysis (Dee et al. 2011) and two members from the CMIP5: National Center for Atmospheric Research (NCAR) Community Climate System Model version 4 (CCSM4) and Geophysical Fluid Dynamics Laboratory Climate Model version 3 (GFDL-CM3; Donner

et al. 2011). The reanalysis data used here cover the period from 1981-2010 and frequently serve as the baseline period that climate model projections are compared against. The projections are presented in 30-year periods (i.e., 2011-2040, 2041-2070, 2071-2100). These are based on representative concentration pathway 8.5 (RCP8.5; Riahi et al. 2011), which best matches the current trajectory of greenhouse gas and aerosol emissions (Peters et al. 2013). The research contained herein uses these data to advance previous work on climate extremes over Alaska by the following three studies:

1. The ETCCDI climate extremes indices are calculated at higher spatial resolution across Alaska than was done previously to help better understand the spatial characteristics of observed and projected changes. The probability density functions of temperature and precipitation across 30-year periods are shown and emphasis is placed on how statistical moments change in relation to others.
2. One of the ETCCDI indices is growing season length. For Alaska, the changing temperature distribution and reduced frequency of cold extremes present new agricultural possibilities. These are investigated using indicators that include: seasonal temperature and precipitation climatology, growing season length, last spring frost, first autumn frost, start-of-field operations date and heat stress.
3. Many of the climate extremes that occur in Alaska relate to the presence or absence of snow and associated feedback mechanisms. Key cold season parameters are assessed, including: the annual cycle of elevation-dependent snowfall and end-of-winter snowpack, snow onset and snow-off dates, and maximum 2-day snowfall amounts.

1.3 Outline of this Dissertation

Chapters 2-4 of this dissertation are arranged into self-contained manuscripts that, together, address the previously stated research objectives. These manuscripts use a standardized format to facilitate navigation between studies. Chapter 5 provides summary conclusions and implications, identifying similarities and differences between the individual study results and methodologies. Following each chapter are figures, tables and references.

1.4 Figures

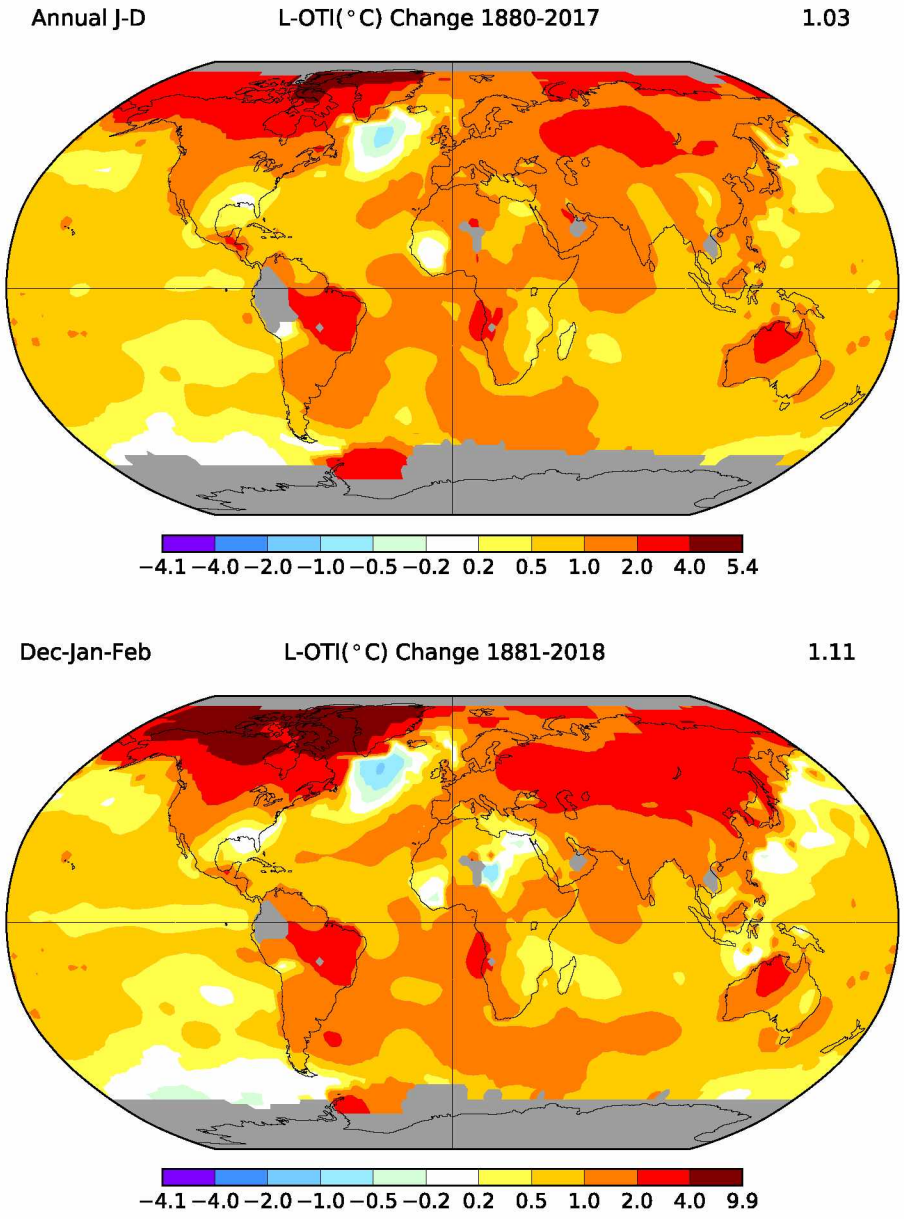

Figure 1.1 Annual temperature change (˚C) from 1880-2017 (top) and Dec-Jan-Feb change from 1881-2018 (bottom). The global average is indicated in the top right of each map (Data source: GISTEMP Team 2018; Hansen et al. 2010).

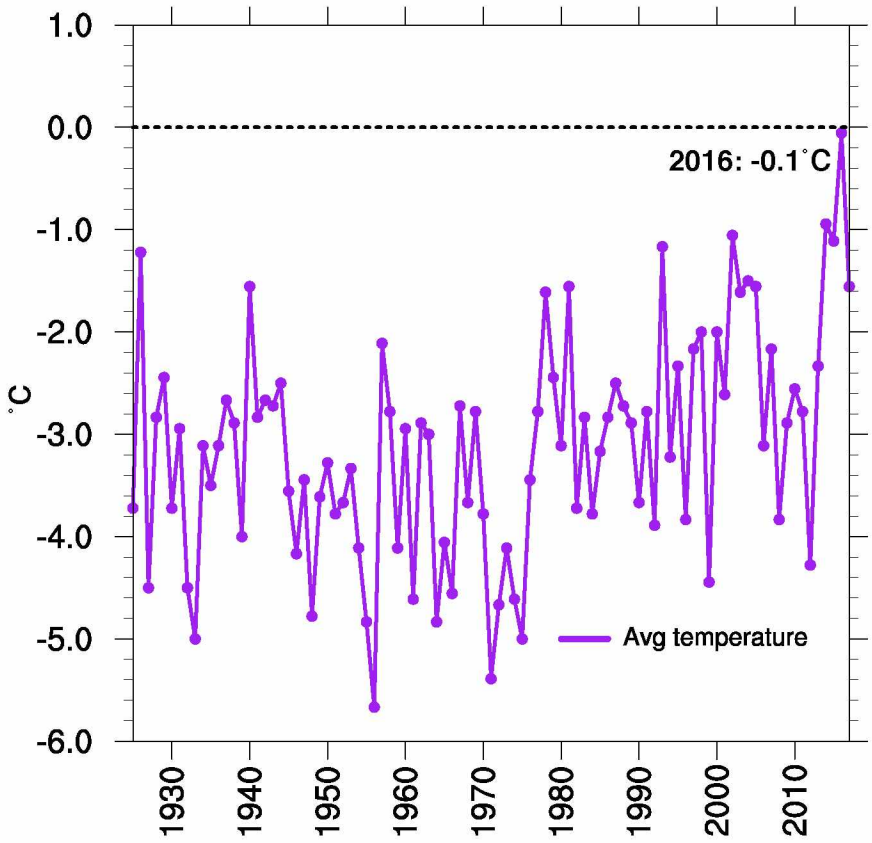

Figure 1.2 Average annual temperature (˚C) for Alaska (1925-2017; Data source: NOAA 2018b).

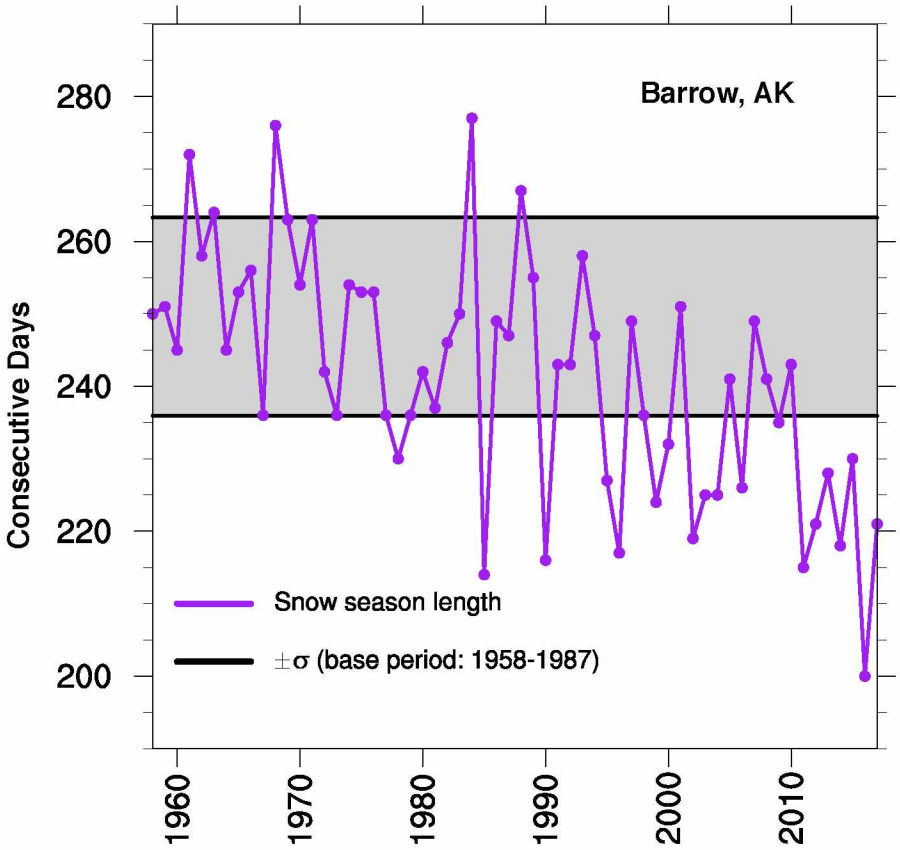

Figure 1.3 Snow season length for Barrow, AK (1958-2017). The shaded area represents ± 1 standard deviation relative to the 1958-1987 base period.

1.5 References

AMAP, 2017: Snow, water, ice and permafrost summary. Summary for policy-makers. Arctic Monitoring and Assessment Programme (AMAP), Oslo, Norway. 20 pp.

Dee, D. P., and Coauthors, 2011: The ERA-Interim reanalysis: Configuration and performance of the data assimilation system. *Quart. J. Roy. Meteor. Soc.*, **137**, 553-597, doi:10.1002/qj.828.

Donat, M. G, A. L. Lowry, L. V. Alexander, P. A. O'Gorman, and N. Maher, 2016: More extreme precipitation in the world's dry and wet regions. *Nat. Clim. Change*, **6**, 508-513, doi:10.1038/nclimate2941.

Donner, L. J., and Coauthors, 2011: The Dynamical Core, Physical Parameterizations, and Basic Simulation Characteristics of the Atmospheric Component AM3 of the GFDL Global Coupled Model CM3. *J. Climate*, **24**, 3484-3519, doi:10.1175/2011JCLI3955.1.

GISTEMP Team, 2018: *GISS Surface Temperature Analysis (GISTEMP)*. NASA Goddard Institute or Space Studies. Dataset accessed 2018-04-30 at https://data.giss.nasa.gov/gistemp/.

Hansen, J., R. Ruedy, M. Sato, and K. Lo, 2010: Global surface temperature change. *Rev. Geophys.*, **48**, RG4004, doi:10.1029/2010RG000345.

Hayhoe, K. A., 2010: A standardized framework for evaluating the skill of regional climate downscaling techniques. Ph.D. dissertation, University of Illinois at Urbana-Champaign, 158 pp. [Available online at http://www.snap.uaf.edu/attachments/1_Hayhoe_Katharine.pdf.]

IPCC, 2012: *Managing the Risks of Extreme Events and Disasters to Advance Climate Change Adaptation*. C. B. Field et al., Eds., Cambridge University Press, 582 pp.

IPCC, 2014: *Climate Change 2014: Synthesis Report. Contribution of Working Groups I, II and III to the Fifth Assessment Report of the Intergovernmental Panel on Climate Change* [Core Writing Team, R. K. Pachauri and L. A. Meyer (eds.)]. IPCC, Geneva, Switzerland, 151 pp.

Klein Tank, A. M. G., F. W. Zwiers, and X. Zhang, 2009: Guidelines on analysis of extremes in a changing climate in support of informed decisions for adaptation. Climate data and monitoring WCDMP-No. 72, WMO-TD No. 1500, 56 pp.

Lader, R., U. S. Bhatt, J. E. Walsh, T. S. Rupp, and P. A. Bieniek, 2016: Two-meter temperature and precipitation from atmospheric reanalysis evaluated for Alaska. *J. Appl. Meteor. Climatol.*, **55**, 901-922, doi:10.1175/JAMC-D-15-0162.1.

Mearns, L. O., W. J. Gutowski, R. Jones, L. –Y. Leung, S. McGinnis, A. M. B. Nunes, and Y. Qian, 2009: A regional climate change assessment program for North America. *EOS*, **90**, 311-312, doi:10.1029/2009EO360002.

Melvin, A. M., and Coauthors, 2016: Climate change damages to Alaska public infrastructure and the economics of proactive adaptation. *Proc. Natl. Acad. Sci.*, **114 (2)**, E122-E131, doi:10.1073/pnas.1611056113.

Menne, M. J., I. Durre, R. S. Vose, B. E. Gleason, and T. G. Houston, 2012: An overview of the Global Historical Climatology Network-Daily Database. *J. Atmos. Ocean Tech.*, **29**, 897-910, doi:10.1175/JTECH-D-11-00103.1.

Monaghan, A. J., M. P. Clark, M. P. Barlage, A. J. Newman, and L. Xue, 2018: High-resolution historical climate simulations over Alaska. *J. Appl. Meteor. Climatol.*, **57**, 709-731, doi:10.1175/JAMC-D-17-0161.1.

National Academies of Sciences, Engineering, and Medicine, 2016: *Attribution of Extreme Weather Events in the Context of Climate Change*. Washington, DC: The National Academies Press, doi:10.17266/21852.

NOAA National Centers for Environmental Information, 2018a: State of the Climate: Global Climate Report for Annual 2017, published online January 2018, retrieved on April 30, 2018 from https://www.ncdc.noaa.gov/sotc/global/201713.

NOAA National Centers for Environmental Information, 2018b: Climate at a Glance: Statewide Time Series, published April 2018, retrieved on April 30, 2018 from http:/ /www.ncd c.noaa.gov/cag/.

Overland, J. E., E. Hanna, I. Hanssen-Bauer, S. –J Kim, J. E. Walsh, M. Wang, U. S. Bhatt, and R. L. Thoman, 2016: Surface Air Temperature [in Arctic Report Card 2016], http://www.arctic.noaa.gov/Report-Card.

Parkinson, C. L., 2014: Global sea ice coverage from satellite data: annual cycle and 35-yr trends. *J. Climate*, **27**, 9377-9382, doi:10.1175/JCLI-D-14-00605.1.

Partain, J. L., and Coauthors, 2016: An assessment of the role of anthropogenic climate change in the Alaska fire season of 2015 [in "Explaining Extremes of 2015 from a Climate Perspective"]. *Bull. Amer. Meteor. Soc.*, **97 (12)**, S14-S18, doi:10.1175/BA MS-D-16-0149.

Pastick, N. J., M. T. Jorgenson, B. K. Wylie, S. J. Nield, K. D. Johnson, and A. O. Finley, 2015: Distribution of near-surface permafrost in Alaska: Estimates of present and future conditions. *Remote Sens. Environ.*, **168**, 301-315, doi:10.1016/j.rse.2015.07.0 19.

Peters, G. P., and Coauthors, 2013: The challenge to keep global warming below 2°C. *Nature Clim. Change*, **3 (1)**, 4-6.

Pithan, F., and T. Mauritsen, 2014: Arctic amplification dominated by temperature feedbacks in contemporary climate models. *Nat. Geosci.*, 7, 181-184, doi:10.1038/NGEO2071.

Riahi, K., S. Rao, V. Krey, C. Cho, V. Chirkov, G. Fischer, G. Kindermann, N. Nakicenovic, and P. Rafaj, 2011: RCP 8.5—A scenario of comparatively high greenhouse gas emissions. *Clim. Change.*, **109**, 33-57, doi:10.1007/s10584-011-0149-y.

Sillmann, J., V. V. Kharin, X. Zhang, F. W. Zwiers, and D. Bronaugh, 2013a: Climate extremes indices in the CMIP5 multimodel ensemble: Part 1. Model evaluation in the present climate. *J. Geophys. Res. Atmos.*, **118**, 1716-1733, doi:10.1002/jgrd.50203.

Sillmann, J., V. V. Kharin, F. W. Zwiers, X. Zhang, and D. Bronaugh, 2013b: Climate extremes indices in the CMIP5 multimodel ensemble: Part 2. Future climate projections. *J. Geophys. Res. Atmos.*, **118**, 2473-2493, doi:10.1002/jgrd.50188.

Skamarock, W. C., and Coauthors, 2008: A description of the Advanced Research WRF version 3. NCAR Tech Note, NCAR/TN-475+STR, 113 pp., doi:10.1056/D68S4MVH.

Smith, A., and R. Katz, 2013: U. S. billion-dollar weather and climate disasters: Data sources, trends, accuracy and biases. *Nat. Hazards*, **67**, 387-410, doi:10.1007/s11069-013-0566-5.

Stott, P. A., and Coauthors, 2016: Attribution of extreme weather and climate-related events. *WIREs Clim.* Change, 7, 23-41, doi:10.1002/wcc.380.

Taylor, K. E., R. J. Stouffer, and G. A. Meehl, 2012: An overview of CMIP5 and the experiment design. *Bull. Amer. Meteor. Soc.*, **93**, 485-498, doi:10.1175/BAMS-D-11-00094.1.

Walsh, J. E., and Coauthors, 2018: The high latitude marine heat wave of 2016 and its impacts on Alaska [in "Explaining Extremes of 2016 from a Climate Perspective"]. *Bull. Amer. Meteor. Soc.*, **99 (1)**, S39-43, doi:10.1175/BAMS-D-17-0105.1.

WMO, 2011: *Guide to Climatological Practices*. Third edition (WMO-No.100), Geneva.

2 PROJECTIONS OF TWENTY-FIRST-CENTURY CLIMATE EXTREMES FOR ALASKA VIA DYNAMICAL DOWNSCALING AND QUANTILE MAPPING[1]

2.1 Abstract

Climate change is expected to alter the frequencies and intensities of at least some types of extreme events. Although Alaska is already experiencing an amplified response to climate change, studies of extreme event occurrences have lagged those for other regions. Forced migration due to coastal erosion, failing infrastructure on thawing permafrost, more severe wildfire seasons, altered ocean chemistry, and an ever-shrinking season for snow and ice are among the most devastating effects, many of which are related to extreme climate events. This study uses regional dynamical downscaling with the Weather Research and Forecasting Model (WRF) to investigate projected 21st-century changes of daily maximum temperature, minimum temperature, and precipitation over Alaska. The forcing data used for the downscaling simulations include the: ERA-Interim reanalysis (1981-2010), GFDL-CM3 historical (1976-2005), and GFDL-CM3 RCP8.5 (2006-2100). Observed trends of temperature and sea ice coverage in the Arctic are large and the present trajectory of global emissions makes a continuation of these trends plausible. The future scenario is bias-adjusted using a quantile mapping procedure. Results indicate an asymmetric warming of climate extremes, namely cold extremes rise fastest, and the greatest changes occur in winter. Maximum 1-day and 5-day precipitation amounts are projected to increase by 53% and 50%, which is larger than the

---

[1] *Lader, R., J. E. Walsh, U. S. Bhatt, and P. A. Bieniek, 2017: Projections of twenty-first-century climate extremes for Alaska via dynamical downscaling and quantile mapping. J. Appl. Meteor. Soc., 56 (9), 2393-2409, doi:10.1175/JAMC-D-16-0415.1.*

corresponding increases for the contiguous United States. When compared to the historical period, the shifts in temperature and precipitation indicate unprecedented heat and rainfall across Alaska during this century.

2.2 Introduction

The effects of climate change and global warming on Alaska are unequivocal. From 1949 to 2012, the annual mean temperature increased 1.7 ˚C and annual precipitation increased 3.1 mm; winter changes were most dramatic with temperatures climbing 3.7 ˚C, and precipitation by 7.2 mm (Bieniek et al. 2014). While the overall signal for warmer, wetter conditions is clear, there also exists substantial spatial variability across Alaska. The trend magnitude for temperature on the North Slope and the northern Interior is consistently higher than the statewide average. For precipitation, Interior locations show little to no trend, but much of Southeast Alaska, while becoming wetter on an annual basis, shows significant drying during the spring months (Bieniek et al. 2014).

Arctic-wide, the 12-month period from October 2015 through September 2016 was the warmest year on record over the period 1900-2016 (Overland et al. 2016a). This broke the previous record set in 2007 that had been matched in 2011 and 2015 (Overland et al. 2016b). Heavy precipitation, defined as exceeding the 95th percentile of the distribution, increased by 18% across southern Alaska during the period from 1950 to 2002 (Groisman et al. 2005). Since 1979, the melt season for sea ice in the Arctic Ocean has lengthened by 37 days (Parkinson 2014); meanwhile, the lowest recorded maximum and minimum Arctic sea ice extents occurred in 2015 and 2012, respectively (US EPA

2016). The trend of Arctic sea ice extent is negative for all months, and the annual trend of loss, globally, is significant at the 99% confidence level (Parkinson 2014).

The Arctic is warming at twice the rate of the Northern Hemisphere, due to positive feedback mechanisms in the climate system, often referred to as Arctic amplification (Bekryaev et al. 2010; Pithan and Mauritsen 2014). One mechanism for the amplification is the sea ice-albedo feedback, wherein reduced sea ice lowers the surface albedo of the ocean, thus enabling greater absorption of solar radiation and promoting further sea ice melt. Warming temperatures are also responsible for thawing permafrost, which leads to drier landscapes in regions of discontinuous permafrost, and an increased wildfire threat. Ocean acidification, a response to the uptake of approximately one quarter of annual carbon dioxide emissions (Walsh et al. 2014), threatens biodiversity, commercial fisheries, and subsistence harvesting over the coastal waters of Alaska (Chapin et al. 2014). Increased river discharge and rapid glacial melt further exacerbate these problems by altering ocean chemistry.

Alaska is projected to experience major changes in extreme weather during the 21st century (IPCC 2012). Natural and human systems are adapted to the recently observed climate, but not necessarily for rare or unobserved conditions, so rapidly changing extreme weather patterns make these systems vulnerable to deterioration and destruction. To help understand how extreme events are changing globally, the Expert Team on Climate Change Detection and Indices (ETCCDI) developed a set of 27 indices (http://www.climdex.org/indices.html) that are based on the distributions of daily surface temperature and precipitation (Klein Tank et al. 2009). These include measures of absolute extremes (e.g., hottest and coldest days of the year), threshold exceedance (e.g.,

number of frost days), time duration (e.g., cold spells), and percentile-based extremes (e.g., heavy precipitation above the 95th percentile).

Sillmann et al. (2013a) used these indices to compare a 31-model ensemble from the Coupled Model Intercomparison Project Phase 5 (CMIP5) with reanalysis output and noted an observed pattern of asymmetric warming of extreme temperatures. That is, cold temperature extremes are rising faster than warm temperature extremes. Observed trends of extreme precipitation are also positive with greater spatial variability (Zhang et al. 2011). This is expected, given that rising temperatures increase the atmosphere's holding capacity for water vapor. While the global climate models generally replicate climate extremes, they also occasionally exhibit large errors owing to coarse resolution, particularly in mountainous regions.

Regional dynamical downscaling of the global models attempts to reduce these errors by providing gridded output at much finer spatial and temporal resolution. The Coordinated Regional Climate Downscaling Experiment (CORDEX) (Giorgi et al. 2009), for example, includes an Arctic domain covering most of Alaska. The global models provide the initial and boundary conditions that are necessary for the regional models to run, as the atmospheric circulation output from regional models is heavily dependent on the forcing global model (Koenigk et al. 2015). The added value of dynamical downscaling will vary spatially and seasonally with the circulation regime.

For Alaska, Bieniek et al. (2016) downscaled the European Center for Medium-Range Weather Forecasts (ECMWF) Reanalysis (ERA-Interim) (Dee et al. 2011) to 20-km spatial resolution using the Advanced Research core of the Weather Research and Forecasting (WRF) Model (Skamarock et al. 2008). Unlike many regional climate model

simulations, the downscaling of historical conditions in this study was constrained by a re-initialization to a reanalysis (ERA-Interim) every 48 hours. They found reduced biases in the downscaled products of monthly temperature and precipitation relative to the input reanalysis data when validated against the statistically downscaled dataset of Hill et al. (2015) and station observations. The improvement was especially apparent near coastlines and in areas of significant topography.

The utility of dynamical downscaling has been shown across Alaska for mass-balance modeling of the Gulkana Glacier (Zhang et al. 2007), studying extreme precipitation (Glisan and Gutowski 2014a,b), quantifying the fraction of attributable risk imposed by climate change to the 2015 Alaska fire season (Partain et al. 2016), and anticipating when the record-warm winter of 2015-2016 could become normal (Walsh et al. 2017b).

Future projections of extreme temperature and precipitation are dependent upon the expected radiative forcing from greenhouse gas emissions and aerosols. The CMIP5 prescribes four Representative Concentration Pathways (RCPs) that provide a range of radiative forcing between 2.6 W m^{-2} and 8.5 W m^{-2} by the end of the 21st century (van Vuuren et al. 2011). Observed carbon dioxide emissions continue to closely track the highest forcing scenario, RCP8.5 (Peters et al. 2013). RCP8.5 assumes a global population increase to 12 billion by 2100, and notes a decoupling between legislation that is aimed to combat air or water pollution as opposed to strictly climate change policy (Riahi et al. 2011). In the Arctic, the observed trend of warming and rate of sea ice loss is even greater than projected by models forced by RCP8.5 (See Figs. 4-5 in Overland et al. 2013).

Sillmann et al. (2013b) studied projected changes to the extremes indices with a multimodel ensemble from CMIP5 using several of the RCPs. For their Alaska region, they found a continued asymmetric warming, with cold extremes increasing more than warm ones. Under the RCP8.5 scenario, the annual minimum temperature is projected to climb 14.3 ˚C by 2100, but the annual maximum only by 4.4 ˚C; meanwhile, the annual maximum five-day precipitation is projected to increase by an average of 16 mm statewide (Bennett and Walsh 2014). These studies also note that the greatest increases in extreme temperature and precipitation occur in winter for Alaska. During summer, the changes to extreme indices are often more comparable to lower latitudes. These studies of the CMIP5 models did not consider the biases or other systematic errors in the CMIP5 global models.

Alaska has a limited observational network, so reanalysis is often used as a gridded tool to assess climate model output (Lader et al. 2016). Therefore, to properly contextualize model projections, it is important to consider the bias of a climate model relative to reanalysis, and also the bias of reanalysis relative to *in situ* observations. This leads to the following questions that this study addresses:

1) Does reanalysis compare more favorably to station observations than the historical climate model in terms of their long-term downscaled distributions?
2) Does dynamical downscaling reduce errors associated with extremes-relevant variables: daily maximum temperature (T_{max}), minimum temperature (T_{min}), and precipitation?

3) Under the RCP8.5 emissions scenario, how do downscaled projections of the climate extremes indices compare to previous studies that use coarser data?

2.3 Data and Methods

This study incorporates the ERA-Interim reanalysis from 1981-2010 (Dee et al. 2011), and two simulations from the Geophysical Fluid Dynamics Laboratory (GFDL)-CM3 (Donner et al. 2011) from 1976-2100. All of these data have been dynamically downscaled with spectral nudging, providing hourly output across 49 vertical levels and 20 km spatial resolution as described in Bieniek et al. (2016). The choice of resolution was based on the decision to improve upon the widely used CORDEX data, which had a 50-km spacing for its first phase, and for computational time efficiency. The WRF Model configuration includes the following physics options: microphysics – Morrison 2-moment (Morrison et al. 2009); radiation – Rapid Radiative Transfer Model (Iacono et al. 2008); cumulus – Grell 3D; planetary boundary layer – Mellor-Yamada-Janjić (Janjić 1994); surface layer – Monin-Obukhov; land surface – Noah land surface model coupled with thermodynamic sea ice (Zhang and Zhang 2001). The two timeframes spanned by the GFDL-CM3 runs are a historical period from 1976-2005, and a future period (2006-2100) based on the RCP8.5 emissions scenario. The study domain covers eastern Russia, Alaska, much of northern Canada, and the adjoining oceans (Figure 2.1).

The National Oceanic and Atmospheric Administration (NOAA) provides a visualization tool (http://www.esrl.noaa.gov/psd/ipcc/cmip5/) that enables users to compare each member of the CMIP5 to the ensemble means of temperature and precipitation. From 1979-2008, the GFDL-CM3 agrees well with these ensemble means

across Alaska. However, from 2006-2100, the GFDL-CM3 projects a higher rate of warming that is nearly twice the CMIP5 ensemble mean for daily air temperature. It also projects a larger increase of precipitation across Interior Alaska, with comparable changes over the southeast. Our choice of the GFDL-CM3 model is motivated in part by the fact that Arctic warming and sea ice loss are occurring more rapidly than in most CMIP5 simulations (Overland et al. 2013). Laliberté et al. (2016) showed that the GFDL-CM3 is one of the top-performing CMIP5 models for capturing the summer sea-ice concentration when compared to a recent decade of passive microwave imagery. Walsh et al. (2017a) show that GFDL-CM3 ranks third among 21 CMIP5 models in the simulation of the seasonal cycles of temperature, precipitation and sea level pressure over Alaska. Finally, as shown in Section 4, indices of extremes based on GFDL-CM3 are generally in the mid-range of the indices based on other CMIP5 models.

A major contribution of this study is the hybrid dynamical downscaling and quantile-mapping approach used to investigate projected changes to extreme climate for Alaska. Dynamical downscaling of the GFDL-CM3 from 2° latitude × 2.5° longitude to 20 km × 20 km is here shown to provide value-added information, particularly for temperature. The subsequent application of a quantile-delta mapping algorithm serves to bias-adjust the GFDL-CM3 RCP8.5 scenario using the observation-based ERA-Interim reanalysis.

Quantile approaches of statistical downscaling are generally superior to a simple delta method because each point in the distribution gets a unique adjustment (Hayhoe et al. 2010). These incorporate changes to the mean and variance, rather than only to the mean. However, the quantile-mapped data are also tied to the relationships between

large-scale features and the climate inherent to the reanalysis, which are assumed to remain stationary.

A quantile-delta mapping algorithm (Cannon et al. 2015) was employed to bias-adjust the downscaled GFDL-CM3 RCP8.5 projections. This takes the relative change at each point in the distribution of the GFDL-CM3 between the projection and the historical period and applies it to the ERA-Interim reanalysis, which acts as an observational dataset. This is described mathematically as follows:

$$x(t) = F_R^{-1}[q(t)] \times \frac{F_P^{-1}[q(t)]}{F_H^{-1}[q(t)]}, \quad (1)$$

where $x(t)$ represents the corrected value, and $F^{-1}[q(t)]$ represents the quantile functions of the observed ERA-Interim reanalysis R, future GFDL-CM3 RCP8.5 projection P, and the historical GFDL-CM3 simulation H. More generally the quantile function is defined as:

$$F^{-1}[q(t)] = \min\{x \in \mathbb{R} : F(x) \geq q(t)\}, q(t) \in \{0,1\}, \quad (2)$$

where $F(x)$ is the cumulative distribution function of the variables, in this case temperature and precipitation, and $\mathbb{R}$ denotes the set of real numbers. For example, the 90th percentile precipitation of the future projected distribution is divided by the 90th percentile precipitation from the GFDL-CM3 historical simulation to obtain a modeled ratio of change. This ratio is then multiplied by the 90th percentile precipitation of the observed reanalysis distribution to obtain a bias-adjusted future projection. The percentile

values, and all other points, are obtained via the quantile function (2). The same procedure is applied to temperature. For precipitation values that are less than one, the modeled change is calculated by subtraction and this delta is then added to the observed reanalysis value.

The procedure works with successive 30-year periods so that bias-adjusted data are produced from 2011-2040, 2041-2070, and 2071-2100, using 1981-2010 as the reanalysis baseline. The period from 1976-2005 is the historical period used for the GFDL-CM3 because the simulation ends in 2005, but this difference should not have a significant effect on the final products. Also note that the quantile-delta algorithm is applied locally, (i.e., at each grid box) to best preserve modeled changes.

This bias-adjustment using reanalysis is justified because the ERA-Interim consistently has a lower root-mean-square-error (RMSE), in terms of statistical distribution, when compared to station observations, than the historical GFDL-CM3 does. This is also true when restricting the sample to the highest and lowest percentiles, which is relevant for extreme events. Figure 2.2 shows this result for daily T_{max}; findings for daily T_{min} and precipitation are similar. The closer correspondence of the station data to ERA-Interim compared to GFDL-CM3 is expected because ERA-Interim assimilates station and satellite observations, whereas the GFDL-CM3 does not. Consider also that the model grid cells used for each station have the same elevation because both downscaling simulations were conducted using WRF.

For the overlapping period of 1980-2005, the annual mean statewide ERA-Interim temperature (-3.1 ˚C) compares more favorably with observations (-2.6 ˚C) than does the GFDL-CM3 (-3.5 ˚C). Figure 2.3a shows the corresponding time series. Similarly, for

precipitation, ERA-Interim (90.3 cm) is closer to observed (95.5 cm) than is the GFDL-CM3 (103.3 cm) (Figure 2.3b). The observations are from NOAA's 'Climate at a Glance' tool, available at (http://www.ncdc.noaa.gov/cag/) (NOAA 2017). The quantile-delta mapping procedure temporarily removes the date associated with any particular value and sorts the respective distributions in ascending order. The date is kept track of, however, so that the correct ratio can be applied to the correct point in the reanalysis distribution, thus producing the projected time series. In this way, the projected data reflects changes to the 30-year distribution more than it does to the trend.

Another test compares the spatially-averaged RMSE of the coarse-scale forcing data with their downscaled products. If ERA-Interim is considered 'truth', both before and especially after downscaling, as previous studies already mentioned suggest, are the errors larger or smaller when comparing the coarse and downscaled GFDL-CM3 datasets with their reanalysis counterparts? Figure 2.4 shows that the RMSE of daily T_{max} and T_{min} for a 25-year climatology from 1981-2005 are lower in the downscaled GFDL-CM3. This is true for the entire study domain and when only comparing grid cells over land. For precipitation, the coarse GFDL has a lower RMSE when averaging over the entire domain, but the values are equal over land. These results indicate that dynamical downscaling, which provides an improved representation of topography, reduces climate model errors for land areas. Along the coastal mountains of southern Alaska, the sign of the model precipitation bias changes from being too dry prior to downscaling, and then too wet after downscaling.

2.4 Results

2.4.1 Projections of extreme temperature

Threshold-based indices of daily T_{max} and T_{min} suggest a further shrinking of the traditional cold season in Alaska and an increase in unprecedented summer heat. The annual number of icing days, those with a daily T_{max} below 0°C, is projected to decrease 38% by 2100 statewide (Table 1). Its counterpart for daily T_{min}, the annual number of frost days (T_{min} < 0°C), shows an average decrease of over two months statewide (Figure 2.5). Meanwhile, the annual count of days with a high temperature above 25°C, so-called 'summer days', is expected to skyrocket from a historical statewide average of 1.5 days $year^{-1}$ up to 29.7 days $year^{-1}$ (Figure 2.6). Similarly, the annual count of tropical nights (T_{min} > 20°C), transitions from a negligible number to a statewide average of 6.8 occurrences per year (Table 1). To date, this magnitude of heat has largely been restricted to interior Alaska, but end-of-century projections indicate an expansion to cover nearly all of the state.

The maximum seasonal value of daily T_{max} (TX_x), when averaged across Alaska over 30-year periods, shows projected increases of 6.2°C, 7.5°C, 7.0°C, and 7.7°C for DJF, MAM, JJA, and SON, respectively, by 2100. For the monthly minimum value of daily T_{min} (TN_n), these increases are 18.2°C, 16.3°C, 6.8°C, and 14.9°C, respectively. Thus, all seasons except summer indicate a much greater warming of extreme cold over extreme warm temperatures. The changes for TX_x and TN_n are approximately 50% and 25% larger, respectively, than those presented by Bennett and Walsh (2014), who used a 6-member ensemble of high-performing CMIP5 models for Alaska. This further suggests that the GFDL-CM3 projects a stronger warming than the CMIP5 ensemble mean.

The asymmetric warming of cold extremes relative to warm extremes is apparent in the probability density functions of daily T_{max} (Figure 2.7) and T_{min} (Figure 2.8) at the nearest grid point to eight primary population centers of Alaska (Figure 2.1). The eight-city average of the 30-year minimum temperature increases by 22°C from 1981-2010 to 2071-2100 for both distributions of daily T_{max} and T_{min}. At the lower quartile, the magnitude of change decreases to approximately half that of the absolute minima, and the least change occurs at the upper quartile and the absolute maxima of the distributions (Table 2). Notable is the bimodality of many of these distributions, often representing cold and warm season modes. With time, extreme cold values warm and populate the bin near freezing, which results in peaky behavior. Despite the warming, Alaska will continue to experience polar night and ice-covered surfaces during winter, which could constrain the temperature to near freezing. The summer mode shifts more uniformly to the right.

The observed inter-annual variability, quantified by standard deviation, decreases at all stations except for Anchorage (T_{max}), and Juneau (both T_{max}, and T_{min}). This points to the importance of sea ice and seasonally permanent snowpack as drivers of extreme cold and high temperature variability. Anchorage and Juneau are much less affected by these drivers in the base period of 1981-2010 than are the other six stations. However, for the other locations proximal to where seasonal sea ice currently exists, sea ice and the presence of long-standing snowpack are projected to diminish by the mid-century and disappear entirely by 2100. As a stark consequence of this, Barrow, which currently has high temperature variability similar to that of Interior Alaska, exhibits comparable variability to Juneau by 2100 (Table 2).

2.4.2 Projections of extreme precipitation

Total precipitation is projected to increase across Alaska through time. The average annual accumulation increases from 79.3 cm yr^{-1} during the base period to 121.2 cm yr^{-1} by the end of the century, representing an increase of 53%. Note that these represent statewide averages; the Gulf of Alaska coast, including Southeast Alaska and the Kenai Peninsula, typically have values exceeding 200 cm yr^{-1}, whereas the Arctic coast is often around 15-30 cm yr^{-1}. The changes to extreme precipitation are similarly striking. The average annual count of heavy precipitation days ($\geq$ 10mm) and very heavy precipitation days ($\geq$ 20mm) increases by 66% and 101%, respectively (Table 1). The average annual maximum 1-day (Table 1) and 5-day (Figure 2.9) precipitation is projected to increase by 53% and 50%, respectively, by the end of the century. The greatest relative change by percentage is expected for the Brooks Range and locations further north. The average annual maximum number of consecutive wet days ($\geq$ 1.0mm) is expected to increase by 23%, whereas the number of consecutive dry days is projected to decrease by 21% (Table 1). This does not necessarily mean that the threat for severe drought would decrease however, because higher temperatures would lead to greater daily evapotranspiration.

At the station (i.e., grid point) level, most locations are expected to see a median increase in daily precipitation, with each successive 30-year period becoming wetter than the previous (Table 3). The exceptions to this are Juneau and Anchorage, which are projected to have comparable or even smaller median precipitation by 2100. The 90^{th} and 99^{th} percentiles of the 30-year distributions are projected to increase at all stations through time. The absolute maximum precipitation amount does not necessarily increase

with each period, but the end-century quantities are larger than those from the base period in all cases.

There is also an apparent connection between diminishing sea ice and extreme precipitation across western Alaska. The average daily sea ice extent during March, when the climatological maximum annual extent is reached, extends well south in the Bering Sea to between St. Paul Island and the Aleutians from 2011-2040, but this line recedes into the Chukchi Sea from 2071-2100 (Figure 2.10). Coincident with these losses of sea ice is an increasing trend for greater extreme precipitation, first for the Aleutians and southwest Alaska from 2041-2070, and then for the Bering Strait and northwest Alaska from 2071-2100 (Table 3). Possible mechanisms for this relationship include shifting storm tracks and dynamics along the ice edge, and greater local evaporation in areas where sea ice has been replaced by open water (Kopec et al. 2015).

2.5 Discussion

The observed and expected changes to extreme climate in Alaska show similarities but also some marked differences when compared to the contiguous United States. For example, the asymmetric shift in the distributions of daily T_{max} and T_{min} is evident beyond Alaska; Meehl et al. (2016) show that for the continental United States there has been an observed 2:1 ratio of record high maximum to record low minimum temperatures set during the early part of the 21st century. A similar analysis for Alaska shows that this ratio routinely exceeds 3:1 beginning in the 1990s, and even climbs to 9:1 for the recent warm year of 2015 (Figure 2.11). The circulation pattern likely contributed to the extreme warmth of 2014 and 2015, which saw both El Niño and strongly positive PDO

conditions. These years are not included in the reference period used for mapping and thus do not affect the projections. However, they highlight how background warming in combination with favorable large-scale teleconnection patterns, which may or may not be captured well in the climate model, can result in extraordinary climate extremes.

The frost-free period in the eastern two-thirds of the contiguous United States is projected to increase by 30-40 days by 2100 (Walsh et al. 2014), whereas for Alaska the statewide average increase of the growing season length in this study is nearly 50 days (Table 1). Whether or not this increased growing potential is realized will largely depend on soil conditions and precipitation.

The average statewide precipitation distribution for Alaska is projected to increase nearly uniformly in a percentage sense; annual mean precipitation and maximum 1-day precipitation are both expected to increase by 53%. The most extreme precipitation in the contiguous United States is expected to increase by smaller amounts of approximately 10-40%, depending on season, and mean precipitation is even projected to decrease in parts of the central and southern United States (Prein et al. 2016). Furthermore, the annual maximum number of consecutive dry days is projected to increase across most of the contiguous United States (Walsh et al. 2014), but is expected to decrease by 21% in Alaska (Table 1).

In terms of Clausius-Clapeyron scaling, the average surface specific humidity is projected to increase 5.7% C^{-1} statewide, and 6.4% C^{-1} for the 99^{th} percentile. For temperature-precipitation scaling, these values are 4.1% C^{-1} and 5.8% C^{-1}, respectively. These values represent changes between 2071-2100 and 1981-2010. The 5.7% C^{-1} rate exactly matches the differential rate of change found by O'Gorman and Muller (2010)

where it is suggested that scaling is lower than the expected 6-7% C^{-1} due to slight decreases in relative humidity over land. The upper percentile values are closer to expected Clausius-Clapeyron scaling possibly because they represent instances of high moisture transport and convergence.

For a signal-to-noise analysis of the extremes indices, the change signal can be represented by the 10-year running mean anomaly relative to the historical GFDL-CM3 and the noise by the inter-annual standard deviation of the same period. A signal-to-noise ratio of two indicates that the decadal mean is twice the historical standard deviation, indicating that a change signal is emergent. For the annual frost days index, the ratio continuously exceeds two from 2026 onward and for the annual maximum consecutive 5-day precipitation from 2043 onward. However, no signal emerges for consecutive wet or dry days through 2100 (Table 1). This suggests that for indices with emergence dates before mid-century, the current level of change is already (or is close to) producing new extremes behavior. However, for indices with emergence dates after mid-century (e.g., tropical nights), the choice of emissions scenario could significantly change their future state. The use of a 10-year running mean anomaly here is designed to provide a robust estimate of signal emergence that accounts for inter-annual variability. The signal emergence dates shown in Table 1 represent a statewide average and are likely to vary considerably by location.

Despite being a warm and wet model for Alaska relative to the CMIP5 RCP8.5 ensemble mean, indices of several extremes computed from the GFDL-CM3 output generally fall near the middle of the range of projections from 29 other models (Figure 2.12). These data were interpolated to the WRF grid, calculated for the Alaska land cells,

and chosen to represent each of the meteorological variables in this study – summer days (T_{max}); frost days (T_{min}); very heavy precipitation days (precipitation). This suggests that, while the downscaling effect can be large, use of different models in this study would likely not offer drastically different results. Global files for each of these models containing the CLIMDEX indices are available from the Canadian Center for Climate Modeling and Analysis (http://climate-modelling.canada.ca/climatemodeldata/climdex/).

2.6 Conclusions

This study investigates multiple dynamically downscaled datasets for Alaska to demonstrate that extreme daily temperatures (T_{max} and T_{min}) are projected to warm asymmetrically, with cold extremes warming the fastest. Total precipitation is expected to increase statewide, largely due to more intense precipitation, and with higher relative changes north of the Brooks Range. The percentage increase in short-duration heavy precipitation amounts is greater than for the contiguous 48 states (Walsh et al. 2014). The combination of these findings suggests that unprecedented heat and precipitation would occur throughout Alaska, and that freezing temperatures and frozen precipitation would become increasingly less frequent by late century. These changes would favor increased plant productivity and an increased growing season length, but would likely also increase the risk for severe fire years, warm season flash flooding and landslides. The exact timing of the most drastic changes is in part a function of when sea ice vanishes entirely, particularly for the Arctic coast; however, the overall signal of the magnitude of change is clear.

The downscaling products in this study are shown to better reflect observations of temperature than are the original coarse input data during the historical period, indicating a value-added response as a result of higher resolution. The GFDL-CM3 RCP8.5 future scenario, which is warmer and wetter than the CMIP5 ensemble means, tracks better with recent trends in Arctic sea ice and near-surface temperatures and, without meaningful diversion away from the current trajectory of greenhouse gas emissions, it remains highly plausible. This future scenario was also bias-adjusted to the downscaled ERA-Interim reanalysis using quantile-delta mapping to further reduce errors. The bias adjustments of the entire distributions represent a value-added contribution to the evaluation of changes in extremes of temperature and precipitation for Alaska.

2.7 Acknowledgements

Support for this work was provided by the NOAA Climate Program Office through Grants NA11OAR4310141 and NA16OAR4310162 to the Alaska Center for Climate Assessment and Policy. This work was also made possible through financial support from the Alaska Climate Science Center, funded by the Cooperative Agreement G10AC00588 from the United States Geological Survey. Its contents are solely the responsibility of the author and do not necessarily represent the official view of the USGS. We thank three anonymous reviewers and the editor for providing excellent suggestions for how to improve our manuscript.

2.8 Figures

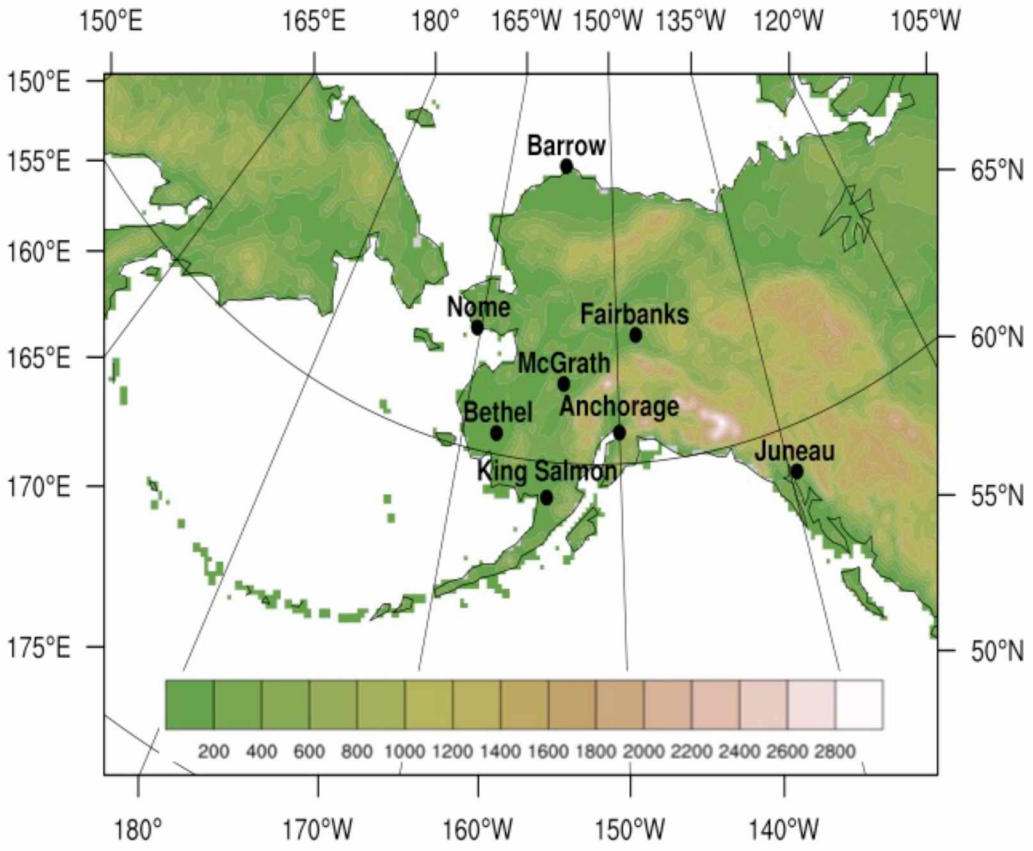

Figure 2.1 Model topography (m) for downscaling domain with selected cities in Alaska.

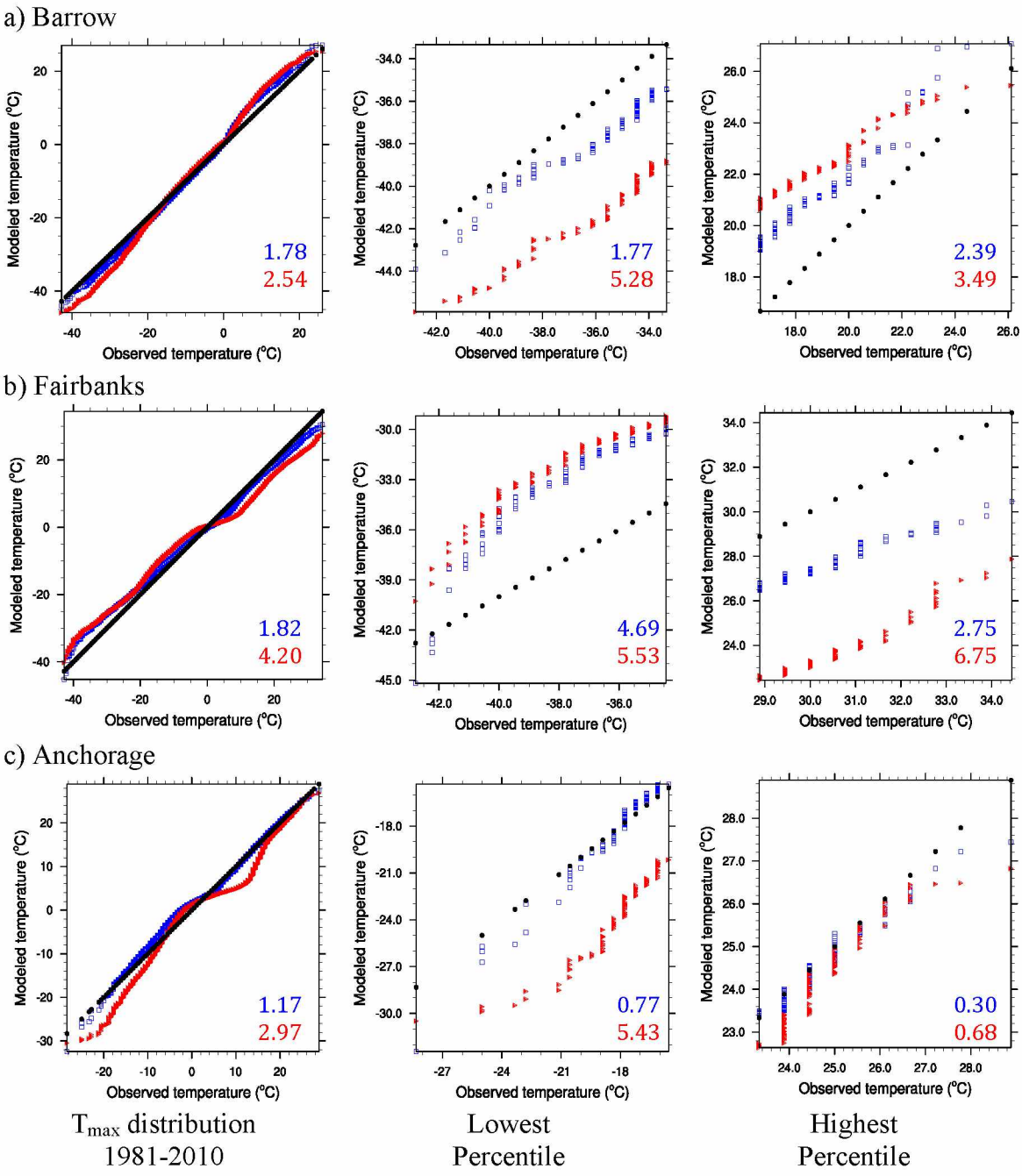

Figure 2.2 The observed distribution of daily T_{max} (˚C) from 1981-2010 (black) is compared to the nearest model grid cell of the downscaled ERA-Interim (blue), and GFDL-CM3 (red) at (a) Barrow, (b) Fairbanks, and (c) Anchorage. This includes the: (left) full 30-year distribution, (middle) lowest percentile, and (right) highest percentile. The RMSE relative to observed is indicated in the bottom right of each plot.

a)

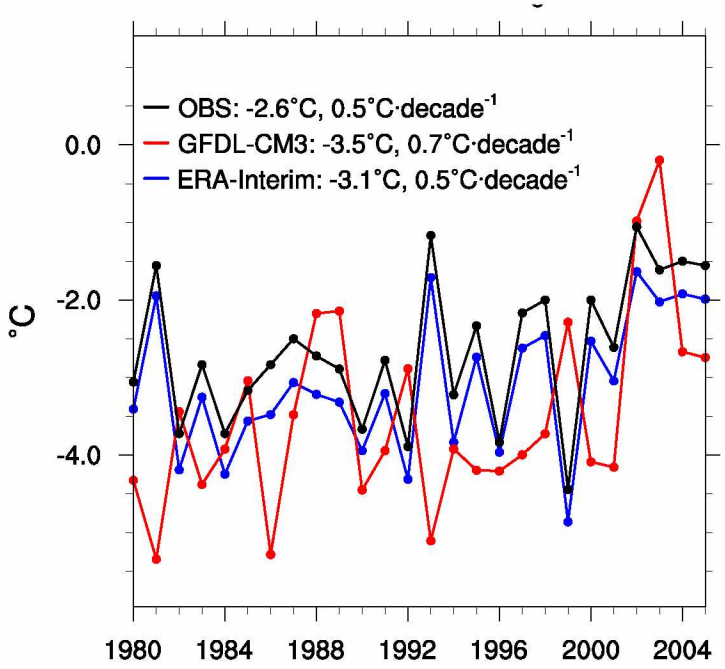

b)

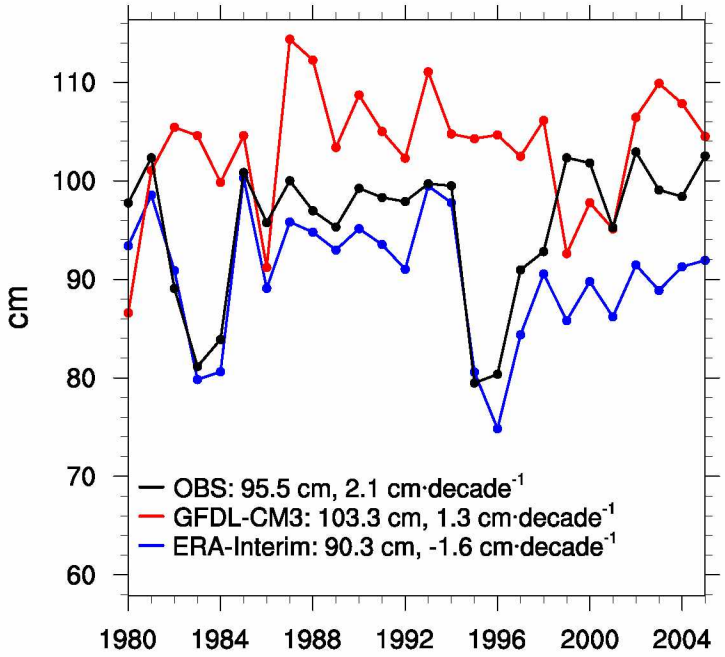

Figure 2.3 Average annual statewide a) temperature and b) precipitation for observations (black), ERA-Interim (blue) and GFDL-CM3 (red) from 1980-2005. The historical mean, and linear trend for each time series are indicated.

a) T_{max} bias

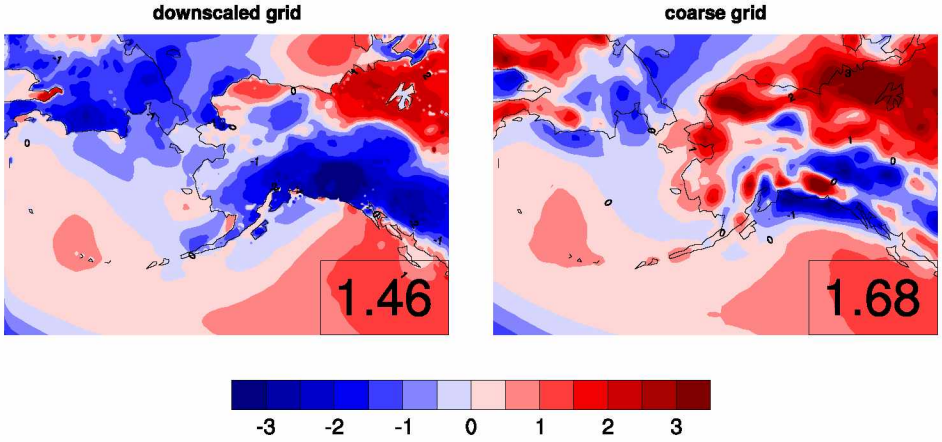

b) T_{min} bias

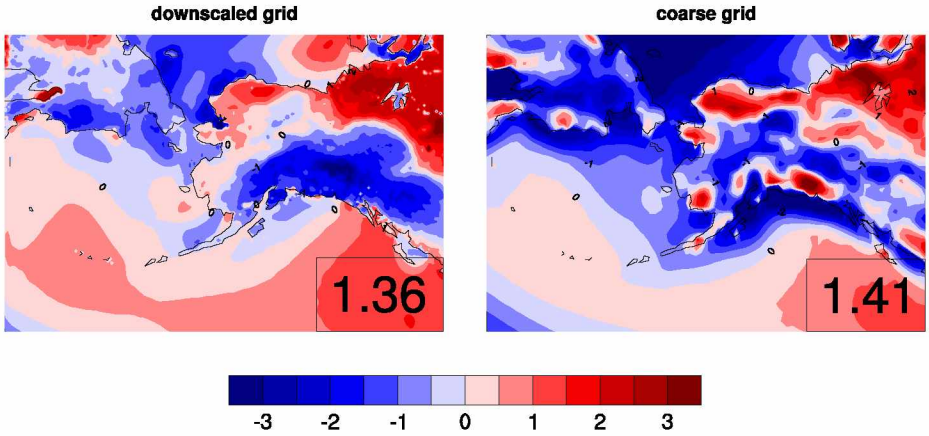

c) Precipitation bias

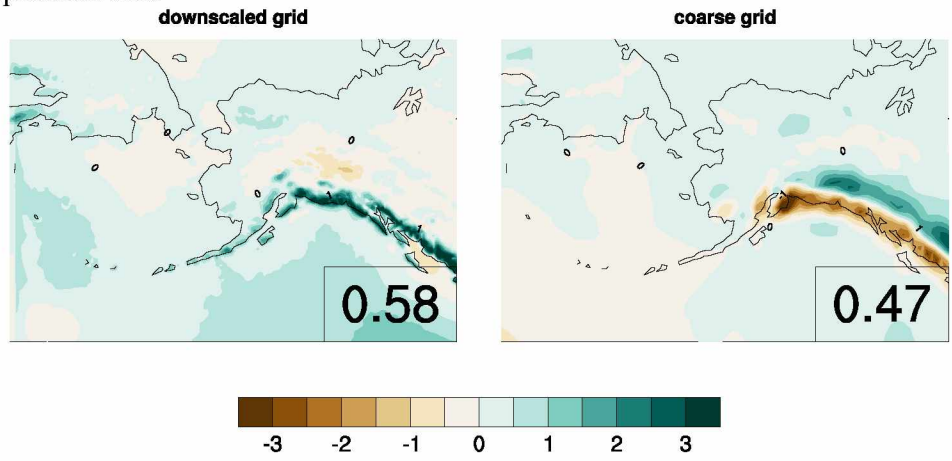

Figure 2.4 RMSE (GFDL-CM3 minus ERA-Interim) of daily a) T_{max} (˚C), b) T_{min} (˚C), and c) precipitation (mm) from 1981-2005 for the downscaled (left column) and coarse (right column) domains. The grid-point average RMSE is shown at the bottom right.

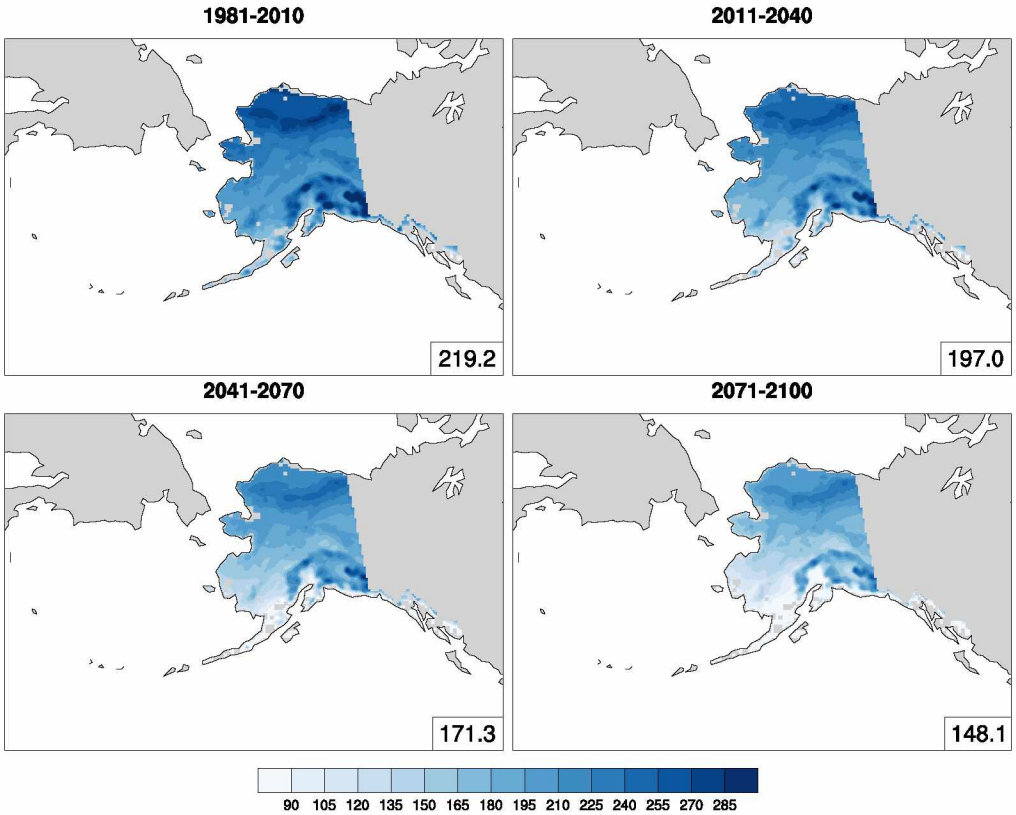

Figure 2.5 Number of frost days (T_{min} < 0°C) per year averaged for successive 30-year periods. The statewide average is located at the bottom right.

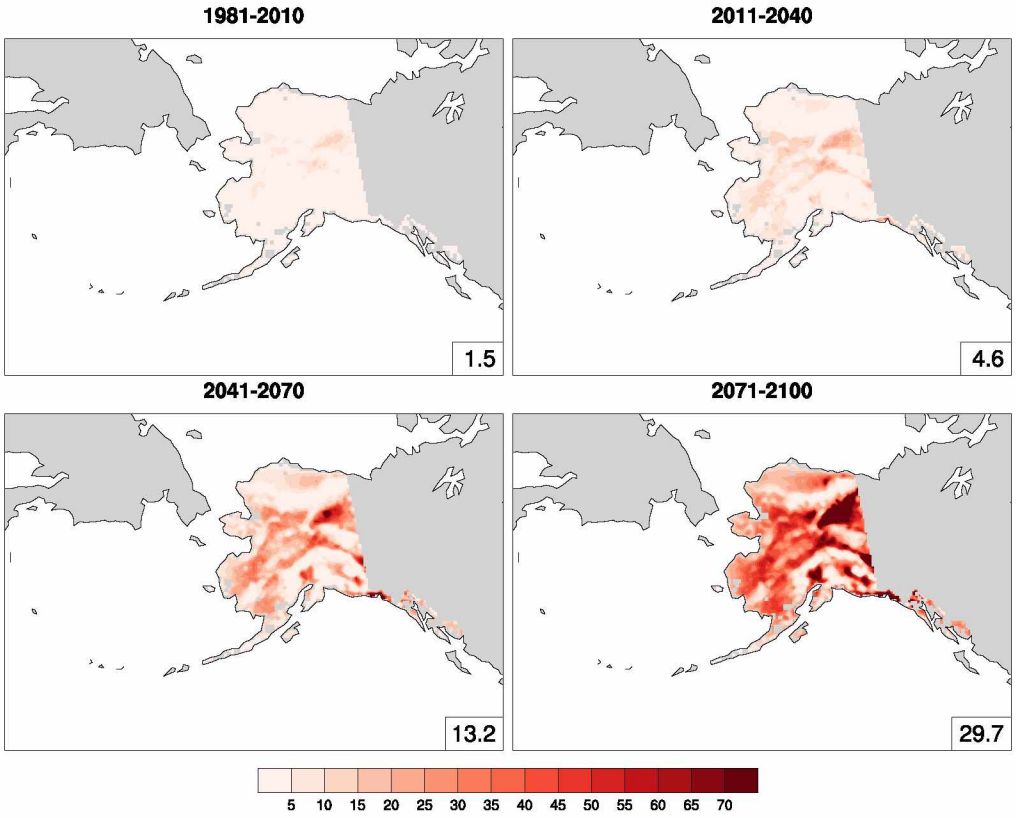

Figure 2.6 Number of summer days (T_{max} > 25˚C) per year averaged for successive 30-year periods. The statewide average is located at the bottom right.

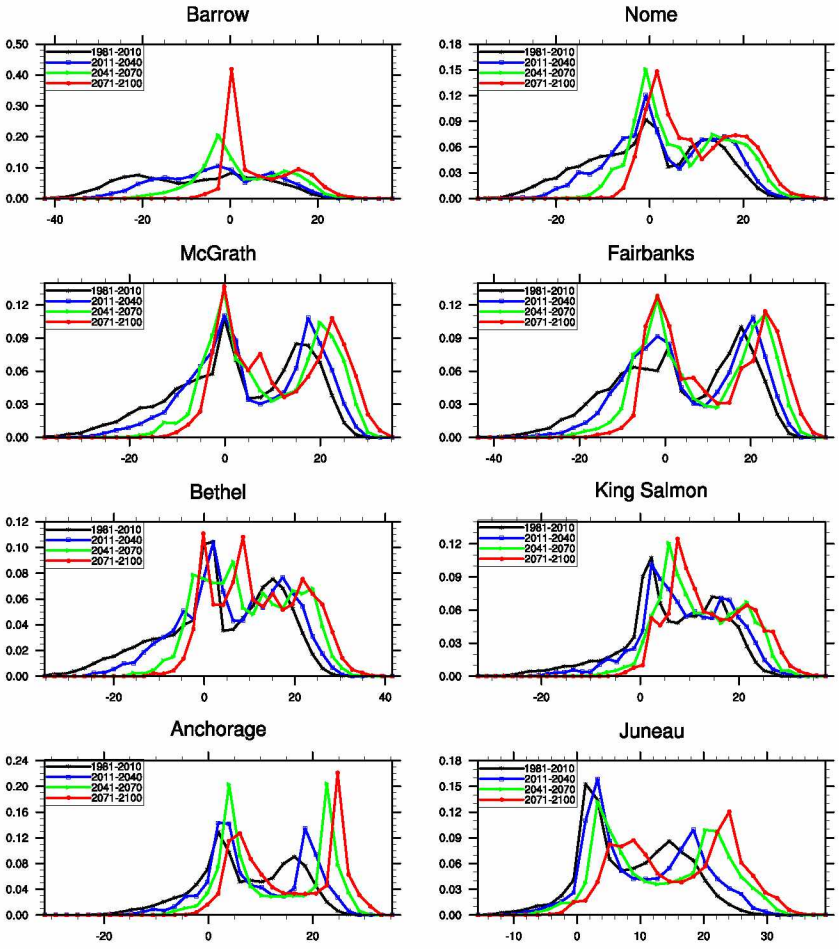

Figure 2.7 Probability density function of daily T_{max} for the nearest downscaled grid cell to selected cities in Alaska for 1981-2010 (black), 2011-2040 (blue), 2041-2070 (green), and 2071-2100 (red).

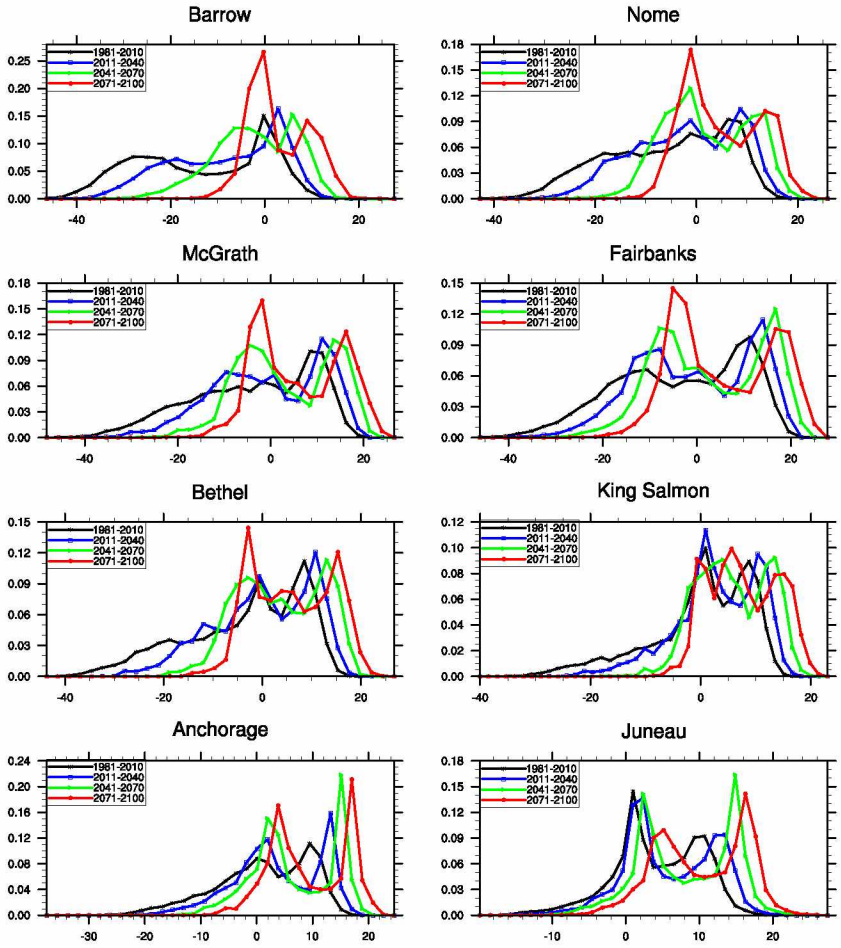

Figure 2.8 Probability density function of daily T_{min} for the nearest downscaled grid cell to selected cities in Alaska for 1981-2010 (black), 2011-2040 (blue), 2041-2070 (green), and 2071-2100 (red).

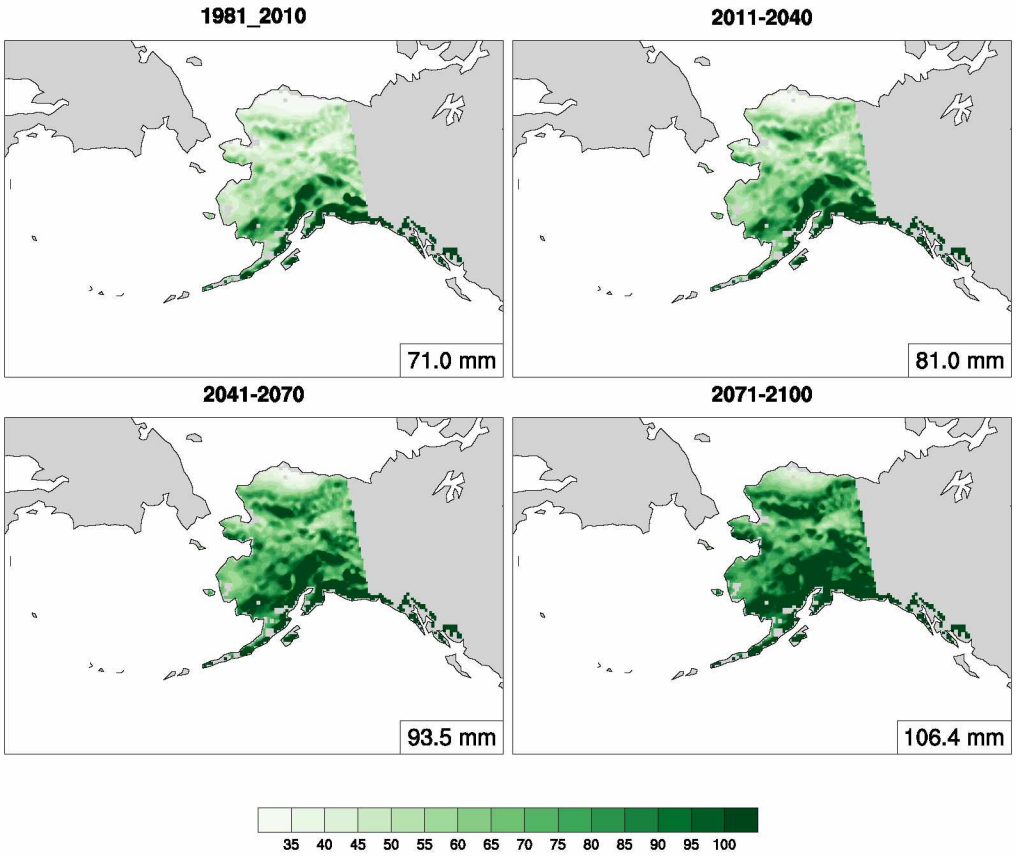

Figure 2.9 Annual maximum consecutive 5-day precipitation (mm) averaged for successive 30-year periods. The statewide average is located at the bottom right.

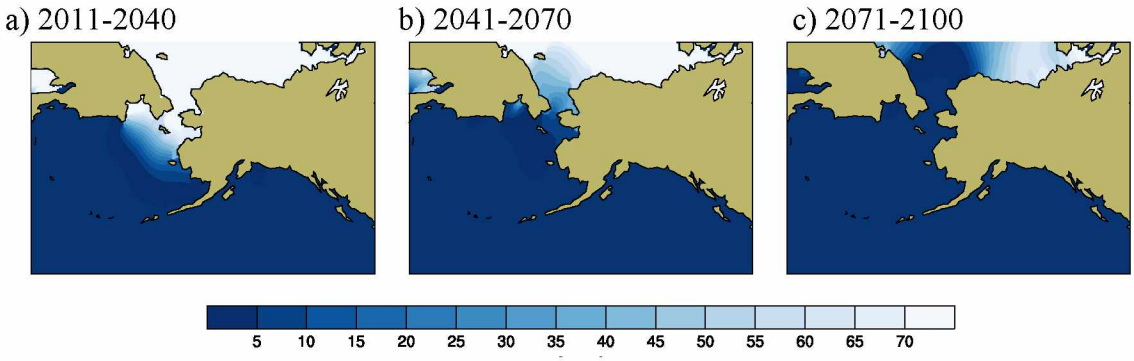

Figure 2.10 Average daily sea ice concentration (%) during March for a) 2011-2040, b) 2041-2070, and c) 2071-2100.

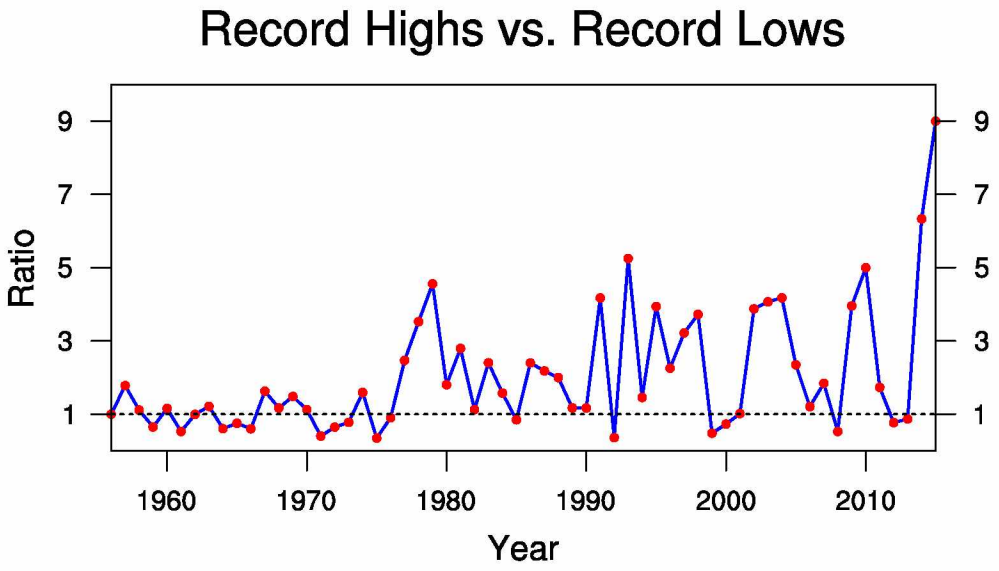

Figure 2.11 Ratio of record high to record low temperatures for an aggregate of eight cities across Alaska from 1956-2015 (blue line). This is based on daily station observations of T_{max} and T_{min} from: Anchorage, Barrow, Bethel, Fairbanks, Juneau, King Salmon, McGrath and Nome. The expected ratio (dashed black line) assumes no change in extreme temperatures.

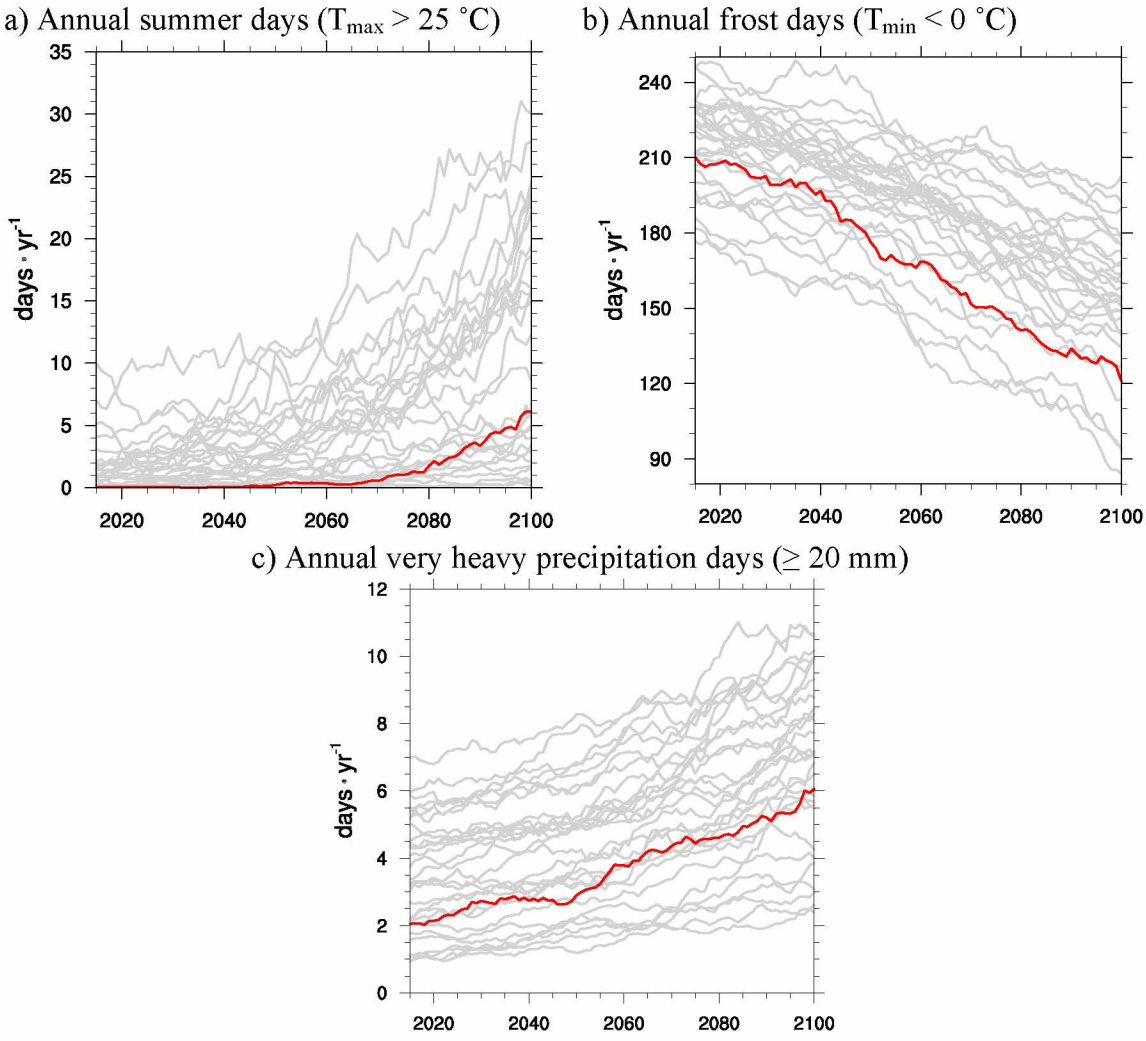

Figure 2.12 Annual statewide 10-year running mean of a) summer days (T_{max} > 25 °C), b) frost days (T_{min} < 0 °C), and c) very heavy precipitation days (≥ 20 mm) from 30 CMIP5 RCP8.5 models. These represent the forcing data used for subsequent downscaling, and here have been re-gridded to the WRF grid. The GFDL-CM3 is indicated (red line).

2.9 Tables

Table 2.1 Statewide average of climate extremes indices for 30-year periods, including: icing days (ID), summer days (SU), growing season length (GSL), frost days (FD), tropical nights (TR), heavy precipitation days (R10), very heavy precipitation days (R20), maximum 1-day precipitation (RX1), maximum consecutive 5-day precipitation (RX5), maximum consecutive wet days (CWD), and maximum consecutive dry days (CDD). The values represent annually averaged counts or magnitudes. Growing season length represents the period beginning on the sixth consecutive day with a daily mean temperature above 5°C in spring, and ends on the sixth consecutive day below 5°C in autumn. The percent change marks the relative difference between 2071-2100 and 1981-2010. Signal emergence denotes when the 10-year running mean anomaly continuously exceeds ± 2σ relative to the historical distribution.

Index	Threshold (if applicable)	Units	1981 – 2010	2011 – 2040	2041 – 2070	2071 – 2100	% change	Signal emergence
ID	$T_{max} < 0°C$	days	165.4	148.7	126.2	102.4	-38.1	2038
SU	$T_{max} > 25°C$	days	1.5	4.6	13.2	29.7	1880.0	2036
GSL		days	114.5	130.8	148.2	163.4	42.7	2035
FD	$T_{min} < 0°C$	days	219.2	197.0	171.3	148.1	-32.4	2026
TR	$T_{min} > 20°C$	days	0.0	0.1	1.2	6.8	n/a	2058
R10	$P \geq 10$ mm	days	22.8	26.8	32.4	37.8	65.8	2026
R20	$P \geq 20$ mm	days	6.7	8.3	10.6	13.5	101.5	2026
RX1		mm	34.4	39.5	45.9	52.7	53.2	2026
RX5		mm	71.0	81.0	93.5	106.4	49.9	2043
CWD		days	9.9	10.6	11.5	12.2	23.2	none
CDD		days	22.9	21.0	19.4	18.2	-20.5	none

Table 2.2 The minimum (Min), lower quartile (Q1), median (Med), upper quartile (Q3), maximum (Max), and standard deviation (SD) of daily T_{max} (˚C), and T_{min} (˚C) for successive 30-year periods for the nearest downscaled grid cell to selected **cities** in Alaska.

STATION		TMAX (˚C)						TMIN (˚C)					
		Min	Q1	Med	Q3	Max	SD	Min	Q1	Med	Q3	Max	SD
Barrow	1981-2010	-43.9	-20.3	-7.1	4.0	27.1	14.3	-48.0	-25.7	-13.1	-0.4	16.6	13.7
	2011-2040	-39.4	-12.2	-2.9	7.3	29.2	12.1	-43.3	-18.0	-6.1	2.0	19.6	11.6
	2041-2070	-29.5	-3.9	-0.2	10.7	30.3	9.5	-34.4	-8.0	-2.0	5.3	19.8	8.6
	2071-2100	-15.7	0.1	2.9	13.6	34.9	7.8	-23.4	-2.0	0.4	8.5	25.0	6.4
Nome	1981-2010	-38.0	-8.8	0.4	11.0	28.8	12.6	-44.0	-15.3	-3.9	4.7	17.6	11.9
	2011-2040	-29.3	-4.5	1.8	13.3	32.4	11.2	-35.6	-9.9	-1.3	6.9	20.6	10.2
	2041-2070	-21.9	-1.1	5.4	15.7	34.1	9.9	-28.4	-4.5	0.8	9.6	24.1	8.3
	2071-2100	-11.8	1.2	8.0	17.8	36.6	9.3	-18.0	-1.7	3.5	11.9	24.5	7.6
McGrath	1981-2010	-39.1	-6.1	1.9	14.9	28.1	13.3	-49.5	-13.7	-2.2	8.0	19.3	13.2
	2011-2040	-31.7	-3.1	3.5	17.2	29.7	12.2	-41.0	-9.5	-0.4	10.4	19.6	11.6
	2041-2070	-25.2	-0.7	7.5	20.0	32.1	11.3	-33.1	-5.0	2.0	13.1	22.4	10.1
	2071-2100	-16.3	1.0	10.0	21.8	34.8	10.8	-25.7	-2.4	4.6	14.9	25.1	9.3
Fairbanks	1981-2010	-45.2	-7.9	2.5	16.5	30.5	14.4	-47.4	-14.3	-2.5	8.7	22.5	13.6
	2011-2040	-39.0	-5.0	3.6	18.9	29.9	13.4	-43.0	-10.5	-0.6	11.4	21.0	12.3
	2041-2070	-30.5	-2.5	7.0	21.3	31.8	12.8	-36.0	-6.9	1.5	14.0	23.1	11.4
	2071-2100	-24.7	-0.7	9.7	23.2	36.8	12.4	-27.2	-3.9	3.6	16.0	26.2	10.7
Bethel	1981-2010	-36.4	-3.7	2.9	14.2	30.5	12.4	-44.9	-11.7	-0.8	7.0	17.7	12.0
	2011-2040	-25.5	-0.9	6.0	16.3	32.4	11.2	-32.3	-6.7	0.7	9.1	19.6	10.0
	2041-2070	-16.7	1.4	8.7	18.8	34.9	10.1	-24.3	-3.3	3.3	11.5	21.7	8.5
	2071-2100	-11.9	4.0	10.8	20.7	39.3	9.7	-19.6	-1.7	5.5	13.5	24.8	8.1
K. Salmon	1981-2010	-33.8	1.1	6.8	14.7	28.3	9.9	-40.9	-4.2	1.3	7.3	16.8	9.3
	2011-2040	-21.2	3.1	8.9	16.5	30.4	8.8	-27.2	-1.1	2.9	9.3	18.8	7.6
	2041-2070	-13.5	5.7	10.9	19.0	32.4	8.0	-18.2	1.0	5.3	11.7	20.3	6.3
	2071-2100	-5.9	7.6	12.6	20.6	36.5	7.9	-13.9	2.7	7.0	13.3	22.7	6.2
Anchorage	1981-2010	-32.4	1.1	6.3	15.2	27.4	9.2	-38.5	-4.3	1.7	8.5	17.7	8.5
	2011-2040	-27.1	2.4	7.2	18.8	29.1	9.2	-33.0	-1.5	2.9	11.9	18.3	7.8
	2041-2070	-21.0	3.9	10.4	22.2	32.2	9.5	-25.4	1.4	4.8	14.9	21.4	7.4
	2071-2100	-13.2	6.1	13.9	24.2	35.0	9.2	-17.5	3.7	7.6	16.6	23.5	6.8
Juneau	1981-2010	-16.6	2.3	7.8	14.9	31.7	7.6	-20.5	0.5	4.0	9.4	21.1	6.0
	2011-2040	-13.9	3.1	9.3	17.7	33.2	8.3	-19.8	1.5	5.1	11.6	21.6	6.1
	2041-2070	-9.9	4.9	13.4	21.4	36.6	9.1	-14.4	2.8	8.0	14.5	23.2	6.4
	2071-2100	-8.6	8.2	16.4	23.3	39.0	8.7	-12.8	5.1	10.2	16.0	26.6	6.1

Table 2.3 The median (Med), 90th percentile (90P), 99th percentile (99P), maximum (Max) and annual total of daily precipitation (mm) averaged over successive 30-year periods for the nearest downscaled grid cell to selected **cities** in Alaska.

STATION		PCPT (mm)				
		Med	90P	99P	Max	Annual
Barrow	1981-2010	0.07	1.73	6.99	24.62	217.72
	2011-2040	0.10	2.06	8.04	30.67	263.93
	2041-2070	0.12	2.69	9.77	28.67	335.84
	2071-2100	0.19	3.58	12.28	34.68	439.88
Nome	1981-2010	0.06	4.66	17.47	43.43	541.55
	2011-2040	0.12	5.61	21.10	48.52	661.58
	2041-2070	0.15	7.02	25.23	62.91	825.44
	2071-2100	0.24	8.62	29.77	93.62	1022.17
McGrath	1981-2010	0.35	5.59	16.50	39.34	683.52
	2011-2040	0.50	6.36	18.72	50.56	794.53
	2041-2070	0.61	7.62	21.61	88.60	944.63
	2071-2100	0.65	7.82	25.02	90.53	1010.98
Fairbanks	1981-2010	0.18	4.02	13.62	45.37	495.86
	2011-2040	0.21	4.62	16.39	68.76	582.42
	2041-2070	0.26	5.48	18.80	97.92	696.25
	2071-2100	0.33	6.22	21.27	65.54	797.80
Bethel	1981-2010	0.31	5.68	15.63	44.18	670.10
	2011-2040	0.37	6.02	17.66	50.09	740.51
	2041-2070	0.55	7.16	20.41	76.77	879.44
	2071-2100	0.64	7.91	23.24	59.90	975.55
K. Salmon	1981-2010	0.47	6.51	16.25	40.92	772.03
	2011-2040	0.54	7.40	18.70	61.02	874.61
	2041-2070	0.75	8.63	23.09	53.15	1050.73
	2071-2100	0.72	9.56	25.61	62.00	1139.54
Anchorage	1981-2010	0.21	5.79	18.49	65.77	686.93
	2011-2040	0.21	6.77	22.25	54.11	796.59
	2041-2070	0.19	7.42	25.09	64.39	879.51
	2071-2100	0.20	8.86	28.51	102.48	1024.03
Juneau	1981-2010	1.37	14.18	32.88	92.07	1747.05
	2011-2040	1.25	15.16	35.72	144.02	1816.60
	2041-2070	0.86	16.77	41.80	137.88	1963.05
	2071-2100	1.16	20.54	47.72	163.74	2353.02

2.10 References

Bekryaev, R. V., I. V. Polyakov, and V. A. Alexeev, 2010: Role of polar amplification in long-term surface air temperature variations and modern Arctic warming. *J. Climate*, **23**, 3888-3906, doi:10.1175/2010JCLI3809.1.

Bennett, K. E., and J. E. Walsh, 2014: Spatial and temporal changes in indices of extreme precipitation and temperature for Alaska. *Int. J. Climatol.*, **35**, 1434-1452.

Bieniek, P. A., J. E. Walsh, R. L. Thoman, and U. S. Bhatt, 2014: Using climate divisions to analyze variations and trends in Alaska temperature and precipitation. *J. Climate*, **27**, 2800-2818, doi:10.1175/JCLI-D-13-00342.1.

Bieniek, P. A., U. S. Bhatt, J. E. Walsh, T. S. Rupp, J. Zhang, J. R. Krieger, and R. Lader, 2016: Dynamical downscaling of ERA-Interim temperature and precipitation for Alaska. *J. Appl. Meteor. Climatol.*, **55**, 635-654, doi:10.1175/JAMC-D-15-0153.1.

Cannon, A. J., S. R. Sobie, and T. Q. Murdock, 2015: Bias correction of GCM precipitation by quantile mapping: How well do methods preserve changes in quantiles and extremes? *J. Climate*, **28**, 6938-6959.

Chapin, F. S., III, S. F. Trainor, P. Cochran, H. Huntington, C. Markon, M. McCammon, A. D. McGuire, and M. Serreze, 2014: Ch. 22: Alaska. *Climate Change Impacts in the United States: The Third National Climate Assessment*, J. M. Melillo, T. C. Richmond, and G. W. Yohe, Eds., U.S. Global Change Research Program, 514-536. [Available online at http://nca2014.globalchange.gov/system/files_force/downloads/high/NCA3_Full_Report_22_Alaska_HighRes.pdf?download=1.]

Dee, D. P., and Coauthors, 2011: The ERA-Interim reanalysis: Configuration and performance of the data assimilation system. *Quart. J. Roy. Meteor. Soc.*, **137**, 553-597, doi:10.1002/qj.828.

Donner, L. J., and Coauthors, 2011: The Dynamical Core, Physical Parameterizations, and Basic Simulation Characteristics of the Atmospheric Component AM3 of the GFDL Global Coupled Model CM3. *J. Climate*, **24**, 3484-3519, doi:10.1175/2011JCLI3955.1.

Giorgi F., C. Jones, and G. R. Asnar, 2009: Addressing climate information needs at the regional level: the CORDEX framework. *WMO Bulletin 58*, 175-183.

Glisan, J. M., and W. J. Gutowski Jr., 2014a: WRF summer extreme daily precipitation over the CORDEX Arctic. *J. Geophys. Res. Atmos.*, **119**, 1720-1732, doi:10.1002/2013JD020697.

_____, and _____, 2014b: WRF winter extreme daily precipitation over the North American CORDEX Arctic. *J. Geophys. Res. Atmos.*, **119**, 10738-10748, doi:10.1002/2014JD021676.

Groisman, P. Y., R. W. Knight, D. R. Easterling, T. R. Karl, G. C. Hegerl, and V. N. Razuvaev, 2005: Trends in intense precipitation in the climate record. *J. Climate*, **18**, 1326-1350, doi:10.1175/JCLI3339.1.

Hayhoe, K. A., 2010: A standardized framework for evaluating the skill of regional climate downscaling techniques. Ph.D. dissertation, University of Illinois at Urbana-Champaign, 158 pp. [Available online at http://www.snap.uaf.edu/attachments/1_Hayhoe_Katharine.pdf.]

Hill, D. F., N. Bruhis, S. E. Calos, A. Arendt, and J. Beamer, 2015: Spatial and temporal variability of freshwater discharge into the Gulf of Alaska. *J. Geophys. Res. Oceans*, **120**, 634-646, doi:10.1002/2014JC010395.

Iacono, M. J., J. S. Delamere, E. J. Mlawer, M. W. Shephard, S. A. Clough, and W. D. Collins, 2008: Radiative forcing by long-lived greenhouse gases: Calculations with the AER radiative transfer models. *J. Geophys. Res.*, **113**, D13103, doi:10.1029/2008JD009944.

IPCC, 2012: Managing the Risks of Extreme Events and Disasters to Advance Climate Change Adaptation. A Special Report of Working Groups I and II of the Intergovernmental Panel on Climate Change, pp. 582, Cambridge University Press, Cambridge, UK, and New York, NY, USA.

Janjić, Z., 1994: The step-mountain Eta coordinate model: Further developments of the convection, viscous sublayer, and turbulence closure schemes. *Mon. Wea. Rev.*, **122**, 927-945, doi:10.1175/1520-0493(1994)122<0927:TSMECM>2.0.C;2.

Klein Tank, A. M. G., F. W. Zwiers, and X. Zhang, 2009: Guidelines on analysis of extremes in a changing climate in support of informed decisions for adaptation. Climate data and monitoring WCDMP-No. 72, WMO-TD No. 1500, 56 pp.

Koenigk, T., P. Berg, and R. Döscher, 2015: Arctic climate change in an ensemble of regional CORDEX simulations. *Polar Research*, **34**, 24603, doi:10.3402/polar.v34.24603.

Kopec, B. G., X. Feng, F. A. Michel, and E. S. Posmentier, 2015: Influence of sea ice on Arctic precipitation. *Proc. Natl. Acad. Sci.*, **113 (1)**, 46-51, doi:10.1073/pnas.1504633133.

Lader, R., U. S. Bhatt, J. E. Walsh, T. S. Rupp, and P. A. Bieniek, 2016: Two-meter temperature and precipitation from atmospheric reanalysis evaluated for Alaska. *J. Appl. Meteor. Climatol.*, **55**, 901-922, doi:10.1175/JAMC-D-15-0162.1.

Laliberté, F., S. E. L. Howell, and P. J. Kushner, 2015: Regional variability of a projected sea ice-free Arctic during the summer months. *Geophys. Res. Lett.*, **43 (1)**, 256-263, doi:10.1002/2015GL066855.

Meehl, G. A., C. Tebaldi, and D. Adams-Smith, 2016: U. S. daily temperature records past, present, and future. *Proc. Natl. Acad. Sci.*, **113 (49)**, doi:10.1073/pnas.1606117 113.

Morrison, H. C., G. Thompson, and V. Tatarskii, 2009: Impact of cloud microphysics on the development of trailing stratiform precipitation in a simulated squall line: Comparison of one- and two-moment schemes. *Mon. Wea. Rev.*, **137**, 991-1007, doi: 10.1175/2008MWR2556.1.

NOAA National Centers for Environmental Information, 2017: Climate at a Glance: U.S. Time Series, published April 2017, retrieved April 13, 2017 from http://www.ncdc.n oaa.gov/cag/.

O'Gorman, P. A., and C. J. Muller, 2010: How closely do changes in surface and column water vapor follow Clausius-Clapeyron scaling in climate change simulations? *Environ. Res. Lett.*, **5**, 025207, doi:10.1088/1748-9326/5/2/025207.

Overland, J., E. Hanna, I. Hanssen-Bauer, S. –J. Kim, J. E. Walsh, M. Wang, U. S. Bhatt, R. L. Thoman 2016a: *Surface Air Temperature [in Arctic Report Card 2015]*, http:// www.arctic.noaa.gov/Report-Card.

Overland, J., E. Hanna, I. Hanssen-Bauer, S.-J. Kim, J. Walsh, M. Wang, U. S. Bhatt, and R. L. Thoman, 2016b: *Air temperature [in "State of the Climate in 2015"]*. Bull. Amer. Meteor. Soc., 97 (8), S132–S134.

Overland, J. E., M. Wang, J. E. Walsh, and J. C. Stroeve, 2013: Future Arctic climate changes: Adaptation and mitigation time scales. *Earth's Future*, **2**, 68-74, doi:10.100 2/2013EF000162.

Parkinson, C. L., 2014: Global sea ice coverage from satellite data: annual cycle and 35-yr trends. *J. Climate*, **27**, 9377-9382, doi:10.1175/JCLI-D-14-00605.1.

Partain, J. L., and Coauthors, 2016: An assessment of the role of anthropogenic climate change in the Alaska fire season of 2015 [in "Explaining Extremes of 2015 from a Climate Perspective"]. *Bull. Amer. Meteor. Soc.*, **97 (12)**, S14-S18, doi:10.1175/BA MS-D-16-0149.

Peters, G. P., and Coauthors, 2013: The challenge to keep global warming below 2°C. *Nature Clim. Change*, **3 (1)**, 4-6.

Pithan, F., and T. Mauritsen, 2014: Arctic amplification dominated by temperature feedbacks in contemporary climate models. *Nat. Geosci.*, **7**, 181-184, doi:10.1038/NGEO2071.

Prein, A. F., R. M. Rasmussen, K. Ikeda, C. Liu, M. P. Clark, and G. J. Holland, 2016: The future intensification of hourly precipitation extremes. *Nature Clim. Change*, **6 (12)**, doi:10.1038/nclimate3168.

Riahi, K., S. Rao, V. Krey, C. Cho, V. Chirkov, G. Fischer, G. Kindermann, N. Nakicenovic, and P. Rafaj, 2011: RCP 8.5—A scenario of comparatively high greenhouse gas emissions. *Clim. Change.*, **109**, 33-57, doi:10.1007/s10584-011-0149-y.

Sillmann, J., V. V. Kharin, X. Zhang, F. W. Zwiers, and D. Bronaugh, 2013a: Climate extremes indices in the CMIP5 multimodel ensemble: Part 1. Model evaluation in the present climate. *J. Geophys. Res. Atmos.*, **118**, 1716-1733, doi:10.1002/jgrd.50203.

Sillmann, J., V. V. Kharin, F. W. Zwiers, X. Zhang, and D. Bronaugh, 2013b: Climate extremes indices in the CMIP5 multimodel ensemble: Part 2. Future climate projections. *J. Geophys. Res. Atmos.*, **118**, 2473-2493, doi:10.1002/jgrd.50188.

Skamarock, W. C., and Coauthors, 2008: A description of the Advanced Research WRF version 3. NCAR Tech Note, NCAR/TN-475+STR, 113 pp., doi:10.1056/D68S4MVH.

U.S. Environmental Protection Agency. 2016. Climate change indicators in the United States, 2016. Fourth edition. EPA 430-R-16-004. [Available online at http://www.epa.gov/climate-indicators.]

van Vuuren, D. P., and Coauthors, 2011: The representative concentration pathways: an overview. *Clim. Change*, **109**, 5-31, doi:10.1007/s10584-011-0148-z.

Walsh, J. E., U. S. Bhatt., J. S. Littell, M. Leonawicz, M. Lindgren, T. A. Kurkowski, P. Bieniek, R. Thoman, S. Gray and T. S. Rupp, 2017a: Downscaling of climate model output for Alaska. Environ. Modeling and Software, submitted.

Walsh, J. E., P. Bieniek, B. Brettschneider, E. Euskirchen, R. Lader, and R. Thoman, 2017b: The exceptionally warm winter of 2015-16 in Alaska. *J. Climate*, **30**, 2069-2088, doi:10.1175/JCLI-D-16-0473.1.

Walsh, J.E., and Coauthors, 2014: Ch. 2: Our Changing Climate. *Climate Change Impacts in the United States: The Third National Climate Assessment*, J. M. Melillo, T. C. Richmond, and G. W. Yohe, Eds., U. S. Global Change Research Program, 19-67. doi:10.7930/J0KW5CXT.

Zhang, J., U. S. Bhatt, W. V. Tangborn, and C. S. Lingle, 2007: Climate downscaling for estimating glacier mass balances in northwestern North America: Validation with a USGS benchmark glacier. *Geophys. Res. Lett.*, **34**, L21505, doi:10.1029/2007GL031139.

Zhang, X., L. Alexander, G. C. Hegerl, P. Jones, A. Klein Tank, T. C. Peterson, B. Trewin, and F. W. Zwiers, 2011: Indices for monitoring changes in extremes based on daily temperature and precipitation data. *WIREs Clim Change*, doi:10/1002.wcc.147.

Zhang, X., and J. Zhang, 2001: Heat and freshwater budgets and pathways in the Arctic Mediterranean in a coupled ocean/sea-ice model. *J. Oceanogr.*, **57**, 207-237, doi:10.1023/A:1011147309004.

3 AGRO-CLIMATE PROJECTIONS FOR A WARMING ALASKA[2]

3.1 Abstract

Climate warming is expected to disproportionately affect crop yields in the Southern United States due to excessive heat stress, while presenting new farming opportunities through a longer growing season further north. Few studies have investigated the impact of this warming on agro-climate indices that link meteorological data with important field dates in northern regions. This study employs regional dynamical downscaling using the Weather Research and Forecasting (WRF) Model to assess changes in growing season length (GSL), spring planting dates, and occurrences of plant heat stress (PHS) for five regions in Alaska. Differences between future representative concentration pathway 8.5 (RCP8.5; 2011-40, 2041-70, 2071-2100) and historical (1981-2010) periods are obtained using boundary forcing from the Geophysical Fluid Dynamics Laboratory Climate Model, version 3 and the NCAR Community Climate System Model, version 4. The model output is bias-corrected using the ERA-Interim reanalysis. Median GSL shows increases of 48-87 days by 2071-2100 with the largest changes in northern Alaska. Similarly by 2071-2100, planting dates advance 2-4 weeks, and PHS days increase from near zero to 5-10 instances per summer in the hottest areas. The largest GSL changes occur in the mid- (2041-2070) and late-century (2071-2100), when a warming signal emerges from the historical inter-annual variability. These periods coincide with the greatest divergence of the RCPs, suggesting that near-term decision-making may effect substantial future change. Early-century (2011-2040) projections show median GSL

---

[2] *Lader, R., J. E. Walsh, U. S. Bhatt, and P. A. Bieniek. Agro-climate projections for a warming Alaska. Conditionally accepted with Earth Interactions.*

increases of 8-27 days, which is close to the historical standard deviation of GSL. Thus, internal variability will remain an important source of uncertainty into the mid-century despite a trend for longer growing seasons.

3.2 Introduction

3.2.1 Agronomic considerations in the context of warming

Climate change, largely influenced by anthropogenic emissions, is expected to disrupt agricultural production, globally and within the United States, due to changes in temperature, precipitation, and the resultant alterations to water availability (IPCC 2014). In 2016, over 800 million people were considered undernourished – an increase from the year before – and extreme drought and flooding were identified as key factors (FAO et al. 2017). The anticipated global agronomic impacts of a warming climate suggest that higher atmospheric CO_2 will support plant fertilization through increased photosynthesis, but these benefits will be offset by greater plant heat stress and declining yields (Tripathi et al. 2016).

The effects of high temperatures on agriculture are particularly notable. In the contiguous United States (CONUS), Hsiang et al. (2017) found an average projected decrease of 9.1% in agricultural yield per ˚C of warming for maize, wheat, soybeans, and cotton; however, locations in the Northwest displayed increases greater than 30%. These findings represent average values, but excessive heat results in negative yield impacts that are non-linear (Schlenker and Roberts 2009). Above a high temperature threshold, a plant must adapt by producing heat shock proteins that promote thermal tolerance; if the heat is too severe, the plant cells lose viability (Krishnan et al. 1989). Typical threshold

values – expressed as daily mean temperature – for corn, rice, wheat, and grain legumes are 38°, 34°, 26°, and 25°C, respectively (Wahid et al. 2007). A warming climate will disproportionately affect agriculture in locations where these thresholds are exceeded, while the reduction of freezing temperatures will provide new opportunities to colder regions.

Amidst increasing atmospheric CO_2 concentrations that now exceed 400 ppm (NOAA/ESRL 2017), no place in the United States is expected to warm at a greater rate than Alaska. The observed rate of warming in the Arctic is approximately twice that of the global average (AMAP 2017), and the 12-month period from September 2015 to October 2016 was the warmest since records began in 1900 (Overland et al. 2016). Over mainland Alaska, 38% of the land is estimated to contain near-surface permafrost, and this is expected to reduce to 10-18% by the end of the century, depending on emissions scenario; the greatest reductions are expected for the Seward Peninsula and Interior Alaska (Pastick et al. 2015). For land areas poleward of 45°N, growing season length increased 2.6 days decade^{-1} from 1982 to 2014, but substantial spatiotemporal variability was observed (Park et al. 2016).

3.2.2 Study area

Given its harsh climate, less than 0.5% of Alaska's land area is comprised of farmland; however, the total cropland in Alaska increased by 55%, or approximately 30,000 acres, from 1982 to 2012, with over one quarter of this area for hay and green silage (USDA/NASS 2014a). The vast majority of this and the lesser-grown barley, oat, and wheat crops are located in the valley locations between Anchorage and Fairbanks

(Figure 3.1a). These Interior valleys exhibit an extreme annual temperature cycle, often marking the coldest and hottest parts of Alaska with temperatures as low as -50°C in winter and up to 35°C during summer. Largely protected from extreme precipitation by surrounding mountains, these valleys receive adequate rainfall and long hours of solar radiation, conducive for plant growth. Outside of field crops in this zone, the state's remaining agricultural production is in berries, fruits, vegetables, and floriculture. Small-scale greenhouses are common in the shoulder seasons to extend activities. Most coastal areas are too cool, cloudy and wet during the summer months for extensive production.

Rapid warming in Alaska could affect these historical conditions, and threshold-based agro-climate indices represent a way to link meteorological data with important field dates and thermal accumulation units. Matthews et al. (2008) co-developed a set of indicators with stakeholders in Scotland's agriculture industry that include the start-of-field operations date, growing season length, first and last air frost, and plant heat stress. Regional climate model projections of these indices across the United Kingdom from 2061-2090 show an increased growing season length of approximately two months with the largest changes occurring in the coldest locations (Harding et al. 2015). Applying these metrics to the CONUS, Monier et al. (2016) found an increased growing season length in excess of three months for parts of the Northwest and Northeast under the business-as-usual scenario (RCP8.5). It is also noted that mitigation of greenhouse gas emissions could greatly reduce the negative impacts of excessive heat, decreased water availability, and subsequent lower yields (Beach et al. 2015), although mitigation of emissions would also reduce the increase of growing season length.

The present study builds on this previous research and assesses projected agricultural opportunity for Alaska to 2100, producing a set of agro-climate variations using downscaled climate model simulations and reanalysis. These indices include: 1) growing season length, defined as the difference in days, between the last frost on or before June 30, and the first frost on or after July 1, 2) start-of-field operations (SFO), which represents the calendar date when the thermal accumulation of daily average temperature (T_{avg}) reaches 200°C, and 3) plant heat stress (PHS), defined as the number of days with a T_{avg} that exceeds 25°C. The resulting information on these metrics helps to inform the following questions:

1) How is Alaska's growing season length (GSL) projected to change this century, both spatially and in terms of differences between the last spring air frost (LF) and first autumn air frost (FF)?
2) Can the SFO index, derived from the downscaled data, be used as a proxy for planting date?

3.3 Data and Methods

3.3.1 Observed growing season trends

The GSL in Alaska, defined as the period between the last air frost (hereinafter frost; $T_{min} \leq 0$°C) in the first half of the year (i.e., no later than June 30) and the first frost in the second half (i.e., on July 1 or later), ranges from over five months in the southeast to effectively zero from the Brooks Range northward. Trends were calculated via linear regression of the annual GSL time series of station observations (Menne et al. 2012; https://www.ncdc.noaa.gov/ghcn-daily-references), and statistical significance of the

regression coefficients was tested using the two-tailed t-test. Station observations during the historical period (1981-2010) show mixed, but primarily increasing GSL trends that range from -9.1 days per decade at Juneau to 6.3 days per decade at Fairbanks (Figure 3.2). Both of these values are statistically significant at the 95% confidence level. The trend of GSL at Fairbanks compares well with results from a 100-year record, beginning in 1906, which show a 45% increase in growing season (Wendler and Shulski 2009).

Over the longest available period of record for each station, GSL trends are generally 1-3 days per decade (Figure 3.2). These trends, in days per decade, are significant at the 95% confidence level at Anchorage (1.9), Barrow (1.2), Bethel (2.7), Fairbanks (2.7), Juneau (3.4), and Nome (3.1). Only King Salmon (-2.0) shows a decreased GSL. These trends are smaller than for the historical period, but are of the same sign, with the exception of Juneau. The opposing rates of change at Juneau highlight an issue with calculating trends over short time intervals when outliers and the starting point used can exert a greater influence. The 10-year running mean results in Figure 3.2, presented to reduce noisiness for illustration, show that these trends are affected by high inter-annual and decadal variability. At Juneau, several of the longest growing seasons occurred in the mid-1980s, at the beginning of the historical period.

3.3.2 Downscaled reanalysis and climate model data

This study includes multiple regional dynamically downscaled variables obtained using the Advanced Research core of the Weather Research and Forecasting Model (WRF; Skamarock et al. 2008) over the Alaska domain (Figure 3.1a). The model simulations were driven by: the ERA-Interim reanalysis (Dee et al. 2011) from 1981-

2010; the Geophysical Fluid Dynamics Laboratory Climate Model version 3 (GFDL-CM3; Donner et al. 2011) from 1981-2100; and the National Center for Atmospheric Research Community Climate System Model version 4 (hereinafter CCSM4) from 1981-2100. The future data come from the business-as-usual representative concentration pathway (RCP8.5; Riahi et al. 2011) of the Coupled Model Intercomparison Project phase 5 (CMIP5; Taylor et al. 2012). Due to the sparseness of station observations in Alaska, the downscaled reanalysis data are considered as gridded observations; however, *in situ* information is used when available for comparison.

The downscaling produced gridded fields at 20-km spatial and hourly time resolution, and was conducted in 2-day segments, each re-initialized to the driving reanalysis or model. In addition, spectral nudging constrained the simulations to the original forcing data. A complete description of the WRF configuration is included in Bieniek et al. (2016). A few of the key physics options used here include the microphysics (Morrison 2-moment; Morrison et al. 2009), radiation (Rapid Radiative Transfer Model; Iacono et al. 2008), the Noah land surface module, and coupling to a thermodynamic sea ice model (Zhang and Zhang 2001). Bieniek et al. (2016) show that the dynamical downscaling reduces temperature and precipitation bias across Alaska when compared to coarse forcing data, and this was particularly true for locations with significant topography.

3.3.3 Bias-correction methodology

The agro-climate analysis in this study utilizes the five operational Census Areas of the United States Department of Agriculture (USDA) to demonstrate the spatial

variability that is characteristic of Alaska, and to highlight regional differences with regard to projected changes. Additionally, a layer that separates soil versus non-soil is superimposed atop the Census Areas (Figure 3.1b). The geographic information for these regions is available from the National Agricultural Statistics Service (USDA/NASS 2014b), and the soil layer from the Natural Resources Conservation Service (Soil Survey Staff 2017). The non-soil grid cells, which are either coastal or mountainous, are not included in any of the indices described by this research. Projected changes to the agro-climate indices are presented in 30-year time slices (i.e., 2011-40, 2041-70, and 2071-2100) from both the CCSM4 and GFDL-CM3. These changes have been bias-corrected according to the observation-based ERA-Interim reanalysis (1981-2010). The ERA-Interim is among the top-performing reanalyses with regard to surface temperature and precipitation for Alaska, frequently exhibiting the lowest root-mean-square error (RMSE) relative to station observations (Lader et al. 2016).

The projections were bias-corrected using quantile mapping or the delta method depending on the variable. For GSL, LF and FF, the historical climate model distribution (1981-2010) is sorted in ascending order and is subtracted from the corresponding sorted 30-year future distribution at each grid cell. These differences are then added to the sorted ERA-Interim distribution (1981-2010). For example, the n^{th} longest growing season modeled by CCSM4 during 1981-2010 is subtracted from the n^{th} longest projected growing season by CCSM4 during 2011-2040. This difference, exclusively according to the climate model (i.e., CCSM4), is then added to the n^{th} longest observed growing season from ERA-Interim. Since 30-year times slices are used, n equals 30. All changes are relative to the 1981-2010 historical period. By applying this quantile-based bias

correction to each point of the 30-year distributions, changes to the mean and variability of GSL, LF and FF are captured. This delineation between time periods also allows investigation into if and when the projected change signal dominates the inter-annual variability.

The 30-year projected changes in the SFO and PHS indices are presented as distributional means. The same delta method (Hayhoe 2010) is applied as before to bias correct the climate model output, but rather than subtracting at all n=30 points of the respective distributions, the 30-year mean is used instead. For example, the 30-year historical (1981-2010) mean SFO date from CCSM4 is subtracted from the 2011-2040 mean CCSM4 SFO date and added to the ERA-Interim (1981-2010) mean SFO date at each grid cell. For all of the agro-climate indices, the resulting grid cell values are further aggregated and averaged by the aforementioned Census Areas (Figure 3.1b).

3.4 Results

3.4.1 Temperature and precipitation climatology and projections

The seasonal ERA-Interim average surface temperature climatology (Figure 3.3, left), derived from daily data, shows a north-to-south gradient for all periods except for summer, when the highest temperatures are found across Interior lowlands, such as the Yukon Flats and Tanana Valley. Late-century temperatures (2071-2100) are projected to warm by 8.1, 4.9, 5.2, and 5.7°C for winter (DJF), spring (MAM), summer (JJA), and autumn (SON), respectively, according to the CCSM4 (Figure 3.3, middle). Larger increases of 10.2, 7.7, 7.0, and 7.7°C are projected for the GFDL-CM3 (Figure 3.3, right). The future results indicate that the largest changes occur during DJF when the coldest

temperatures are found across the Interior; concurrently, Arctic waters adjacent to Alaska stay close to freezing. The average temperature across Alaska transitions from below to above freezing for MAM and SON.

The seasonal ERA-Interim total precipitation climatology (Figure 3.4, left), also derived from daily data, shows that MAM is the driest season, and JJA is the wettest for Alaska when convective precipitation occurs. In all seasons, total precipitation is projected to increase; the largest changes with respect to magnitude and percentage for CCSM4 occur in DJF, and in SON for GFDL-CM3. The CCSM4 (Figure 3.4, middle) shows increases that are approximately half of those depicted by the GFDL-CM3 (Figure 3.4, right). For CCSM4 the smallest percentage change (17.1%) is in SON, while for GFDL-CM3 the smallest increases are in MAM (34.8%). The smallest change in actual magnitude for both models is during MAM.

3.4.2 Growing season length projections for Alaska

The widespread observed increases in GSL are projected to continue and the rate is expected to accelerate across Alaska. The late-century (2071-2100) median increase in CCSM4 ranges from 48 days for the Fairbanks Census Area up to 63 days for the Aleutian Islands. Increases driven by the warmer GFDL-CM3 range from 67 to 87 days for the same Census Areas (Table 3.1). The future (2071-2100) and historical (1981-2010) periods are separated by 90 years, meaning that the modeled increases yield approximate trends of 5-10 days per decade. The lower end of this range compares well with historical trends (days per decade) at Anchorage (5.1), Barrow (4.4), Bethel (5.7), Fairbanks (6.3) and Nome (4.4), but is considerably higher than those from the full period

of record (Figure 3.2). The projected changes indicate that the shortest late-century growing season is outside (i.e., longer) the historical interquartile growing season range for all Census Areas (Figure 3.5). The GSL distributions, including the median value and the extremes, become successively longer with each 30-year time period. However, despite these large GSL increases, the projected Census Area GSL minima continue to exhibit overlap with the historical distributions in the CCSM4 results.

Projections from CCSM4 for the early-century period (2011-2040) show increases to median GSL, depending on Census Area, that range between 8 days (Fairbanks) to 15 days (Juneau) when compared to the historical period (Table 3.1). Greater changes are found for the absolute minima and first quartile of the 30-year distributions, but not necessarily for the third quartiles and maxima. For GFDL-CM3, median GSL increases from 17 (Juneau) to 27 (Aleutians) days. Similar to CCSM4, larger increases are found for the minima and first quartiles, while mixed results are shown for the upper points of the distributions. These changes have the effect of lowering the standard deviation of annual GSL for all Census Areas according to CCSM4, and all regions except for the Juneau Census Area in GFDL-CM3.

For the mid-century period (2041-2070), CCSM4 shows further median GSL increases, relative to the 2011-2040 period, that vary between 18 (Fairbanks) to 23 (Aleutians) days (Table 3.1). These increases are more pronounced for GFDL-CM3, which shows increases of 27-37 days for the Fairbanks and Anchorage Census Areas, respectively. One notable difference between the two models when comparing the mid-century with the early-century periods is their inter-annual variability. For CCSM4, each Census Area has a higher standard deviation of annual GSL from 2041-2070 than during

the 2011-2040 period; the opposite is true for GFDL-CM3. This is reflected visually in Figure 3.5 by comparing the changes between the red and green box and whisker diagrams.

The late-century period (2071-2100) shows the greatest GSL increases for CCSM4, ranging from 19-27 days longer than the mid-century period for the Juneau and Aleutian Islands Census Areas, respectively; the range of increases according to GFDL-CM3 is comparable at 18-27 days for the Fairbanks and Aleutian Islands Census Areas, respectively (Table 3.1). The projected variability of GSL for Alaska again shows considerable spatial variations. Relative to the historical period, both models indicate a decreased late-century standard deviation of up to one week across much of the Interior and increases of up to one week from 60°N and points southward (Figure 3.6). The CCSM4 shows increases in variability (standard deviation) of up to 10 days along parts of the North Slope (Figure 3.6, top), while the GFDL-CM3 has decreased GSL variability exceeding 10 days for a large swath of this area (Figure 3.6, bottom). This is likely due to differences in the model sea ice state. From 2071-2100, the GFDL-CM3 shows essentially no sea ice in the study domain, producing more of a maritime climate for Arctic Alaska; however, the CCSM4 depicts high inter-annual sea ice variability during this period. These differences are evident in the GSL boxplots for the Aleutian Islands Census Area in Figure 3.5.

Analysis of the components that determine GSL, namely the last spring frost (LF; Figure 3.7) and the first autumn frost (FF; Figure 3.8), demonstrates that with each successive 30-year period, the median date of LF is earlier and the median date of FF is later. For CCSM4, the relative advances to median LF by Census Area, in number of

days, range from 1-7 (2011-2040), 10-13 (2041-2070), and 8-12 (2071-2100) when compared to the preceding 30-year period; for GFDL-CM3 these values are generally larger: 9-12 (2011-2040), 12-19 (2041-2070), and 7-14 (2071-2100) (Table 3.2). The relative delays to median FF by Census Area, also in number of days, range from 6-10 (2011-2040), 4-11 (2041-2070), and 8-12 (2071-2100) for CCSM4, and 8-17 (2011-2040), 4-20 (2041-2070), and 10-17 (2071-2100) for GFDL-CM3 (Table 3.3).

When comparing the late-century period (2071-2100) with the historical reference period (1981-2010) there is a tendency for larger changes to occur with the FF, indicating that the lengthening GSL is due more to later autumn frost than to earlier spring thaws. The primary exception to this is for the Juneau Census Area where the change in the LF is about one week greater (i.e., earlier) than the change to later FF. It is speculated that the dearth of late-century snow cover in this southern region is the main reason for this difference. Much of the solar energy in the spring currently goes into melting snow and is projected to continue to do so to a lesser extent in northern regions, but not in the south. The late-century (2071-2100) CCSM4 shows an earlier date of LF compared to the historical period, ranging from an advance of 19 days (Fairbanks) to 31 (Juneau). For FF, the geographical range of values is larger: 23 (Juneau) to 40 (Aleutians) days later. The analogous ranges from the GFDL-CM3 for LF are 30 (Fairbanks) to 45 (Anchorage) days earlier than historical, and 31 (Juneau) to 53 (Aleutians) days later for FF.

3.4.3 Start-of-field operations date

A more robust measure for the start of the agricultural season than the last spring frost is the SFO index, which represents the date when the thermal accumulation

(beginning January 1) of daily T_{avg} reaches 200°C. When compared to the visually observed 'green-up' time series at Fairbanks (Figure 3.9), the independent time series of SFO derived from Fairbanks International Airport data, and the nearest ERA-Interim grid cell have correlation coefficients of 0.91 and 0.90, respectively. Green-up refers to the period when deciduous plants leaf out in the spring. The photoperiod characteristic of Interior Alaska during the spring allows this change to occur over the course of one day, and is striking to the visual observer as the landscape hue transitions from brown to green. Fathauer (2012) notes a concurrent relationship between green-up and grass pollen release. Due to its phenological importance, the onset of green-up in the Interior was statistically tested with daily maximum temperature as the primary predictor (Thoman and Fathauer 1998).

With the assumption that this temperature/green-up relationship can be extrapolated beyond Fairbanks, historical SFO dates range from late April over Southeast Alaska, to late May across most of the Interior, to late June for the North Slope. The CCSM4 projects earlier SFO dates, with changes ranging from less than a week (2011-2040), 1-2 weeks (2041-2070), to about 2-4 weeks across Alaska (2071-2100; Figure 3.10 a-c), while GFDL-CM3 shows earlier start dates of 1 week, 2 weeks, and approximately one month, respectively (Figure 3.10 d-f).

3.4.4 Plant heat stress

Higher precipitation and a longer growing season are conducive to greater agricultural opportunity, but warmer temperatures pose a risk of increased plant heat stress (PHS). Exposure to extremely high daily maximum temperature (e.g., > 35°C)

disrupts the carbon cycle in plants by reducing photosynthesis and increasing respiration (Barnabas et al. 2008). Wheat, a primary field crop currently grown in Alaska, shows cell deterioration with maximum temperatures above 25°C, and anthesis (i.e., flowering) is stunted above 32°C (Sánchez et al. 2014). Excessive heat causes plants to use energy to mitigate structural damage, and this lost energy can no longer be used for growth.

Following the results of Wahid et al. (2007), a typical metric used to indicate PHS for cool season crops that are common to Alaska is the number of days with T_{avg} greater than 25°C. Using T_{avg} instead of daily maximum temperature means that the plants have sustained prolonged exposure to high temperatures. No location in Alaska currently averages one PHS day per year (figure not shown), however Alaska's Interior occasionally experiences this level of heat during a hot summer. Future projections indicate an increased number of heat stress days per year in the Interior, and an introduction of such days to places that previously had none. The CCSM4 shows greater increases (Figure 3.11 a-c) compared to the GFDL-CM3 (Figure 3.11 d-f) with maximum frequencies exceeding seven days per year in parts of the Yukon Flats and Tanana Valley by 2071-2100. Each 30-year projected period shows a slight increase in PHS days compared to the previous 30 years.

3.5 Discussion

This study depicts changes in 30-year segments beyond the historical period of 1981-2010 to allow for a climate change signal to emerge from the natural variability. Table 3.1 identifies the greatest relative GSL changes from successive periods in bold for each of the five Census Areas and for each of the five statistical points, for a total of 25 per

model. By adding these instances together and binning them into each of the three projected periods, it is found that the greatest GSL changes according to CCSM4 occur in the late-century period, and in the mid-century for the GFDL-CM3. Similarly for LF (Table 3.2), the greatest changes occur in the mid-century period for both models, and none of the highest relative changes occur in the early-century (2011-2040). For FF (Table 3.3), both models indicate that the greatest changes occur during the late-century.

The relative increases in median GSL from the historical period to the early-century are comparable to the historical standard deviation of GSL, meaning that internal variability will continue to be as important as the underlying trend into the mid-century. However, the signal of increased GSL largely emerges in all five Census Areas (Figure 3.5), such that most late-century growing seasons (2071-2100) will be reliably longer than currently observed, even in a relatively cold year. This is important for long-term planning, but highlights an ongoing problem. That is, despite rapid warming in the high latitudes, the economic risk of a failed crop due to a cold summer is an impediment to changing agricultural practices. The RCP8.5 emissions scenario used in this study shows the current trajectory of agro-climate indices for Alaska, but mitigation efforts could result in smaller observed changes.

Field sites near Fairbanks show a close relationship between planting date and green-up. The average planting date from 1978-2002 was May 10 (Van Veldhuizen and Knight 2004) and the average green-up date from 1981-2010 was May 9 (Figure 3.9). The average last frost at Fairbanks from 1978-2002 was May 16 (NOAA/NWS 2017), which coincides with the average SFO date from the Fairbanks International Airport and the nearest downscaled ERA-Interim grid cell (Figure 3.9). Given the statistically significant

correlation between green-up and the SFO, these findings imply that the model output can provide a proxy for planting date. Heat accumulation metrics are commonly used to anticipate plant growth and maturation, usually measured in growing-degree days (GDD; Miller et al. 2001); the SFO uses heat units to estimate when the planting process can begin.

This study delineated soil versus non-soil areas. A defining characteristic for much of the soil in Alaska is the presence of permafrost beneath the surface, which drains poorly and is classified by the gelisol taxonomic order (Soil Survey Staff 2014). Given the observed and projected rates of warming for Alaska, near-surface permafrost is expected to thaw over much of mainland Alaska. Thawing permafrost facilitates drainage of surface water, but in a climatologically-dry area like mainland Alaska, the amount of soil water necessary for farming is a delicate balance that can rapidly transition from saturated to too dry. Thawing permafrost often leads to irregular subsidence and irregular surfaces (gullies and ridges) known as thermokarst, especially where the near-surface layers have high ice content. In such cases, extreme surface roughness can preclude agriculture. Furthermore, while the dynamically downscaled data used here provide a better representation of temperature and precipitation than the coarser forcing data (Bieniek et al. 2016; Lader et al. 2017), the 20-km resolution does not resolve the landscape at the individual field level. The feasibility of particular crop varieties can vary widely with small changes in elevation and prevailing meteorological quantities (Van Veldhuizen and Knight 2004).

One potential indicator of the changing feasibility of agriculture is the prevalence of biomass. While summer warming has been linked to higher biomass across the Arctic,

several locations in Alaska have shown decreases in recent decades, pointing to a role of internal variability in complicating a warming climate. For example, southwest Alaska saw a reduction of biomass (i.e., browning) from 1982-2011 (Bhatt et al. 2013). Later spring snowmelt that delayed green-up has been suggested as a plausible reason for this finding (Bieniek et al. 2015). This is consistent with a pan-Arctic study of snow showing that while the region has decreasing snow-cover duration and snow-water equivalent (SWE) in general, southwest Alaska represents one area with increased SWE and later snowmelt dates from 1979-2009 (Liston and Hiemstra 2011). Conversely, increased winter snow acts to insulate the soil underneath, keeping it warmer and more vulnerable to thawing in the summer. Surface water from permafrost thawing reduces the remotely–sensed Normalized Difference Vegetation Index (NDVI) which is sensitive to soil moisture and water, thus potentially leading trends suggesting vegetation browning (Raynolds and Walker 2016). Parent and Verbyla (2010) suggest that an area of vegetation browning in eastern Interior Alaska resulted from drought stress and insect infestation, which together with warming temperatures and thawing permafrost, overwhelmed any precipitation changes.

Greater agricultural opportunity has been noted for other high-latitude regions, but with a few causes for concern. Winter and spring wheat yields are projected to increase by an average of 37% and 70%, respectively, across western Canada from 2040-2069, but there are concerns about pests and new diseases (Smith et al. 2013). The potential for longer growing seasons has been recognized in Sweden and Finland, although the integration of transformational practices such as changing land usage for farming has been limited by short-term economic and regulatory concerns (Juhola et al. 2017).

Uncertainty about changes in water stress at northern locations remains high, too. While precipitation is projected to increase, higher temperatures and longer summers will increase evapotranspiration. However, there is evidence that higher CO_2 will decrease stomatal conductance in plants, helping them to retain water (Yu et al. 2004).

3.6 Conclusions

This study investigates projected changes (2011-2040, 2041-2070, 2071-2100) to agro-climate indices for Alaska using downscaled regional climate model simulations under the RCP8.5 emissions scenario, together with observed meteorological and reanalysis data. The average GSL is projected to increase by 48-87 days per year when comparing the late-century (2071-2100) with the historical reference period (1981-2010), with the largest changes in the coldest locations. Most areas exhibit more change to the first autumn frost than to the last spring frost. Southern Alaska is the exception to this, which could implicate the lack of seasonal snowpack here at the end of winter. The heat-unit based SFO index exhibits a significant correlation with the independently observed green-up date at Fairbanks, which is subsequently related to observed planting date. These relationships indicate, by means of projections of the SFO across Alaska, the feasibility of earlier spring cultivation by 2-4 weeks. Increasing heat is also expected to result in greater PHS for field crops. Interior sites rarely have days with $T_{avg} > 25°C$ at present, but these events are anticipated to occur 5-10 times per year in the hottest valleys at the end of this century.

The most pronounced GSL changes are projected to occur in the mid- and late-century periods, which also coincides with when the RCPs diverge the most (Kunreuther

et al. 2014) and when the choice of scenario represents the highest source of uncertainty compared to model spread and internal variability (Hodson et al. 2013). Utilizing a forcing scenario lower than RCP8.5 would reduce the anticipated late-century increases to temperature and precipitation. This would subsequently reduce the GSL, changes to the SFO, and PHS, while acting to preserve the current landscape of Alaska. Without land-use alterations and transformational changes to infrastructure, water management, and soil treatment, it is plausible that much of Alaska will remain untilled, despite the more favorable climate described here. However, the projections indicate far fewer days with freezing temperatures in Alaska. Thus plants will be less susceptible to lethal cold temperatures, allowing for both an expansion in the acreage of crops that are currently grown and the introduction of new crops (e.g., maize) that require more growing-degree days. Additional investigation into the changing soil water balance and other effects of permafrost thaw would greatly improve further agriculture feasibility studies for Alaska.

3.7 Acknowledgements

We thank two anonymous reviewers who provided invaluable recommendations to help improve this manuscript. Support for this work was provided by the National Science Foundation, Office of Polar Programs through Grant PLR-1268350, and by the NOAA Climate Program Office through Grant NA16OAR4310162 to the Alaska Center for Climate Assessment and Policy. The project described in this publication was supported by Cooperative Agreement No. G17AC00213 from the United States Geological Survey. Its contents are solely the responsibility of the authors and do not necessarily represent the views of the Alaska Climate Adaptation Science Center or the

USGS. This manuscript is submitted for publication with the understanding that the United States Government is authorized to reproduce and distribute reprints for Governmental purposes. This work was supported in part by the high-performance computing and data storage resources operated by the Research Computing Systems Group at the University of Alaska Fairbanks, Geophysical Institute. Rick Thoman of the National Weather Service Alaska Region provided the historical green-up dates used in this study.

3.8 Figures

a)

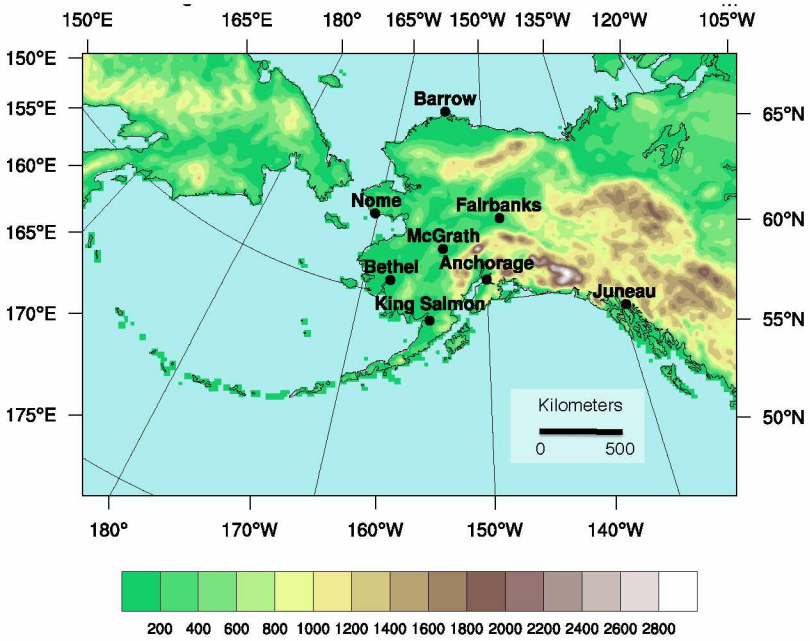

b)

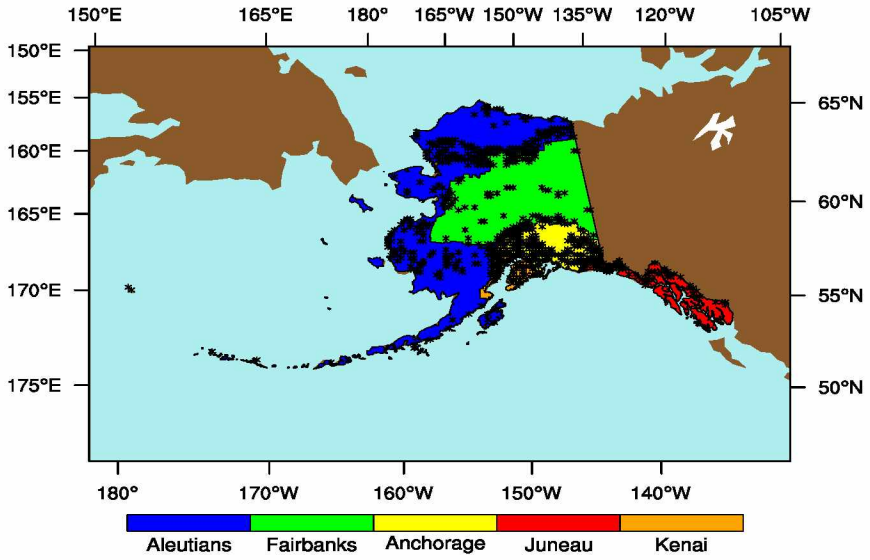

Figure 3.1 (a) Model terrain height (m) and (b) USDA Alaska Census Areas. Black hatching denotes non-soil grid cells. The latitude (˚N), and longitude (˚W) coordinates for the cities are: Anchorage (61.17, 150.02), Barrow (71.30, 156.78), Bethel (60.78, 161.80), Fairbanks (64.80, 147.88), Juneau (58.30, 134.41), King Salmon (58.68, 156.65), McGrath (62.97, 155.62), and Nome (64.50, 165.43).

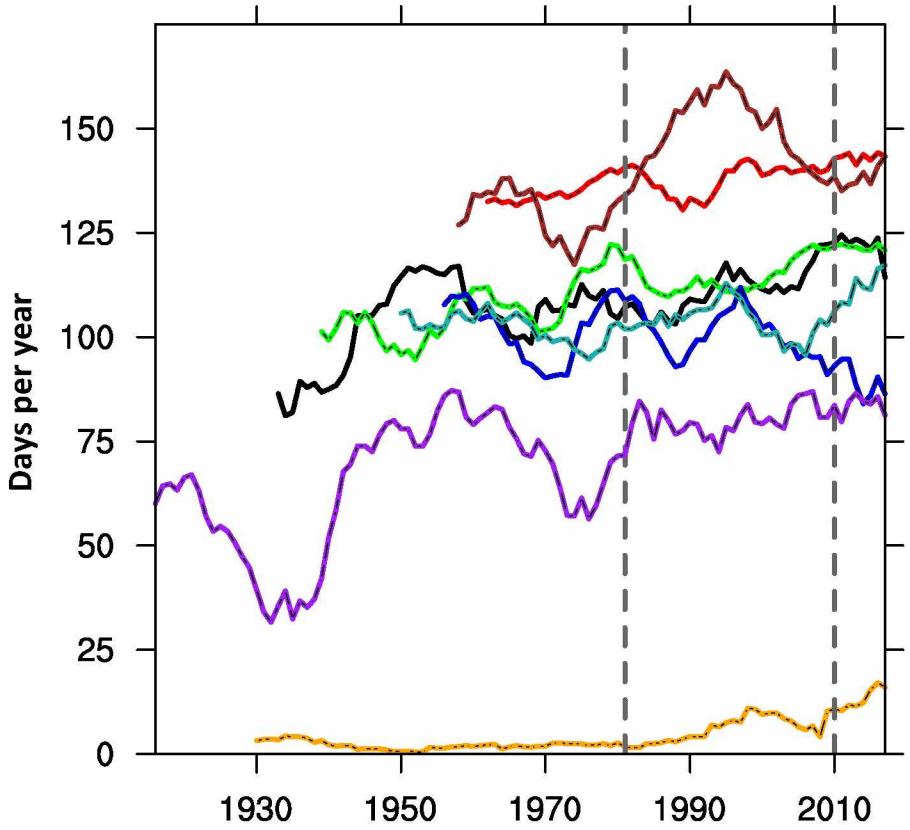

City	Full Period of Record	1981-2010
Anchorage	**1.9**	5.1
Barrow	**1.2**	4.4
Bethel	**2.7**	5.7
Fairbanks	**2.7**	**6.3**
Juneau	**3.4**	**-9.1**
King Salmon	-2.0	-2.1
McGrath	1.1	1.0
Nome	**3.1**	4.4

Figure 3.2 Observed 10-year running mean of annual growing season length for 8 cities in Alaska. The points represent the last year of the 10-year sliding window used for averaging (e.g., 1917 signifies 1908-1917). Vertical dashed lines demarcate the historical period in this study (1981-2010). The linear trend in days per decade is shown with significance at the 95% confidence level indicated in bold for both periods.

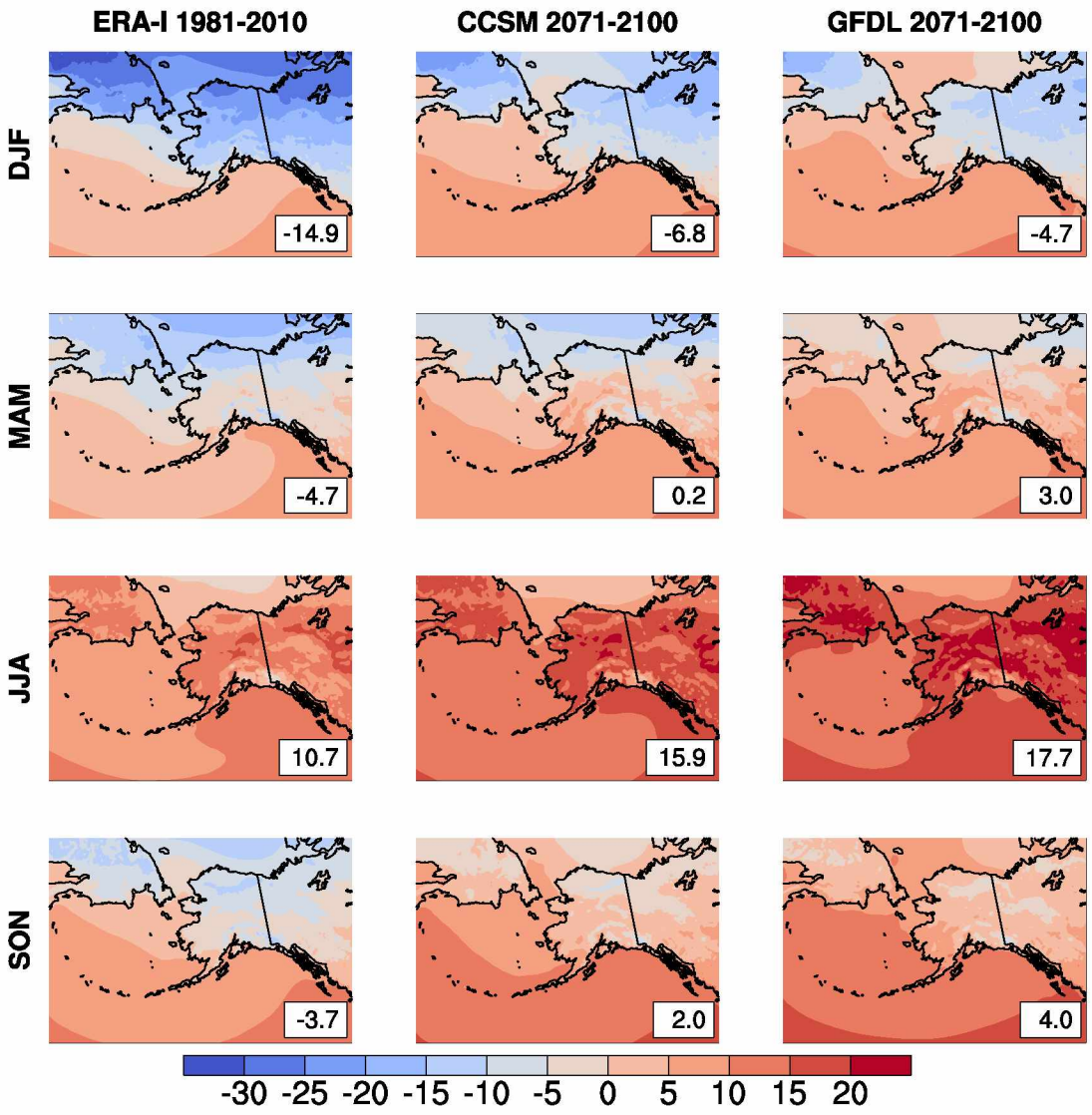

Figure 3.3 Seasonal 2-m temperature climatology (˚C) from (left) ERA-Interim (1981-2010), (middle) CCSM4 projected change (2071-2100 minus 1981-2010) added to ERA-Interim, (right) GFDL-CM3 projected change (2071-2100 minus 1981-2010) added to ERA-Interim. The land grid cell average for Alaska is indicated in the bottom right.

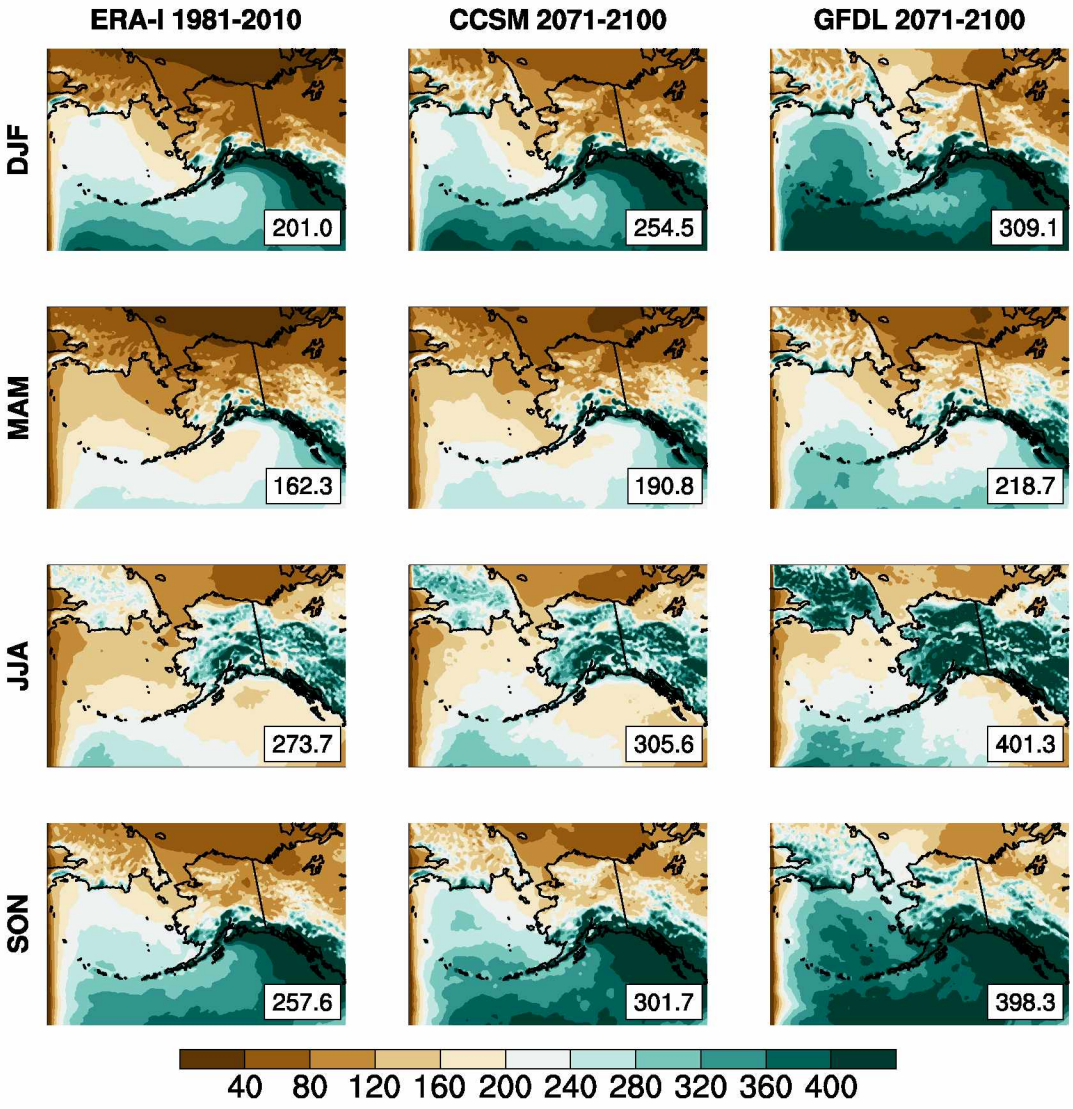

Figure 3.4 Total seasonal precipitation (mm) from (left) ERA-Interim (1981-2010), (middle) CCSM4 projected change (2071-2100 minus 1981-2010) added to ERA-Interim, (right) GFDL-CM3 projected change (2071-2100 minus 1981-2010) added to ERA-Interim. The land grid cell average for Alaska is indicated in the bottom right.

a) CCSM4

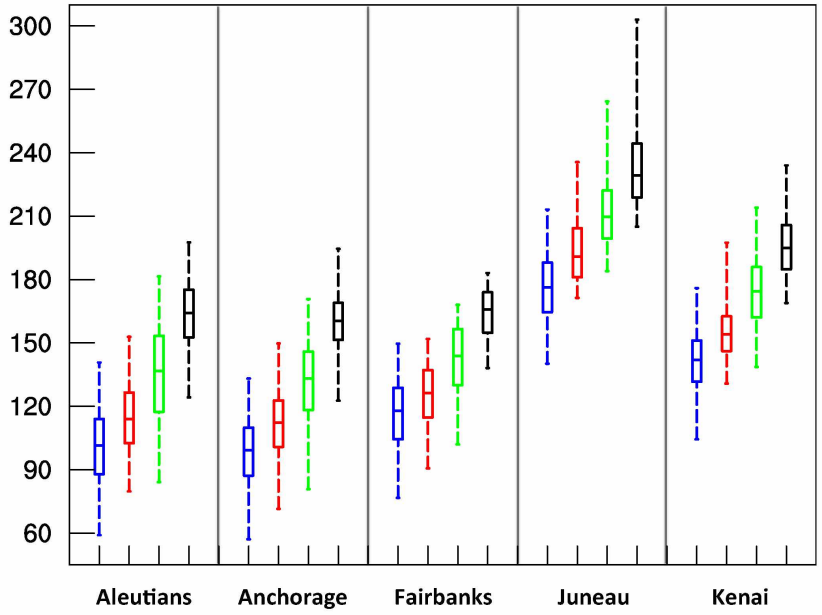

b) GFDL-CM3

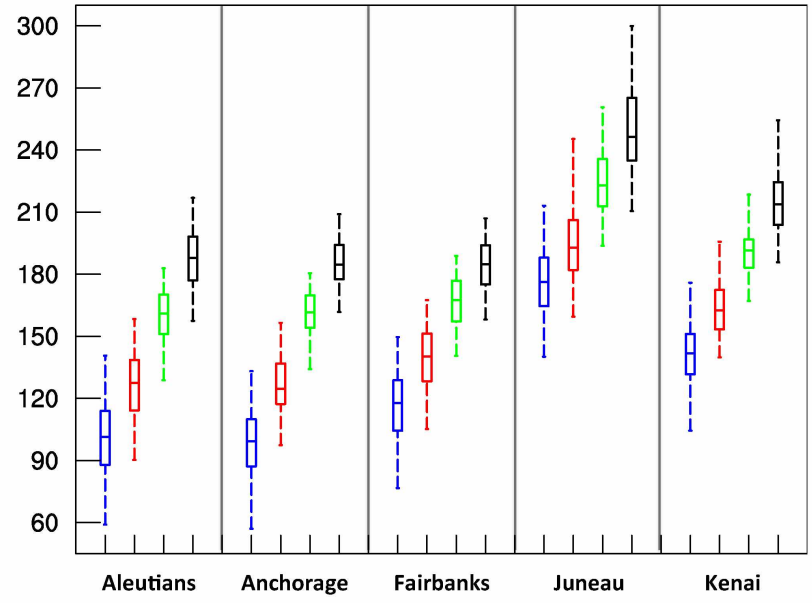

Figure 3.5 Growing season length (days per year) across five USDA Census Areas for a) CCSM4 and b) GFDL-CM3. Boxes represent the interquartile range, and whiskers show the extremes. Projected change, relative to model climatology, for 2011-2040 (red), 2041-2070 (green) and 2071-2100 (black) has been bias-corrected with ERA-Interim (1981-2010; blue).

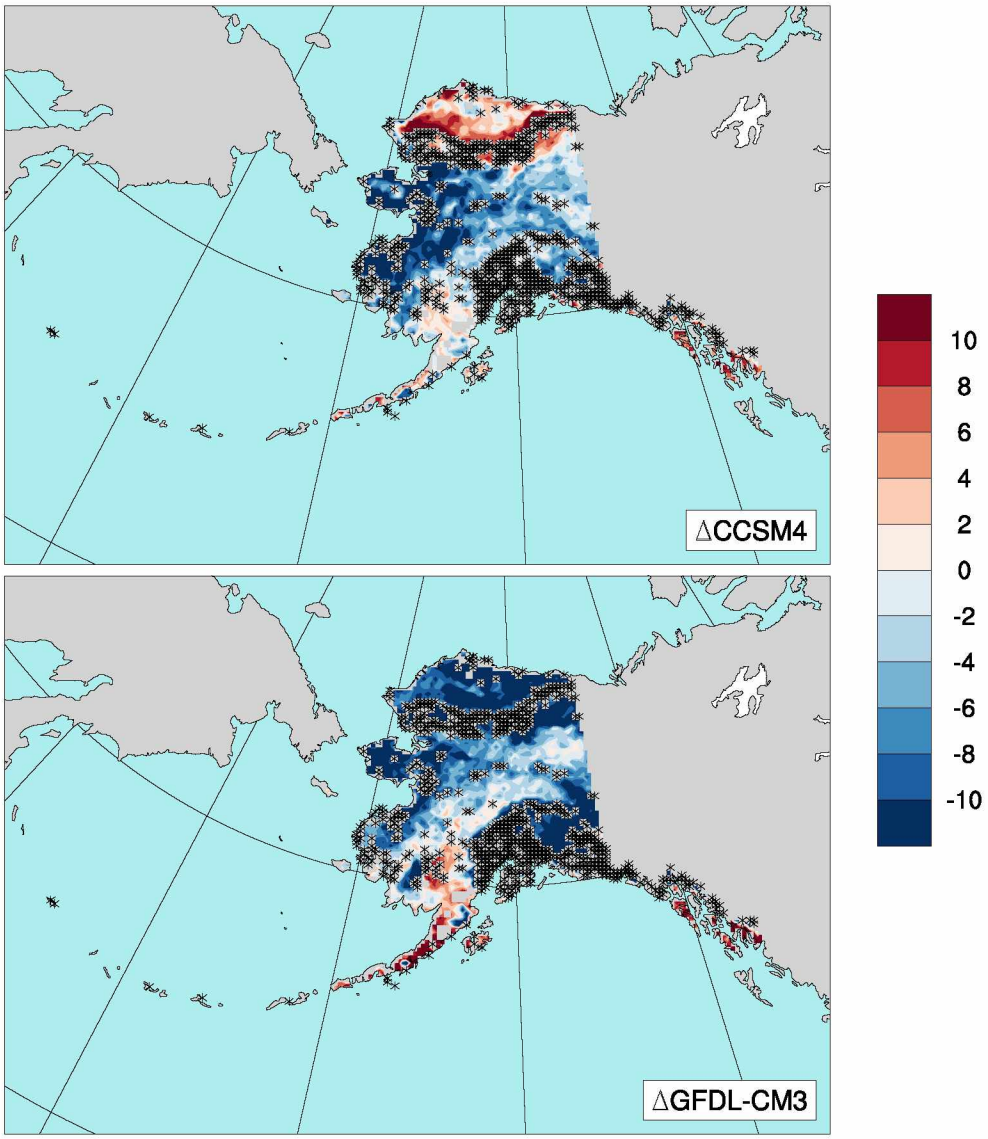

Figure 3.6 Projected changes (2071-2100), relative to climatology (1981-2010), of detrended standard deviation of growing season length (days) for CCSM4 (top), and GFDL-CM3 (bottom). Black hatching denotes non-soil grid cells. The latitude and longitude are identical to Figure 3.1.

a) CCSM4

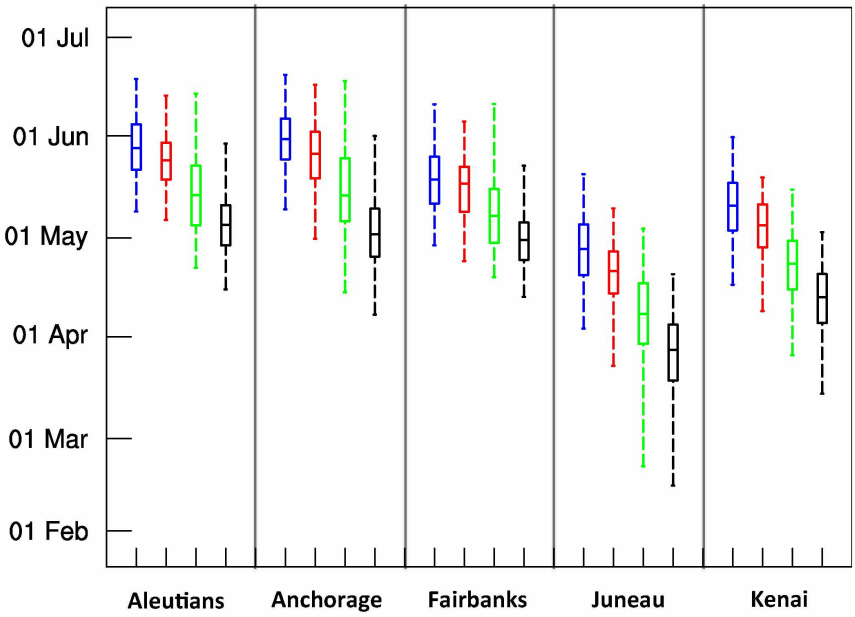

b) GFDL-CM3

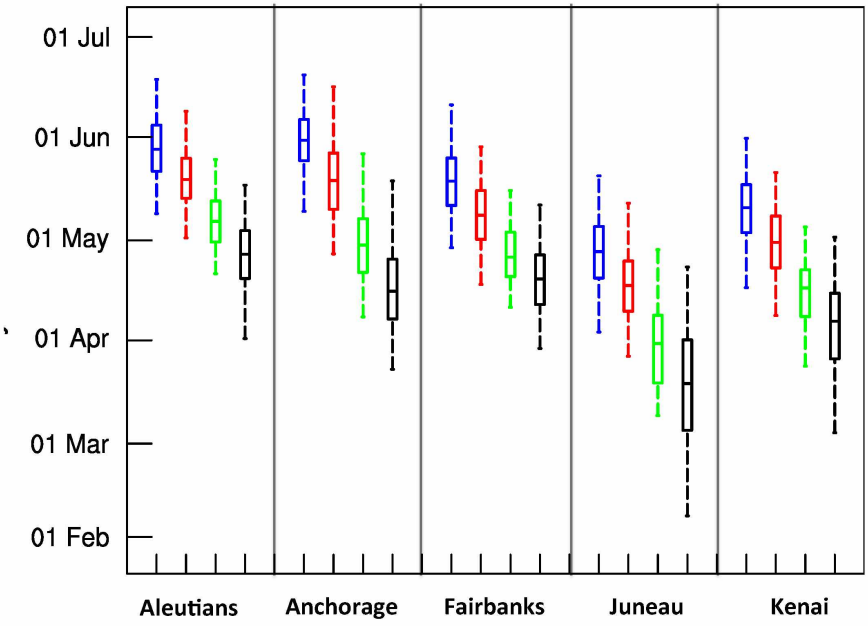

Figure 3.7 Average last date of spring frost across five USDA Census Areas for a) CCSM4 and b) GFDL-CM3. Boxes represent the interquartile range, and whiskers show the extremes. Projected change, relative to model climatology, for 2011-2040 (red), 2041-2070 (green) and 2071-2100 (black) has been bias-corrected with ERA-Interim (1981-2010; blue).

a) CCSM4

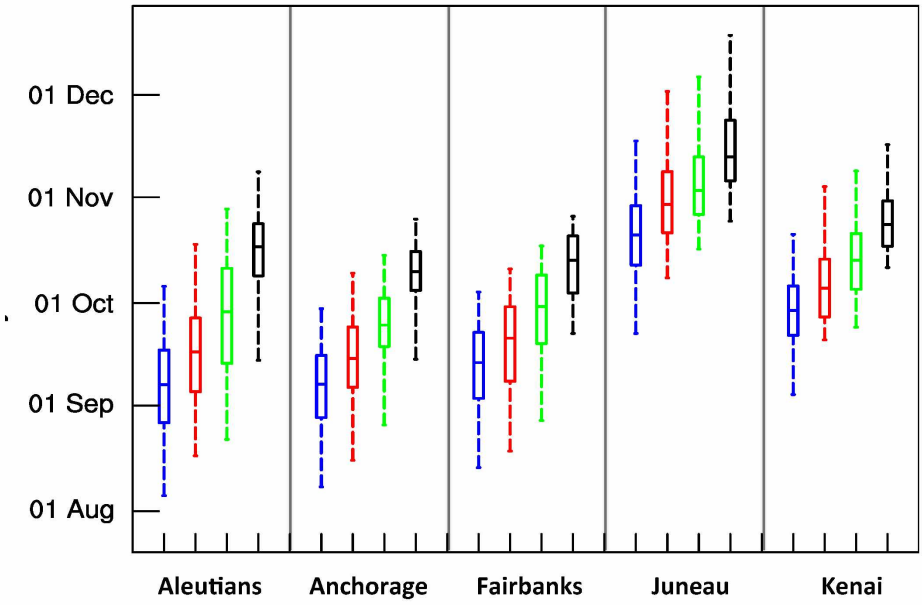

b) GFDL-CM3

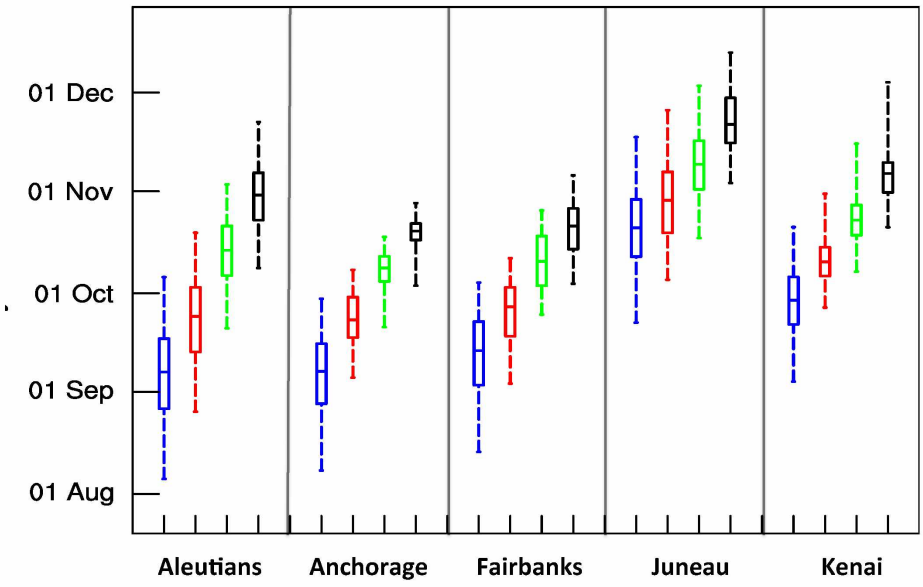

Figure 3.8 Average first date of autumn frost across five USDA Census Areas for a) CCSM4 and b) GFDL-CM3. Boxes represent the interquartile range, and whiskers show the extremes. Projected change, relative to model climatology, for 2011-2040 (red), 2041-2070 (green) and 2071-2100 (black) has been bias-corrected with ERA-Interim (1981-2010; blue).

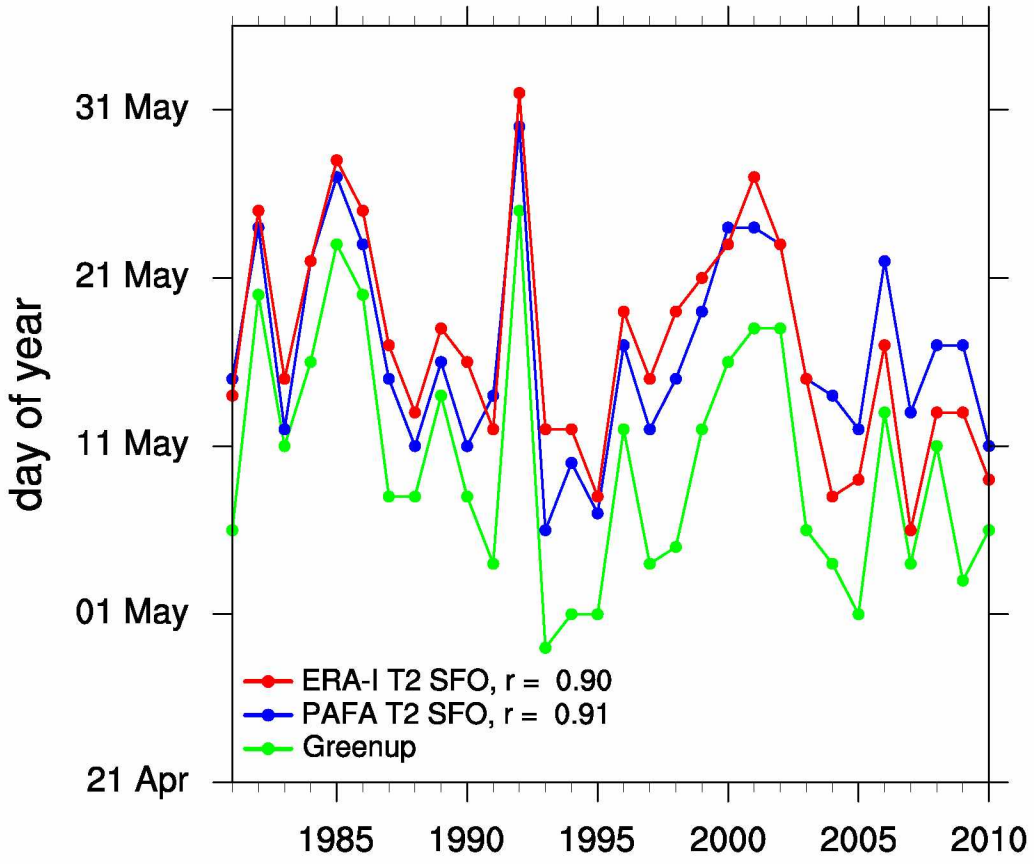

Figure 3.9 Annual time series (1981-2010) of visually observed green-up date (green), start-of-field operations date (SFO) for Fairbanks International Airport (blue), and the SFO for the nearest grid cell from the downscaled ERA-Interim (red). The correlation coefficient (r) of each SFO time series compared to green-up is indicated.

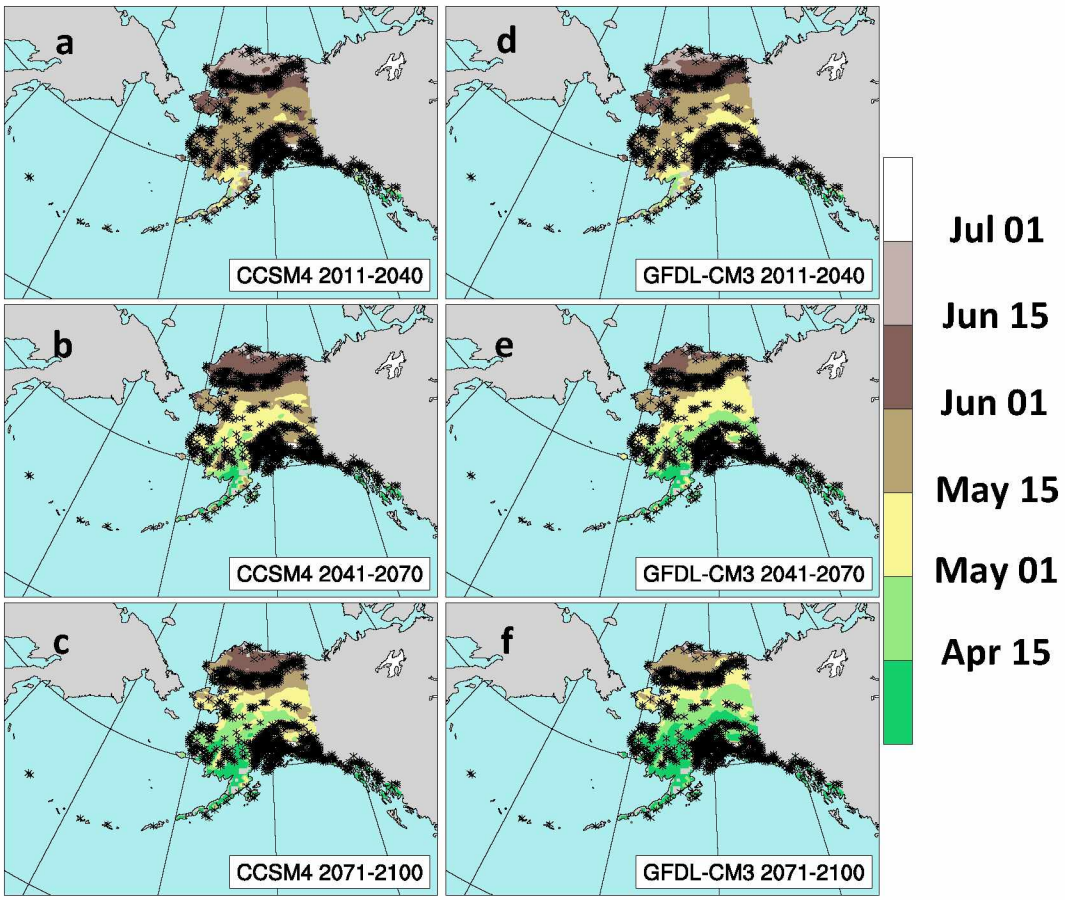

Figure 3.10 Average start-of-field operations date (SFO) for CCSM4 (a-c) and GFDL-CM3 (d-f) by 30-year period. Modeled change has been bias-corrected with ERA-Interim (1981-2010). Black hatching denotes non-soil grid cells. The latitude and longitude is identical to Figure 3.1.

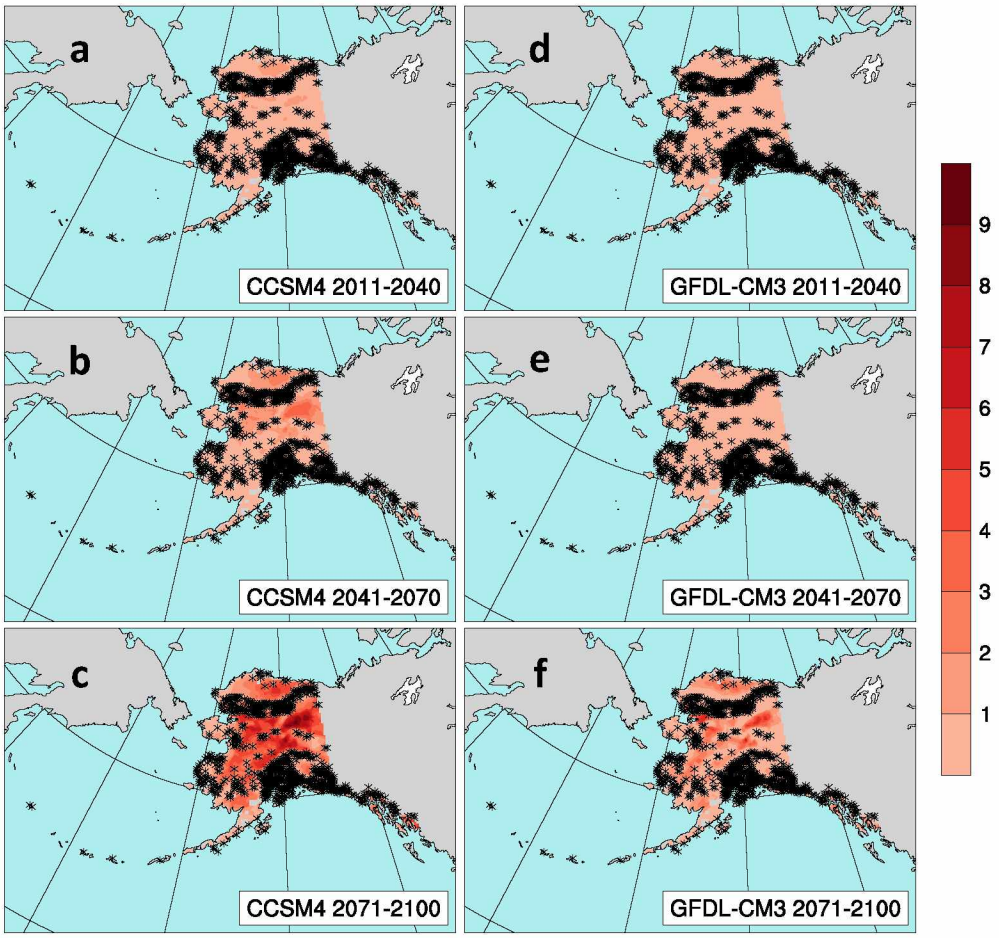

Figure 3.11 Number of plant heat stress days per year (T_{avg} > 25˚C) for CCSM4 (a-c) and GFDL-CM3 (d-f) by 30-year period. Modeled change has been bias-corrected with ERA-Interim (1981-2010). Black hatching denotes non-soil grid cells. The latitude and longitude is identical to Figure 3.1.

3.9 Tables

Table 3.1 Minimum (Min), lower quartile (Q1), median (Med), upper quartile (Q3), and maximum (Max) growing season length (days) averaged over USDA Census Areas for ERA-Interim (1981-2010) and bias-corrected scenarios for CCSM4 and GFDL-CM3. The greatest relative changes from successive periods for each Census Area and statistical point are indicated with the ending period in bold.

		CCSM4					GFDL-CM3				
Area	Period	Min	Q1	Med	Q3	Max	Min	Q1	Med	Q3	Max
Aleutians	1981-2010	59	88	101	114	141	59	88	101	114	141
	2011-40	80	103	114	127	153	90	114	128	139	158
	2041-70	84	117	137	**153**	**181**	**129**	**151**	**161**	**170**	183
	2071-2100	**124**	**153**	**164**	175	198	157	177	188	198	**217**
Anchorage	1981-2010	57	87	99	110	133	57	87	99	110	133
	2011-40	71	101	112	123	150	**97**	117	125	**137**	157
	2041-70	81	118	133	**146**	171	134	**154**	**162**	170	181
	2071-2100	**123**	**151**	**160**	169	**195**	162	178	185	194	**209**
Fairbanks	1981-2010	77	104	118	129	150	77	104	118	129	150
	2011-40	91	115	126	137	152	105	128	140	151	168
	2041-70	102	130	144	**156**	**168**	**141**	**157**	**167**	**177**	**189**
	2071-2100	**138**	**155**	**166**	174	183	158	175	185	194	207
Juneau	1981-2010	140	165	176	188	213	140	165	176	188	213
	2011-2040	**171**	181	191	204	236	160	182	193	206	245
	2041-2070	184	199	210	222	264	**194**	**213**	**223**	**236**	261
	2071-2100	205	**219**	**229**	**244**	**303**	211	235	246	265	**300**
Kenai	1981-2010	104	132	142	151	176	104	132	142	151	176
	2011-2040	131	146	154	163	**197**	**140**	153	163	172	196
	2041-2070	138	162	174	186	214	167	**183**	**191**	197	218
	2071-2100	**169**	**185**	**195**	**206**	234	186	204	214	**224**	**254**

Table 3.2 Minimum (Min), lower quartile (Q1), median (Med), upper quartile (Q3), and maximum (Max) date of last spring frost (Julian day) averaged over USDA Census Areas for ERA-Interim (1981-2010) and bias-corrected scenarios for CCSM4 and GFDL-CM3. The greatest relative changes from successive periods for each Census Area and statistical point are indicated with the ending period in bold.

		CCSM4					GFDL-CM3				
Area	Period	Min	Q1	Med	Q3	Max	Min	Q1	Med	Q3	Max
Aleutians	1981-2010	128	141	147	155	168	128	141	147	155	168
	2011-40	125	138	144	149	163	121	133	138	145	159
	2041-70	**111**	**124**	**133**	142	164	110	**120**	**126**	**132**	**144**
	2071-2100	104	118	124	**130**	**149**	**91**	109	116	123	137
Anchorage	1981-2010	129	144	150	156	170	129	144	150	156	170
	2011-40	120	138	146	152	167	116	129	138	146	166
	2041-70	**103**	**125**	**133**	144	168	**97**	**110**	**119**	**127**	**146**
	2071-2100	97	114	121	**129**	**151**	81	96	105	114	138
Fairbanks	1981-2010	118	130	138	145	161	118	130	138	145	161
	2011-40	113	128	137	142	155	107	120	128	135	148
	2041-70	108	**118**	**127**	135	161	100	**109**	**115**	**122**	**135**
	2071-2100	**102**	113	119	**125**	**142**	**88**	101	108	116	131
Juneau	1981-2010	92	109	117	124	139	92	109	117	124	139
	2011-2040	81	103	110	116	129	85	99	106	114	131
	2041-2070	**51**	**88**	**97**	106	123	67	**77**	**89**	**98**	**117**
	2071-2100	45	77	86	**94**	**109**	**37**	63	77	90	112
Kenai	1981-2010	106	122	130	137	151	106	122	130	137	151
	2011-2040	98	117	124	130	138	97	112	119	127	140
	2041-2070	**84**	**104**	**112**	**119**	135	82	**97**	**106**	**111**	**124**
	2071-2100	73	94	102	109	**122**	**62**	84	96	104	121

Table 3.3 Minimum (Min), lower quartile (Q1), median (Med), upper quartile (Q3), and maximum (Max) date of first autumn frost (Julian day) averaged over USDA Census Areas for ERA-Interim (1981-2010) and bias-corrected scenarios for CCSM4 and GFDL-CM3. The greatest relative changes from successive periods for each Census Area and statistical point are indicated with the ending period in bold.

		CCSM4					GFDL-CM3				
Area	Period	Min	Q1	Med	Q3	Max	Min	Q1	Med	Q3	Max
Aleutians	1981-2010	217	238	249	259	278	217	238	249	259	278
	2011-40	228	247	259	269	**290**	**237**	**255**	266	275	291
	2041-70	233	255	270	**283**	301	262	278	**286**	**293**	306
	2071-2100	**256**	**281**	**289**	296	311	281	295	303	310	**325**
Anchorage	1981-2010	219	239	249	258	271	219	239	249	258	271
	2011-40	227	248	257	266	282	**247**	**260**	**265**	**272**	280
	2041-70	237	260	267	274	287	263	277	281	284	290
	2071-2100	**257**	**277**	**282**	**288**	**298**	275	289	292	294	**300**
Fairbanks	1981-2010	225	245	256	264	276	225	245	256	264	276
	2011-40	230	250	263	272	283	246	260	269	275	284
	2041-70	239	261	272	281	290	**267**	**275**	**283**	**290**	**298**
	2071-2100	**264**	**276**	**286**	**293**	**298**	276	286	293	299	309
Juneau	1981-2010	264	284	293	302	320	264	284	293	302	320
	2011-2040	**280**	294	302	312	335	277	291	301	310	329
	2041-2070	289	299	306	316	339	290	305	312	319	336
	2071-2100	297	**309**	**316**	**327**	**351**	**307**	**319**	**324**	**332**	**346**
Kenai	1981-2010	246	264	271	278	293	246	264	271	278	293
	2011-2040	262	269	277	286	**307**	**269**	**278**	283	287	303
	2041-2070	266	277	286	293	312	280	291	295	300	318
	2071-2100	**283**	**290**	**296**	**303**	319	293	304	**309**	**313**	**337**

3.10 References

AMAP, 2017: Snow, water, ice and permafrost. Summary for policy-makers. Arctic Monitoring and Assessment Programme (AMAP), Oslo, Norway. 20 pp.

Barnabas, B., K. Jäger, and A. Fehér, 2008: The effect of drought and heat stress on reproductive processes in cereals. *Plant Cell Environ.*, **31**, 11-38, doi:10.1111/j.1365-3040.2007.01727.x.

Beach, R. H., and Coauthors, 2015: Climate change impacts on US agriculture and forestry: benefits of global climate stabilization. *Environ. Res. Lett.*, **10**, 095004, doi:10.1088/1748-9326/10/9/095004.

Bhatt, U. S., and Coauthors, 2013: Recent declines in warming and vegetation greening trends over pan-Arctic tundra. *Remote Sens.*, **5**, 4229-4254, doi:10.3390/rs5094229.

Bieniek, P. A., and Coauthors, 2015: Climate drivers linked to changing seasonality of Alaska coastal tundra vegetation productivity. *Earth Interact.*, **19**, doi:10.1175/EI-D-15-0013.1.

Bieniek, P. A., U. S. Bhatt, J. E. Walsh, T. S. Rupp, J. Zhang, J. R. Krieger, and R. Lader, 2016: Dynamical downscaling of ERA-Interim temperature and precipitation for Alaska. *J. Appl. Meteor. Climatol.*, **55**, 635-654, doi:10.1175/JAMC-D-15-0153.1.

Dee, D. P., and Coauthors, 2011: The ERA-Interim reanalysis: Configuration and performance of the data assimilation system. *Quart. J. Roy. Meteor. Soc.*, **137**, 553-597, doi:10.1002/qj.828.

Donner, L. J., and Coauthors, 2011: The dynamical core, physical parameterizations, and basic simulation characteristics of the atmosphere component AM3 of the GFDL global coupled model CM3. *J. Climate*, **24**, 3484-3519, doi:10.1175/2011JCLI3955.1.

FAO, IFAD, UNICEF, WFP and WHO, 2017. *The State of Food Security and Nutrition in the World 2017. Building resilience for peace and food security*. Rome, FAO.

Fathauer, T., 2012: The relation of spring pollen release to weather in Fairbanks, Alaska. M.S. thesis, University of Alaska at Fairbanks, 85 pp. [Available online at http://ffden-2.phys.uaf.edu/atm/atm/theses/Fathauer_Ted_MS2012.pdf.]

Harding, A. E., M. Rivington, and M. J. Mineter, 2015: Agro-meteorological indices and climate model uncertainty over the UK. *Climatic Change*, **128**, 113-126, doi:10.1007s10584-014-1296-8.

Hayhoe, K. A., 2010: A standardized framework for evaluating the skill of regional climate downscaling techniques. Ph.D. dissertation, University of Illinois at Urbana-Champaign, 158 pp. [Available online at http://www.snap.uaf.edu/attachments/1_Hayhoe_Katharine.pdf.]

Hodson, D. L. R., S. P. E. Keeley, A. West, J. Ridley, E. Hawkins, and H. T. Hewitt, 2013: Identifying uncertainties in Arctic climate change projections. *Clim. Dyn.*, **40**, 2849-2865, doi:10.1007/s00382-012-1512-z.

Hsiang, S., and Coauthors, 2017: Estimating economic damage from climate change in the United States. *Science*, **356**, 1362-1369, doi:10.1126/science.aal4369.

Iacono, M. J., J. S. Delamere, E. J. Mlawer, M. W. Shephard, S. A. Clough, and W. D. Collins, 2008: Radiative forcing by long-lived greenhouse gases: Calculations with the AER radiative transfer models. *J. Geophys. Res.*, **113**, D13103, doi:10.1029/2008JD009944.

IPCC, 2014: *Climate Change 2014: Synthesis Report. Contribution of Working Groups I, II and III to the Fifth Assessment Report of the Intergovernmental Panel on Climate Change* [Core Writing Team, R. K. Pachauri and L. A. Meyer (eds.)]. IPCC, Geneva, Switzerland, 151 pp.

Juhola, S., N. Klein, J. Käyhkö, and T. S. Neset, 2017: Climate change transformations in Nordic agriculture. *J. Rural Stud.*, **51**, 28-36, doi:10.1016/j.jrurstud.2017.01.013.

Krishnan, M. H. T. Nyugen, and J. J. Burke, 1989: Heat shock protein synthesis and thermal tolerance in wheat. *Plant Physiol.*, **90**, 140-145, doi:10.1104/pp.90.1.140.

Kunreuther H., and Coauthors, 2014: Integrated Risk and Uncertainty Assessment of Climate Change Response Policies. In: *Climate Change 2014: Mitigation of Climate Change. Contribution of Working Group III to the Fifth Assessment Report of the Intergovernmental Panel on Climate Change* [Edenhofer, O., R. Pichs-Madruga, Y. Sokona, E. Farahani, S. Kadner, K. Seyboth, A. Adler, I. Baum, S. Brunner, P. Eickemeier, B. Kriemann, J. Savolainen, S. Schlömer, C. von Stechow, T. Zwickel and J.C. Minx (eds.)]. Cambridge University Press, Cambridge, United Kingdom and New York, NY, USA.

Lader, R., J. E. Walsh, U. S. Bhatt, and P. A. Bieniek, 2017: Projections of twenty-first-century climate extremes for Alaska via dynamical downscaling and quantile mapping. *J. Appl. Climatol. Meteorol.*, **56**, 2393-2409, doi:10.1175/JAMC-D-16-0415.1.

Lader, R., U. S. Bhatt, J. E. Walsh, T. S. Rupp, and P. A. Bieniek, 2016: Two-meter temperature and precipitation from atmospheric reanalysis evaluated for Alaska. *J. Appl. Meteor. Climatol.*, **55**, 901-922, doi:10.1175/JAMC-D-15-0162.1.

Liston, G. E., C. A. Hiemstra, 2011: The changing cryosphere: Pan-Arctic snow trends (1979-2009). *J. Climate*, **24**, 5691-5712, doi:10.1175/JCLI-D-11-00081.1.

Matthews, K. B., M. Rivington, K. Buchan, D. Miller, and G. Bellocchi, 2008: Characterising the agro-meteorological implications of climate change scenarios for land management stakeholders. *Clim. Res.*, **365**, 59-75, doi:10.3354/cr00751.

Menne, M. J., I. Durre, R. S. Vose, B. E. Gleason, and T. G. Houston, 2012: An overview of the Global Historical Climatology Network-Daily Database. *J. Atmos. Ocean Tech.*, **29**, 897-910, doi:10.1175/JTECH-D-11-00103.1.

Miller, P., W. Lanier, and S. Brandt, 2001: Using growing degree days to predict plant stages. Ag/Extension Service. Montana State University-Bozeman, Bozeman, MT.

Monier, E., L. Xu, and R. Snyder, 2016: Uncertainty in future agro-climate projections in the United States and benefits of greenhouse gas mitigation. *Environ. Res. Lett.*, **11**, 055001, doi:10.1088/1748-9326/11/5/055001.

Morrison, H. C., G. Thompson, and V. Tatarskii, 2009: Impact of cloud microphysics on the development of trailing stratiform precipitation in a simulated squall line: Comparison of one- and two-moment schemes. *Mon. Wea. Rev.*, **137**, 991-1007, doi: 10.1175/2008MWR2556.1.

NOAA/ESRL, 2017: Trends in atmospheric carbon dioxide. Global Monitoring Division. [Available online at https://www.esrl.noaa.gov/gmd/ccgg/trends/.]

NOAA/NWS, 2017: Fairbanks area frost and growing season information. [Available online at https://www.weather.gov/media/afg/climate/Fairbanks_growing_season.pdf .]

Overland, J. E., E. Hanna, I. Hanssen-Bauer, S.-J Kim, J. E. Walsh, M. Wang, U. S. Bhatt, and R. L. Thoman, 2016: Surface air temperature. NOAA. [Available online at http://www.arctic.noaa.gov/Report-Card/Report-Card-2016/ArtMID/5022/ArticleID/271/Surface-Air-Temperature.]

Parent, M. B., and D. Verbyla, 2010: The browning of Alaska's boreal forest. *Remote Sens.*, **2**, 2729-2747, doi:10.3390/rs2122729.

Park, T., and Coauthors, 2016: Changes in growing season duration and productivity of northern vegetation inferred from long-term remote sensing data. *Environ. Res. Lett.*, **11**, 084001, doi:10.1088/1748-9326/11/8/084001.

Pastick, N. J., M. T. Jorgenson, B. K. Wylie, S. J. Nield, K. D. Johnson, and A. O. Finley, 2015: Distribution of near-surface permafrost in Alaska: Estimates of present and future conditions. *Remote Sens. Environ.*, **168**, 301-315, doi:10.1016/j.rse.2015.07.019.

Raynolds, M. K., and D. A. Walker, 2016: Increased wetness confounds landsat-derived NDVI trends in the central Alaska North Slope region, 1985–2011. *Environ. Res. Lett.*, 11, 085004, doi:10.1088/1748-9326/11/8/085004.

Riahi, K., and Coauthors, 2011: RCP 8.5—A scenario of comparatively high greenhouse gas emissions. *Climatic Change*, **109**, 33-57, doi:10.1007/s10584-011-0149-y.

Sánchez, B., A. Rasmussen, and J. Porter, 2014: Temperatures and the growth and development of maize and rice: a review. *Glob. Change Biol.*, **20**, 408-417:10.1111/gcb.12389.

Schlenker, W., and M. J. Roberts, 2009: Nonlinear temperature effects indicate severe damages to U.S. crop yields under climate change. *Proc. Natl. Acad. Sci. USA*, **106**, 15594-15598, doi:10.1073/pnas.0906865106.

Skamarock, W. C., and Coauthors, 2008: A description of the Advanced Research WRF version 3. NCAR Tech. Note NCAR/TN-475+STR, 113 pp., doi:10.1056/D68S4MVH.

Smith, W. N., and Coauthors, 2013: Assessing the effects of climate change on crop production and GHG emissions in Canada. *Agr. Ecosyst. Environ.*, **179**, 139-150, doi:10.1016/j.agee.2013.08.015.

Soil Survey Staff, NCRS, USDA, 2014: Keys to soil taxonomy. 12th edition.

Soil Survey Staff, NRCS, USDA, 2017: Web Soil Survey. Available online at [http://websoilsurvey.nrcs.usda.gov/.]

Taylor, K. E., R. J. Stouffer, and G. A. Meehl, 2012: An overview of CMIP5 and the experiment design. *Bull. Amer. Meteor. Soc.*, **93**, 485-498, doi:10.1175/BAMS-D-11-00094.1.

Thoman, R., and T. Fathauer, 1998: An investigation into estimating greenup dates around Fairbanks Alaska using thermal indices. *Proceedings of the 49th Arctic Science Conference*, Fairbanks, AK, University of Alaska Fairbanks.

Tripathi, A., D. K. Tripathi, D. K. Chauhan, and N. Kumar, 2016: Paradigms of climate change impacts on some major food sources of the world: A review of current knowledge and future prospects. *Agr. Ecosyst. Environ.*, **216**, 356-373, doi:10.1016/j.agee.2015.09.034.

USDA/NASS, 2014a: 2012 Census of Agriculture. Alaska. State and Area Data. Available online at [https://www.agcensus.usda.gov/Publications/2012/Full_Report/Volume_1,_Chapter_1_State_Level/Alaska/akv1.txt.]

USDA/NASS, 2014b: 2012 Census of Agriculture County-Level Boundaries, (CoAK_GCS12.shp -.shx, -.dbf, -.sbn, -.sbx, -.prj): USDA, NASS, Fairfax, Virginia. [Available online at http://www.agcensus.usda.gov/Publications/2012 /Online_Resources/Ag_Atlas_Maps/mapfiles/CoGenAll_GCS12.zip.]

Van Veldhuizen, R. M., and C. W. Knight, 2004: Performance of agronomic crop varieties in Alaska 1978-2002. Bulletin 111. AFES, UAF. [Available online at https://www.uaf.edu/files/snre/B111.pdf.]

Wahid, A., S. Gelani, M. Ashraf, and M. R. Foolad, 2007: Heat tolerance in plants: An overview. *Environ. Exp. Bot.*, **61**, 199-223, doi:10.1016/j.envexpbot.2007.05.011.

Wendler, G., and M. Shulski, 2009: A century of climate change for Fairbanks, Alaska. *Arctic*, **62**, 295-300, doi:10.14430/arctic149.

Yu, Q., Y. Zhang, Y. Liu, and P. Shi, 2004: Simulation of the stomatal conductance of winter wheat in response to light, temperature and CO_2 changes. *Ann. Bot-London*, **93**, 435-441, doi:10.1093/aob/mch023.

Zhang, X., and J. Zhang, 2001: Heat and freshwater budgets and pathways in the Arctic Mediterranean in a coupled ocean/sea-ice model. *J. Oceangr.*, **57**, 207-237, doi:10.1023/A:1011147309004.

4 ANTICIPATED CHANGES TO THE SNOW SEASON IN ALASKA: ELEVATION DEPENDENCY, TIMING AND EXTREMES[3]

4.1 Abstract

Snowfall and snow season length across Alaska act as controls of temperature, surface hydrology and underlying soil properties. Current projections of warming suggest that considerable change will occur to key snow parameters, possibly contributing to: excessive infrastructure damage from thawing permafrost, reduced soil recharge in the spring due to shallow end-of-winter snowpack, and an increased frequency of rain-on-snow events. This study investigates projected changes to mean annual snowfall, dates of snow onset and snow-off, and extreme snowfall for Alaska, using dynamically downscaled reanalysis and climate model simulations. These include the ERA-Interim reanalysis from 1981-2010, and two Coupled Model Intercomparison Project phase 5 models: NCAR Community Climate System Model version 4 (CCSM4) and Geophysical Fluid Dynamics Laboratory Climate Model version 3 (GFDL-CM3) from 1981-2100. The analysis is presented in 30-year periods (i.e., 1981-2010, 2011-2040, 2041-2070, and 2071-2100) with the future scenarios from Representative Concentration Pathway 8.5. Late-century projections of average annual snowfall at low elevations (0-1000 m) show decreases of 41.3% and 40.6% for CCSM4 and GFDL-CM3, respectively. At high elevations (1000-2000 m), the reductions are smaller at 13.5%, and 14.2%, respectively. End-of-winter snow-water equivalent displays reductions at all elevations with the advance of each 30-year period. Snow season length is shortened due to later snow onset

[3] *Lader, R., J. E. Walsh, U. S. Bhatt, and P. A. Bieniek. Anticipated changes to the snow season in Alaska: Elevation dependency, timing and extremes. In preparation for Journal of Applied Meteorology and Climatology.*

and earlier snow-off; many locations in southwest Alaska no longer experience continuous winter snowpack by the late-century period. Maximum 2-day snowfall amounts are projected to decrease at Anchorage and Nome, while Fairbanks and Barrow show no significant trend.

4.2 Introduction

Snow cover and snowfall are prominent features of the climate of Alaska that help regulate surface temperature and physical attributes of the near-surface soil. With its high albedo, snow reflects solar energy back toward space, and deeper snow cover tends to have a higher albedo (Hall 2004). However, in the context of rising greenhouse gas concentrations, this snow-albedo feedback has contributed to a rate of surface warming in the Arctic that is nearly double the global average during the most recent decades (AMAP, 2017; Overland et al. 2016). Studies of Northern Hemisphere snow cover extent and snow season duration indicate large reductions that are most severe in the spring (Brown and Robinson 2011; Derksen et al. 2016; Estilow et al. 2015; IPCC 2013).

It is estimated that 38% of mainland Alaska contains near-surface permafrost (Pastick et al. 2015), which represents soil that is continually frozen throughout the year. The presence of snow cover acts to insulate the soil directly beneath it, keeping it warmer in the winter and making permafrost more vulnerable to thaw in the spring and summer. Alternatively, delayed spring melt keeps the surface closer to freezing and slows warming of the permafrost. Thus, projections of snow season characteristics (e.g., onset, depth, duration) have important implications. In many areas, an active layer that exists above the permafrost is frozen for part of the year and thaws in the summer. Trends of

near-surface permafrost temperature (i.e., 0-20 m beneath the surface) in Alaska indicate a warming of 0.5-2.0°C since the early 1980s (Brown and Romanovsky 2008). When permafrost thaws, it causes subsidence of the land surface, which damages any built infrastructure on it (e.g., roads, buildings, pipelines). Projections of 21st-century warming suggest that permafrost thaw will lead to the second highest costs associated with climate change in Alaska, behind only flooding (Melvin et al. 2016).

Snowfall represents the dominant precipitation type at many locations in Alaska for several months of the year and its water content gets stored on the landscape, rather than immediately running off. During the spring melt season - typically the driest period across Alaska (see Figure 6, Bieniek et al. 2012) – the snowpack serves as the primary water source for soil recharge that is needed for plant life (Clilverd et al. 2011), including uptake by trees in the boreal forest (Young-Robertson et al. 2016). As the future climate is projected to warm, however, some of the precipitation that historically fell as snow is expected to fall as rain instead (McAfee et al. 2013). One of the factors involved in this rain/snow partitioning is elevation, and it is anticipated that, while most locations will experience reduced snowfall, high elevations could see an increase (Frei et al. 2017).

Total precipitation is expected to increase in the Arctic (Walsh et al. 2008; AMAP 2017) given that a warmer atmosphere has a higher holding capacity for water vapor, and this is being supported by observations of increased poleward atmospheric moisture transport (Zhang et al. 2012). To date, surface observations have largely shown a mix of increasing and decreasing precipitation trends, depending on season and location (Hinzman et al. 2005; Wendler and Shulski 2009). However, observations of snow water equivalent from the GlobSnow v2.0 dataset (ESA 2014) indicate significant ($p < 0.05$;

two tailed t-test) decreases across North America for both February and April from 1980-2012; March also showed declines, but these have not quite reached the level of statistical significance (Jeong et al. 2017). Meanwhile, from 1988-2010 significant snow cover increases ($p < 0.01$) have been found during October across Eurasia, and these are posited to be the result of changing large-scale atmospheric patterns (Cohen et al. 2012).

Alterations to snow-related hydrological processes in Alaska have the capacity to change the frequency and intensity of extreme and hazardous weather. Rain-on-snow events produce a layer of ice on the surface that makes travel dangerous and inhibits foraging animals from accessing their winter food sources. Warming temperatures are expected to lead to an increased frequency of these events across the Arctic, including Alaska (Bieniek et al. 2018; Rennert 2009). Unlike locations outside the Arctic - where temperatures often temporarily rise above freezing during winter - when a layer of ice forms on the surface in mainland Alaska, it can persist for months.

Warmer temperatures elevate the atmosphere's holding capacity for water vapor and can also promote extreme snowfall, given the necessary thermodynamics. Heavy snowfall has a deleterious impact on transportation, causes infrastructure failure, and makes it difficult for fauna (e.g., moose, caribou) to navigate the landscape and access food sources. River-ice breakup also shows a slight dependence on snowfall and snowmelt, although spring temperatures appear to be the dominant predictor (Bieniek et al. 2011; Lesack et al. 2014).

This research investigates projections of important snow season characteristics for Alaska using a set of dynamical downscaled climate model and reanalysis simulations from 1981-2100. The relatively high resolution of the downscaled simulations (20 km)

represents an improvement on previous work that relied on coarse global climate models. Moreover, the dynamical forcing produces a full suite of daily meteorological variables, which is often not feasible for statistically downscaled datasets that rely on limited observational data as a basis for their empirical relationships. The primary targets of this assessment of recent and future changes of snow in Alaska are: 1) the anticipated change of the annual snowfall cycle according to elevation, 2) the resultant end-of-winter snow-water equivalent as a function of elevation, 3) expected variations to snow onset and snow melt out dates and 4) expected changes in extreme snowfall events for population centers across Alaska.

4.3 Data and Methods

Regional dynamical downscaled climate model simulations are used to investigate projected snow season changes by 30-year periods (i.e., 2011-2040, 2041-2070 and 2071-2100), relative to a historical period from 1981-2010 across the Alaska domain (Figure 4.1). Specifically, the National Center for Atmospheric Research (NCAR) Community Climate System Model version 4 (CCSM4) and National Oceanic and Atmospheric Administration (NOAA) Geophysical Fluid Dynamics Laboratory Climate Model version 3 (GFDL-CM3; Donner et al. 2011) are downscaled using the Weather Research and Forecasting Model (WRF; Skamarock et al. 2008). The CCSM4 and GFDL-CM3 are members of the Coupled Model Intercomparison Project Phase 5 (CMIP5; Taylor et al. 2012) with atmospheric model resolutions (latitude × longitude) of approximately 1° × 1.25° and 2° × 2.5°, respectively. Thus the downscaled data, which have a spatial resolution of 20-km, are more than four times finer than the original forcing data. The

future simulations are based on representative concentration pathway 8.5 (RCP8.5; Riahi et al. 2011), which best tracks the current trajectory of greenhouse gas emissions (Peters et al. 2013).

Regional orography, represented by the downscaling procedure, is displayed in Figure 4.1. Superimposed on this map are 21 stations across Alaska that have a minimum of 95% daily coverage of precipitation, snowfall and snow depth during the historical period (1981-2010). These data are available from the Global Historical Climatology Network Daily (GHCN-D) database (Menne et al. 2012; https://www.ncdc.noaa.gov/ghcn-daily-references). For the cold season (i.e., all months excluding May-September), Table 4.1 lists information for each of these stations, including total precipitation and snowfall. The stations all have relatively low elevation in common; the highest location, Eagle, is at 259 m, and 15 of the stations are situated less than 100 m above sea level. They have widely varying cold season precipitation and snowfall amounts, however. Yakutat receives 2475 mm of precipitation, on average, each cold season, whereas Barrow typically records 33 mm. Barrow also displays the least snowfall (74 cm), and Alyeska shows the highest, averaging 547 cm.

Given the paucity of meteorological observations with adequate temporal coverage for climate studies across Alaska, reanalysis data can be used instead as a proxy source of gridded observations. This study utilizes a dynamical downscaled simulation of the ERA-Interim reanalysis (Dee et al. 2011) that covers the historical period (1981-2010), and uses the same WRF parameterizations as was done with simulations driven by CCSM4 and GFDL-CM3. Among reanalysis models, the ERA-Interim frequently displays the lowest temperature and precipitation bias when compared to observations in Alaska

(Lader et al. 2016) and the broader Arctic (Lindsay et al. 2014). The downscaling simulations are initialized every 48 hours, and forecasts are produced to 54 hours with every first 6 hours discarded to allow for spin-up. Spectral nudging is used to constrain the downscaled products to the original ERA-Interim. The downscaled reanalysis data have been shown to provide a closer representation of daily temperature and precipitation when compared to observations (Bieniek et al. 2016; Lader et al. 2017).

The spatial distributions of daily water equivalent of accumulated snow depth (ACSNOW) from the downscaled ERA-Interim, after summation by month and averaging over the historical period, are displayed in Figure 4.2. Mainland Alaska experiences its greatest ACSNOW during October (Figure 4.2b) and November (Figure 4.2c). Thereafter, monthly ACSNOW decreases as the winter sea ice develops and cyclones track further south. Much of southern Alaska displays its largest ACSNOW amounts during December (Figure 4.2d) and January (Figure 4.2e). Mountainous locations, particularly the high peaks of the Alaska Range, receive accumulating snowfall during all months, albeit considerably less in the summer.

Note that the gridded ACSNOW variable and snowfall are used interchangeably hereafter because ACSNOW merely represents snowfall in terms of liquid equivalent. Snowfall is particularly difficult to measure; in fact, 8 of the 21 stations in Table 4.1 display opposing trends of observed precipitation and snowfall during the historical period. Given that the vast majority of this winter precipitation fell as snow, it should follow that the trends are of the same sign. While it is possible that there is a physical basis for this discrepancy, previous studies have documented the challenges associated with *in situ* snowfall measurements (Adam and Lettenmaier 2003; Kotlarski et al. 2012;

Yang et al. 1998). Thus, there are reasons to use the historical gridded ACSNOW variable in comparison to observed cold season precipitation, when the predominant precipitation type is snow.

The correlations between historically observed winter precipitation at Barrow, Fairbanks and Nome and the ACSNOW variable from their coincident downscaled ERA-Interim grid cells is statistically significant ($p < 0.05$, student's t-test; Figure 4.3). It is assumed that snow is the predominant precipitation type at these stations from December through March; the 1981-2010 average temperature during these months at Barrow, Nome and Fairbanks is -24.6 ˚C, -17.8 ˚C and -13.3 ˚C, respectively (NOAA 2018). From December through March, the monthly linear regression between observed precipitation and ERA-Interim ACSNOW provides slope values (i.e., change in ACSNOW per change in observed PCPT) that range between 0.94-1.09 for Fairbanks, 1.31-2.83 for Barrow, and 1.06-1.37 for Nome. This indicates that the largest overestimation of snowfall from the reanalysis occurs at Barrow. These relationships, at widely disparate locations, provide a measure of confidence that the downscaled ACSNOW variable reasonably captures snowfall across Alaska. However, a limitation to this assumption is that these stations are all at low elevation, and thus the 'observed precipitation/modeled ACSNOW' relationship might not hold at higher elevations. Furthermore, the downscaled reanalysis shows a tendency to produce greater snowfall amounts.

Future projections in the results section are frequently discussed in reference to the downscaled CCSM4 and GFDL-CM3 historical periods, but are not bias-corrected according to the ERA-Interim. This is because the coarse ERA-Interim SWE parameterizations leads many alpine grid cells in Alaska to have 10,000 mm of SWE, an

unrealistically high value (Drusch et al. 2004). This, in turn, produces unrealistic SWE values in the downscaled simulation. The future projections utilize both the ACSNOW and SWE variables, thus it is for consistency that none of the snow season projections are presented and discussed in relation to the ERA-Interim.

4.4 Results

4.4.1 Elevation dependency of projected snowfall

The statewide annual cycle of monthly ACSNOW, produced by the summation of daily values that are averaged by 30-year periods, is shown in Figure 4.4. These time series represent the historical period (1981-2010) and three future periods (2011-2040; 2041-2070; 2071-2100) that are based on the RCP8.5 emissions scenario for CCSM4 (Figure 4.4, left) and GFDL-CM3 (Figure 4.4, right) The time series are further divided into two elevation bins: low grid cells (0-1000 m; Figure 4.4a) and high grid cells (1000-2000 m Figure 4.4b). Above 2000 m, the downscaled model topography has fewer than 10 grid cells for every 100 m higher, so elevations above 2000 m were left out of the analysis.

At low elevations (Figure 4.4a), CCSM4 and GFDL-CM3 show decreased snowfall in nearly every month with the advance of each 30-year period. CCSM4 produces more snowfall than GFDL-CM3 during all periods; however, the magnitude of the discrepancy between the two models is lowest at the end of the century. The greatest monthly ACSNOW depicted by CCSM4 during the historical period is 70.1 mm for January, but for GFDL-CM3 the highest value occurs in December (47.1 mm). For the late-century (2071-2100), the peak monthly value for CCSM is 50.8 mm, and for GFDL-CM3 it is

39.7 mm, both in December. When comparing the late-century with the historical period, the annual ACSNOW reductions at low elevations, by percentage, are 41.3% and 40.6% for CCSM4 and GFDL-CM3, respectively.

At high elevations (Figure 4.4b), projected changes in the annual ACSNOW cycle are dependent on the month. From May-October, both models show reduced amounts, with the summer months depicting nearly no snowfall by the late century. During the months with the least incoming solar radiation (i.e., November, December and January), GFDL-CM3 shows increased ACSNOW during the late-century; likewise, CCSM4 displays increases in December. The combination of increased winter snowfall and decreased warm season snowfall leads to annual reductions of 13.5% and 14.2% for CCSM4 and GFDL-CM3, respectively. The percentage reductions are much smaller than at lower elevations. In comparison to the low elevation grid cells, CCSM4 produces more snowfall at high elevations than does the GFDL-CM3.

The April 1 (e.g., end-of-winter) SWE, binned into 100 m elevation intervals and averaged over the same 30-year periods as before, is shown for CCSM4 (Figure 4.5a) and GFDL-CM3 (Figure 4.5b). Historically, the models exhibit similar April 1 SWE up to 500 m; however, higher up, the GFDL-CM3 depicts a thicker snowpack that is 80.8 mm deeper than CCSM4 in the 1900-2000 m bin. With each 30-year advance, April 1 SWE is projected to decrease and the greatest reductions, by percentage, occur at the lowest elevations. At the lowest interval (i.e., 0-100 m), CCSM4 shows a 63.3% decrease from 98.0 mm to 36.0 mm when comparing the historical period with the late century. For GFDL-CM3, these values are 88.6 mm to 16.4 mm, representing an 81.5% decrease. GFDL-CM3 shows larger reductions at every level, such that despite having greater SWE

during the historical period, it displays lower values at every elevation by the late century.

One reason for these SWE reductions is that the ratio of snow to total precipitation is projected to decrease. During the historical period, snow represented 47.8% and 41.5% of the total precipitation that fell in Alaska from September-November (SON) for CCSM4, and GFDL-CM3, respectively. For the late-century period, these values are projected to drop to 24.8% and 16.7%. For meteorological winter (DJF), 80.7% (CCSM4) and 75.9% (GFDL-CM3) historically fell as snow; however, these percentages drop to 51.4%, and 46.8% by the late-century, respectively. Thus, considerably more rainfall is anticipated during the cold season, which also suggests that temperatures will be near and above freezing more frequently.

4.4.2 Changes to snow season length

Each cold season, mainland Alaska has historically experienced a continuous period with snow cover. The average first snow-free date of the year, defined as SWE $\leq$ 2.0 mm, exhibits a wide range across Alaska according to both the CCSM4 (Figure 4.6, top left) and GFDL-CM3 (Figure 4.6, top right). Many mountainous and northern locations do not melt out until after the summer solstice, if at all. Interior areas generally lose their snowpack during May, while low elevations in southern Alaska melt out during March and April. Some coastal areas in the Aleutian Islands and southeast Alaska do not have continuous snow cover during the winter. The CCSM4 shows a tendency for later snow-free dates compared to GFDL-CM3.

Projections of snow-free dates indicate earlier melt outs that range from approximately one month across high terrain to complete loss of continuous winter snowpack. For the nearest downscaled CCSM4 grid cell to Barrow, the historical snow-free date is June 15 and is projected to advance to May 27 during 2071-2100; for GFDL-CM3 these dates are June 22 and April 16. The Nome grid cell displays much larger changes, however. The analogous historical values for CCSM4 and GFDL-CM3 are May 24 and April 19, and these advance to February 7 and January 26, respectively. This is possibly due to Nome's closer proximity to the seasonal sea-ice edge, wherein the trajectory of incoming cyclones increasingly is projected to cross open water as opposed to ice, bringing warmer air and rainfall. Such early dates indicate an effective end to the presence of continuous winter snowpack at Nome. By the late-century period, mountain grid cells that did not previously melt out (e.g., in the Wrangell Mountains) now show earlier snow-free dates, suggesting the potential for rapid glacial ice loss. For reference, the historical spring snow-off dates (i.e., first date with a snow depth below 2.54 mm) from the GHCN-D station data for Barrow and Nome are May 27 and May 9, respectively. These discrepancies between the nearest grid cells and the stations arise from the spatial-scale mismatch between the gridded data, which represent areal averages, and point observations from coastal locations.

The onset of snow date, when SWE is continuously greater than or equal to 2.0 mm, shows similarly pronounced changes with each 30-year period. Historically, the snowpack develops during late September for mountain areas and the North Slope, October for the Interior, and November for south and southwest Alaska. The historical CCSM4 (Figure 4.7, top left) and GFDL-CM3 (Figure 4.7, top right) display comparable

spatial patterns. GFDL-CM3 shows a more delayed onset of snowpack in the future periods, but both models indicate a later start to the snow season. The nearest downscaled CCSM grid cell to Fairbanks shows a historical snow onset of October 20 to a late-century onset of November 17. For GFDL-CM3 the onset shifts from October 17, changing to December 4. Along the Arctic coast at Barrow, CCSM4 shows a change from October 8 to November 11, and GFDL-CM3 indicates a change from October 3 to December 14. The latter coincides with the absence of sea ice in the Chukchi and Beaufort Seas from 2071-2100 (see Figure 10, Lader et al. 2017), which would support a maritime climate at Barrow even during winter. The historical average snow onset date for Fairbanks and Barrow from the GHCN-D station data is October 16 and September 30, respectively.

4.4.3 Projections of extreme snowfall

The annual maximum 2-day ACSNOW for the nearest downscaled grid cells to Anchorage, Barrow, Fairbanks and Nome (Figure 4.8, a-d) show different responses that depend on location and time period. The total ACSNOW amount for two consecutive days is used, rather than a single day, to account for events that begin one day and continue into the next. At Anchorage, the average annual maximum ACSNOW reduces from 17.6 mm (CCSM4) and 17.2 mm (GFDL-CM3) during the historical period to 11.2 mm (CCSM4) and 8.2 mm (GFDL-CM3) for the late century. There is also a clear tendency for the absolute highest totals at Anchorage to occur during the historical and early-century periods. For Barrow and Fairbanks, a trend is not evident. When comparing the historical and late-century periods, CCSM4 indicates a slight decrease in the average

annual maximum ACSNOW amount, but GFDL-CM3 shows an increase. The largest events at Barrow and Fairbanks tend to occur in the early time periods; however, there are amounts from the late-century that are among the top 10 highest of all 120 years for each simulation. Nome is similar to Anchorage in that the average annual maximum amount is reduced from 30.0 mm to 20.5 mm according to CCSM4 and from 21.7 mm to 15.9 mm for GFDL-CM3. The highest amounts at Nome (e.g., top 10) all occur in the earlier periods and by the late century there are annual maxima ACSNOW amounts in the 5-15 mm range.

Historical sea-level pressure (SLP) composites that occur concurrently with the top 10 annual 2-day snowfall maxima for Anchorage, Barrow, Fairbanks and Nome are displayed in Figure 4.9. These events are based on actual snowfall observations from the GHCN-D database from 1981-2010, and represent the 2-day average SLP for each ERA-Interim grid cell. The SLP pattern for extreme snowfall events at Anchorage indicates a low-pressure center located directly to the south, bringing in relatively warm, moisture-laden air. For Barrow, the circulation pattern is less coherent, but most of the region is under low pressure. The Fairbanks composite indicates a gradient with low SLP over Bering Strait and high SLP anchored in the western Gulf of Alaska, generating a southwesterly flow that supports moisture flux to the north of the Alaska Range. For Nome, a strong pressure gradient is evident with low pressure east of the Kamchatka Peninsula and high pressure across the eastern interior of Alaska. This promotes a broad southerly flow, bringing moisture northward across southwest Alaska and the Seward Peninsula.

The historical (1981-2010) SLP composites from the CCSM4 (Figure 4.10, left), representing the top 10 annual 2-day ACSNOW amounts from the climate model, display varying agreement with the ERA-Interim patterns. For Anchorage, the CCSM4 shows low pressure to the south-southwest of Anchorage, similar to ERA-Interim, but it exhibits a large discrepancy between the observed (ERA-Interim) SLP composites for events at Barrow. For Fairbanks, the CCSM4 displays a strong pressure gradient, comparable to ERA-Interim, directing warm, moist air northeastward across Interior Alaska. The SLP composites for Nome are similar to the ERA-Interim pattern, but CCSM4 appears to have much higher pressure across the domain. Late-century (2071-2100) changes to the CCSM4 SLP patterns (Figure 4.10, right) generally portray lower pressure region-wide, and weaker pressure gradients. However, the broad patterns remain comparable in the late-century period.

The analogous historical SLP composites from the GFDL-CM3 (Figure 4.11, left) agree well with the ERA-Interim patterns at Anchorage and Nome, and show a closer agreement at Barrow than does the CCSM4. However, the GFDL-CM3 pattern for Fairbanks shows little resemblance to ERA-Interim. It is not readily apparent that one model captures the ERA-Interim SLP patterns better than the other when comparing the four locations. Late-century changes from the GFDL-CM3 (Figure 4.11, right) again indicate weaker pressure gradients, which could help explain the trend for lower extreme snowfall amounts at Anchorage and Nome. If moisture transport from the south were reduced, then this would limit snowfall potential. Warmer temperatures are also anticipated under the RCP8.5 emissions scenario, which could cause some of the precipitation that historically fell as snow to fall as rain instead. The late-century GFDL-

CM3 tends to have higher pressure than during the historical and displays little atmospheric steering for its high snowfall events except at Nome. An alternative explanation for the reduced pressure gradients in the SLP composites is that the individual event patterns could be more diverse than previously observed.

4.5 Discussion

A comparison of the projected annual cycle of ACSNOW with end-of-winter (i.e., April 1) SWE at high elevations highlights the competing effects at work in future changes of snow over Alaska. For locations above 1000 m, CCSM4 shows the highest December snowfall occurring in the late-century period, and GFDL-CM3 shows this for the three-month stretch from November-January (Figure 4.4b). Yet, end-of-winter SWE is projected to decline for all elevations with the advance of each period (Figure 4.5). This reduction cannot be fully explained by lower monthly snowfall in the late summer and autumn. The 8-month ACSNOW sum, beginning in August and ending in March, is only 5-10% lower in the late-century period than in the historical, depending on the model. The analogous high-elevation reductions of SWE average between 31-65% for CCSM4 and GFDL-CM3, respectively. The implication here is that considerable snowfall is projected to melt and run off after it falls.

Snow-season length, defined here as the continuous period with a minimum of 2.0 mm of SWE on the ground, shows unambiguous declines, but the rate of decrease depends on location and time period. The greatest changes are projected for the last two 30-year periods, which corresponds to when the changes in projected radiative forcing from the RCPs diverge (Kunreuther et al. 2014), thus suggesting that current decision-

making can meaningfully impact the future. Location-specific changes to snow season timing indicate a tendency for earlier snow-off than for later snow onset. This is true for the nearest downscaled grid cell to Anchorage, Fairbanks and Nome for both models. Barrow shows a larger change to later snow onset than for earlier snow-off. The projected rate of decline of snow-season length over the full period is generally higher than recently observed. Liston and Hiemstra (2011) noted a rate of -2.6% days decade^{-1} from 1979-2009 across the Arctic, but the rates found here are generally 2-5 times higher. In closer comparison, however, Barrow has shown an earlier snow-off date of -2.86 days decade^{-1} and a later onset date of 4.6 days decade^{-1} from 1975-2016 (Cox et al. 2017), which taken together, suggests approximately a one week reduction in snow season length per decade.

Accurate simulations of snow season length, snowfall, and air temperature are critical to the future states of near-surface permafrost (NSP) and seasonally frozen ground. Using a multi-model ensemble from the CMIP5, Peng et al. 2018 found that active layer thicknesses across northern Alaska are projected to increase by 20 cm when comparing 2071-2100 with 1971-2000. Overall, they found that soil temperatures at 1 m depth are projected to warm between 1-4 ˚C (2080-2099 minus 1950-1969). Lawrence and Slater (2010) studied the relative impacts of changes to snow season length and snow depth, finding mixed results. Later onset of snow in Alaska cooled the soil due to sub-freezing temperatures with minimal absorbed solar radiation, but an earlier melt yielded increasing soil temperatures. A shallower winter snowpack reduced the snow's insulating effect and contributed to cooling. A subsequent study by Lawrence et al. (2012) investigated how climate model biases of temperature and snow depth impact projections of NSP by 2100. Using an offline version of the land model from CCSM4, one that used

observed meteorological data, rather than the warm and wet biased climate model, the magnitude of permafrost loss was 29% less.

Projected changes to snowfall extremes described in Figure 4.8 are consistent with previous studies that examined a large set of CMIP5 models across the Northern Hemisphere (Danco et al. 2016; Krasting et al. 2013). That is, despite a decrease in total annual snowfall for most locations, many sites are expected to continue to see high daily snowfall amounts. This is particularly true for more northerly, continental or high-elevation locations and for the core winter months. The four locations chosen in this study exhibit these patterns. Anchorage (Figure 4.8a) has a maritime climate and shows late-century decreases in annual maximum ACSNOW amount of 36% (CCSM4) and 53% (GFDL-CM3). Similarly, Nome (Figure 4.8b) has a seasonally maritime climate and displays reductions of 32% and 27%, respectively. Fairbanks (Figure 4.8c), with its cold continental climate, and Barrow (Figure 4.8d), located at high latitude and seasonally continental, do not show large changes in projected extreme snow amounts. O'Gorman et al. (2014) suggest that snowfall extremes tend to occur within a favorable temperature range that will continue to be realized in the Arctic, even under rapid warming.

4.6 Conclusions

This study investigates projected changes of important snow season indicators for Alaska over 30-year periods (i.e., 1981-2010, 2011-2040, 2041-2070, and 2071-2100) using a combination of observations, downscaled reanalysis and climate model simulations. The dynamical downscaling provides finer spatial detail than previous research that analyzed a set of CMIP5 models, and a more comprehensive set of variables

than is made available from statistical downscaling. Total annual snowfall is projected to decrease with the advance of each 30-year period for all elevations at and below 2000 m; however, low elevations (0-1000 m) reveal more substantial decreases. This discrepancy results from increased snowfall during the core winter months at high elevations. Despite these differences, all elevations show reduced end-of-winter (April 1) SWE with each successive 30-year period.

The most pronounced changes tend to occur in the mid- and late-century periods, which coincides with the RCP scenario divergence. The full-century projections of snow onset and snow-off dates show trends that are 2-5 times higher than recently observed. However, modeled trends between the early-century period (2011-2040) and the historical are similar. This suggests that short-term policy decisions that shape the trajectory of greenhouse gas emissions could substantially impact the long-term snow season characteristics of Alaska. This is especially important for spring soil recharge, which utilizes snow meltwater almost exclusively. Furthermore, despite projected snowfall increases at high elevations during the coldest months and no apparent changes to extreme snowfall at Fairbanks and Barrow, these distributions show a seasonal compression. That is, with continued warming to the coldest months, all locations will eventually experience reduced mean and extreme snowfall, regardless of latitude or elevation.

4.7 Acknowledgements

Support for this work was provided by the National Science Foundation, Office of Polar Programs through Grant PLR-1268350, and by the NOAA Climate Program Office

through Grant NA16OAR4310162 to the Alaska Center for Climate Assessment and Policy. The project described in this publication was supported by Cooperative Agreement No. G17AC00213 from the United States Geological Survey. Its contents are solely the responsibility of the authors and do not necessarily represent the views of the Alaska Climate Adaptation Science Center or the USGS. This manuscript is submitted for publication with the understanding that the United States Government is authorized to reproduce and distribute reprints for Governmental purposes. This work was supported in part by the high-performance computing and data storage resources operated by the Research Computing Systems Group at the University of Alaska Fairbanks, Geophysical Institute.

4.8 Figures

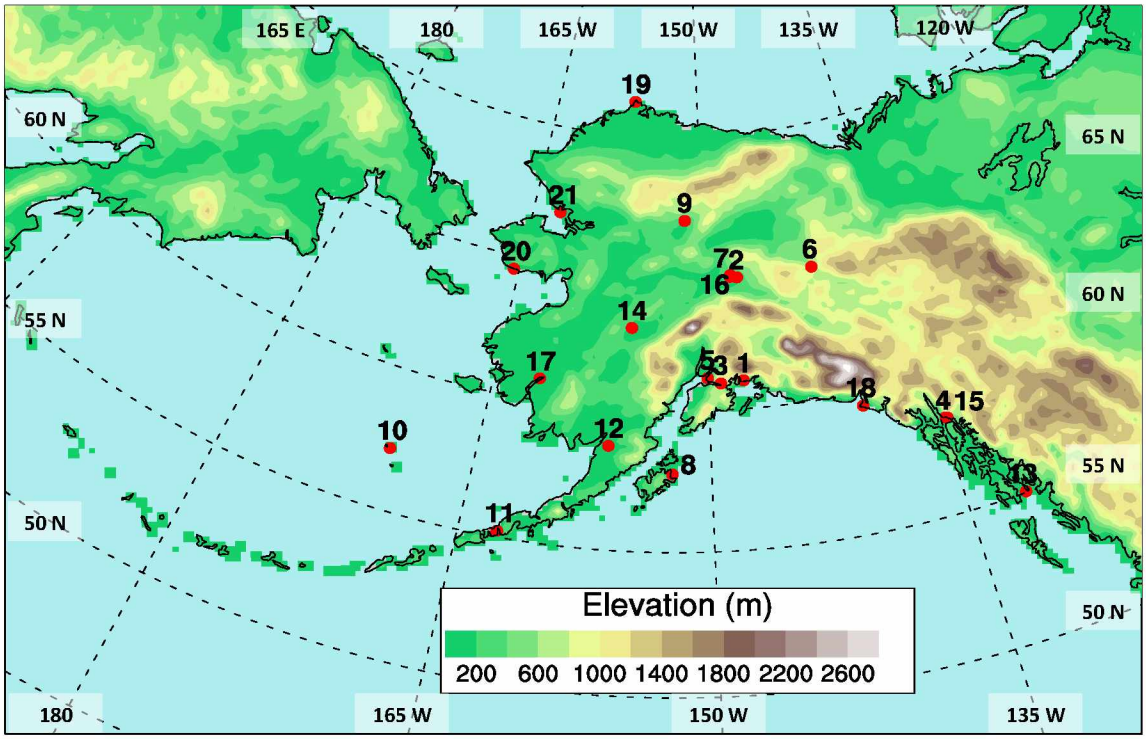

Figure 4.1 Distribution of stations, superimposed on regional orography, with ≥ 95% daily coverage (1981-2010) of precipitation, snowfall, and snow depth. A description of the numbered stations is located in Table 1.

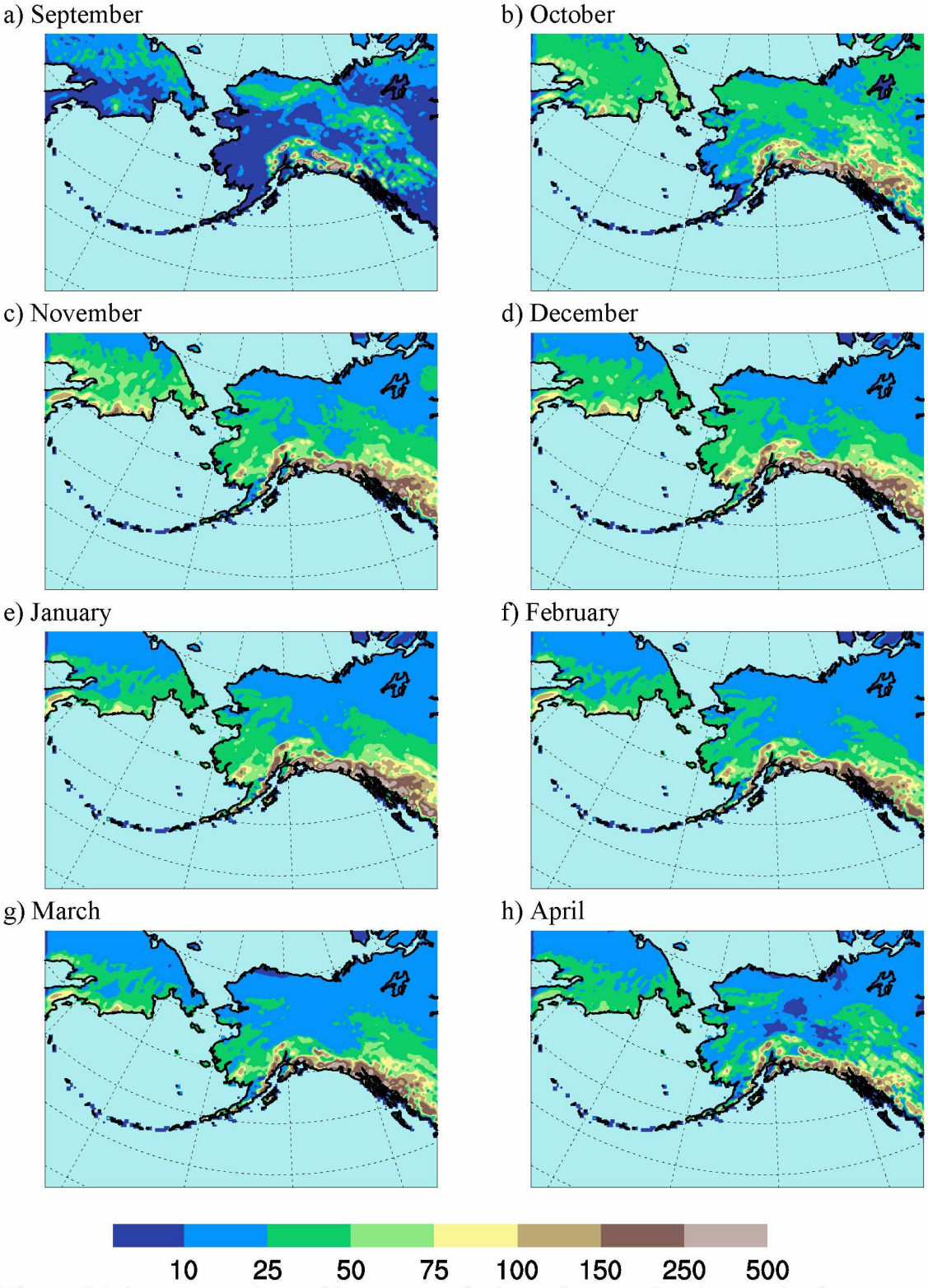

Figure 4.2 Average total monthly water equivalent of accumulated snow depth (ACSNOW; mm) from downscaled ERA-Interim (1981-2010).

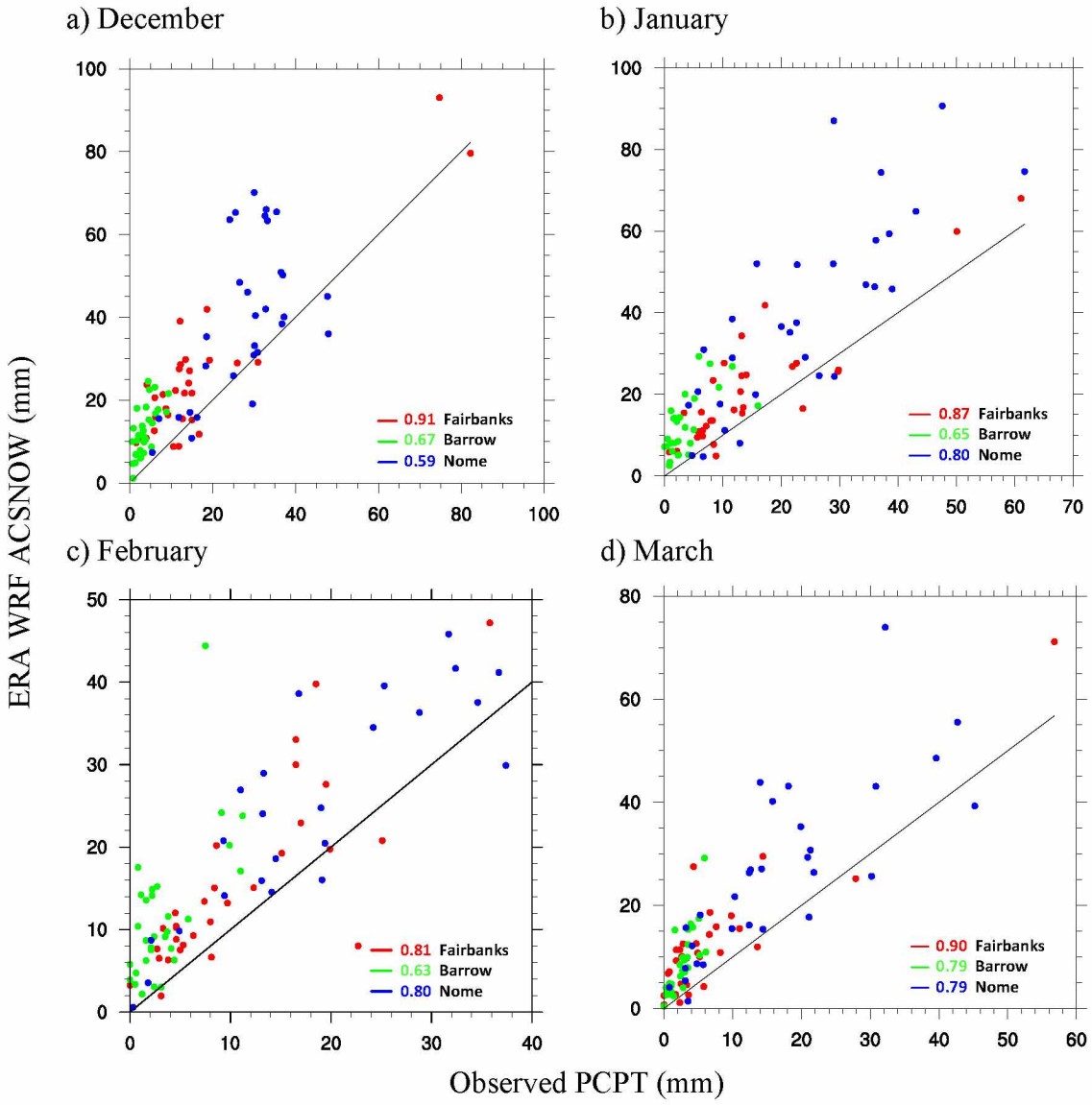

Figure 4.3 Scatterplots between total monthly observed precipitation (PCPT; mm) at three stations: Fairbanks International Airport (red), Wiley Post-Will Rogers Memorial Airport (Barrow; green), and Nome Airport (blue) and downscaled ERA-Interim water equivalent of accumulated snow depth (ACSNOW; mm) from 1981-2010. Correlation coefficient (r) is provided with the legend and all values are statistically significant ($p < 0.05$; student's t-test).

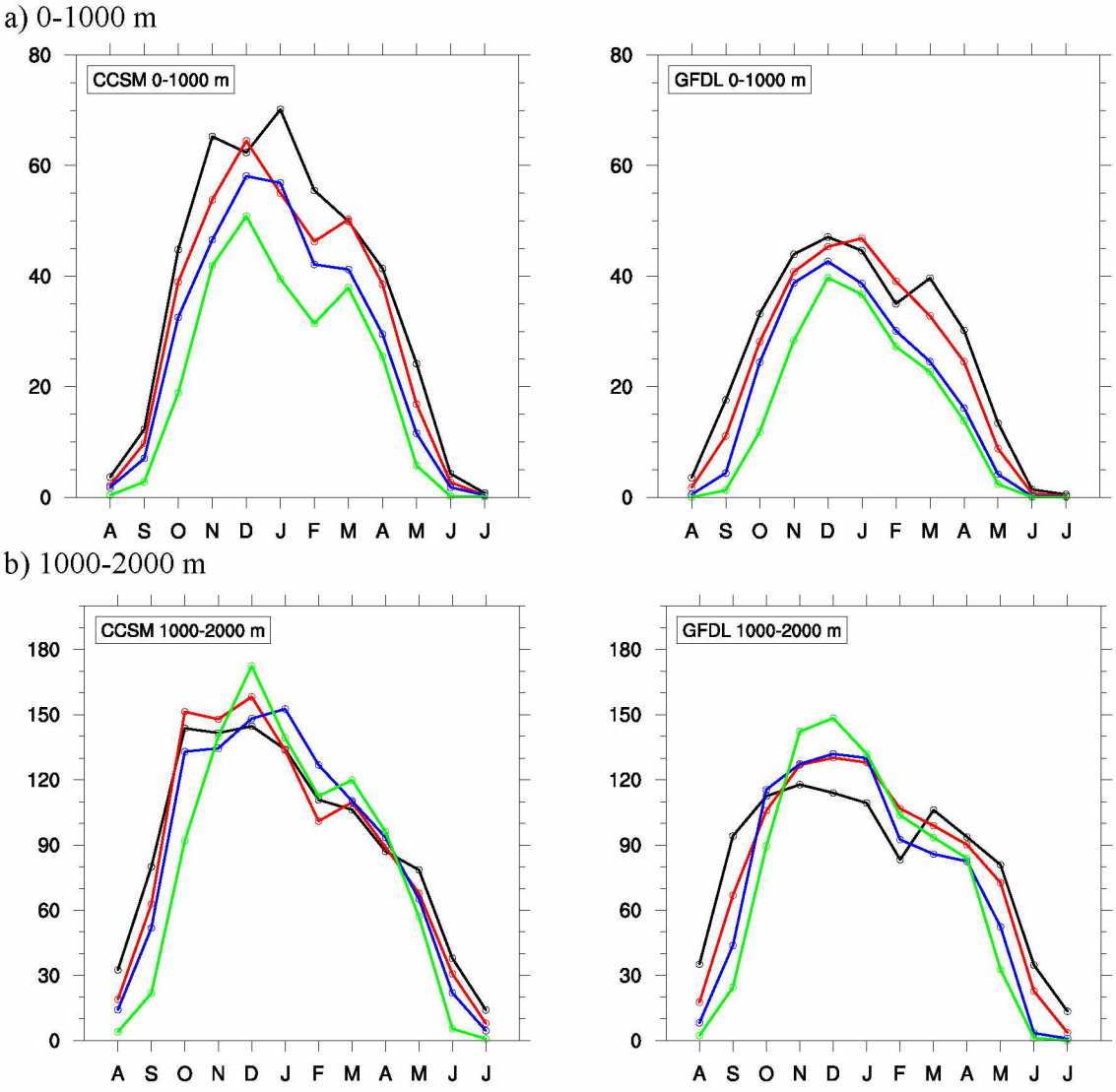

Figure 4.4 Monthly averaged water equivalent of accumulated snow depth (ACSNOW; mm) for elevations a) 0-1000 m and b) 1000-2000 m. Time series represent the downscaled CCSM (left) and GFDL (right) for 30-year periods across Alaska. These include: 1981-2010 (black), 2011-2040 (red), 2041-2070 (blue), and 2071-2100 (green).

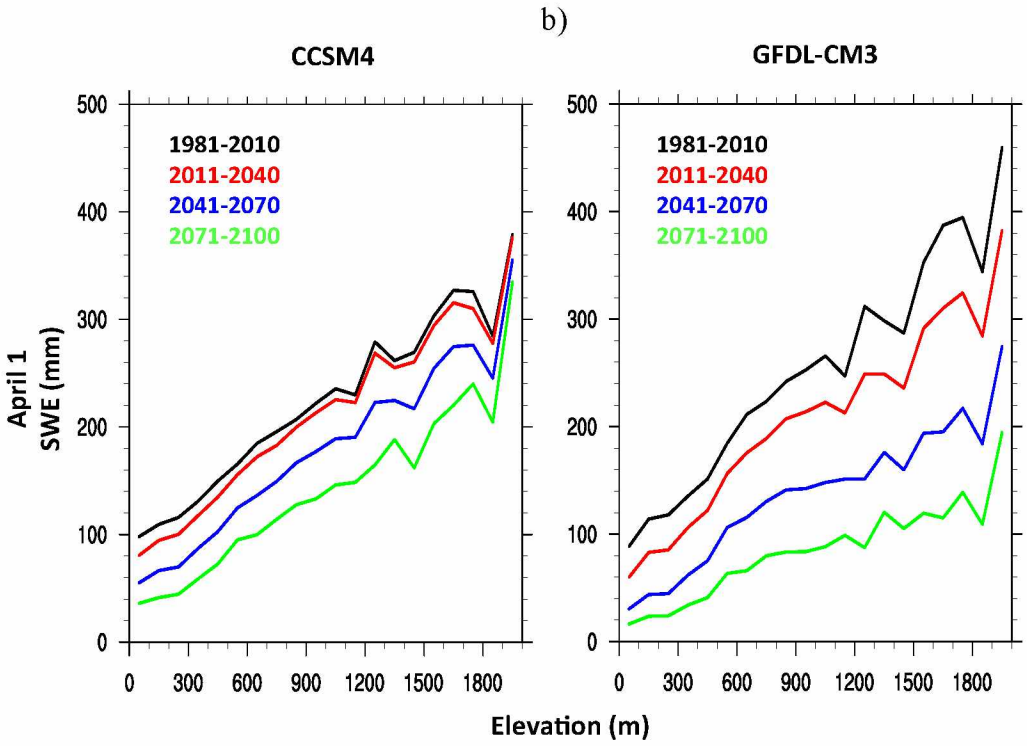

Figure 4.5 April 1 snow-water equivalent (SWE; mm) for a) CCSM and b) GFDL. Downscaled grid cells have been binned in 100-m elevation intervals and averaged for 30-year periods across Alaska. These include: 1981-2010 (black), 2011-2040 (red), 2041-2070 (blue), and 2071-2100 (green).

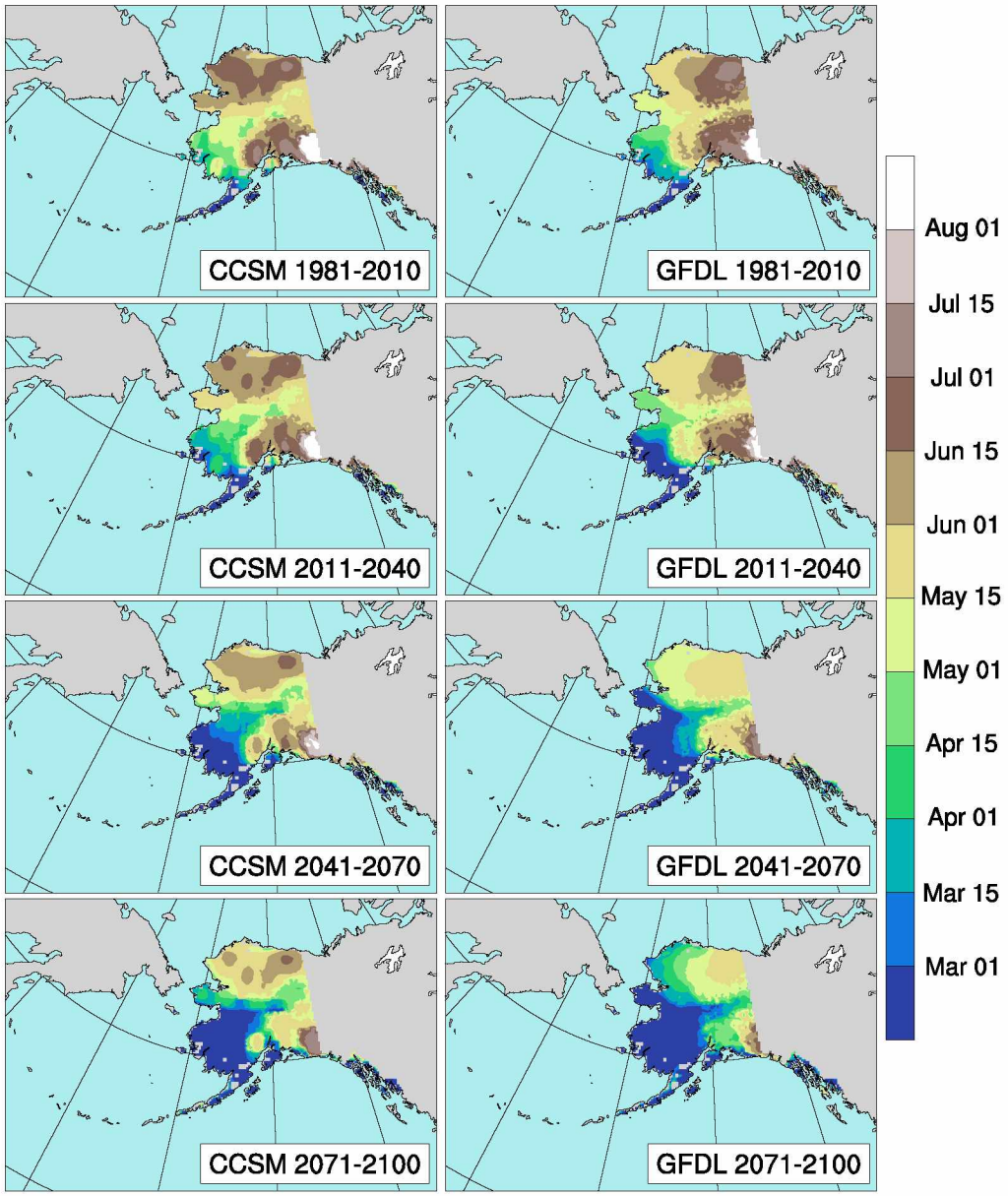

Figure 4.6 First snow-free date (SWE ≤ 2 mm) averaged for downscaled CCSM (left) and GFDL (right) over the indicated 30-year periods across Alaska.

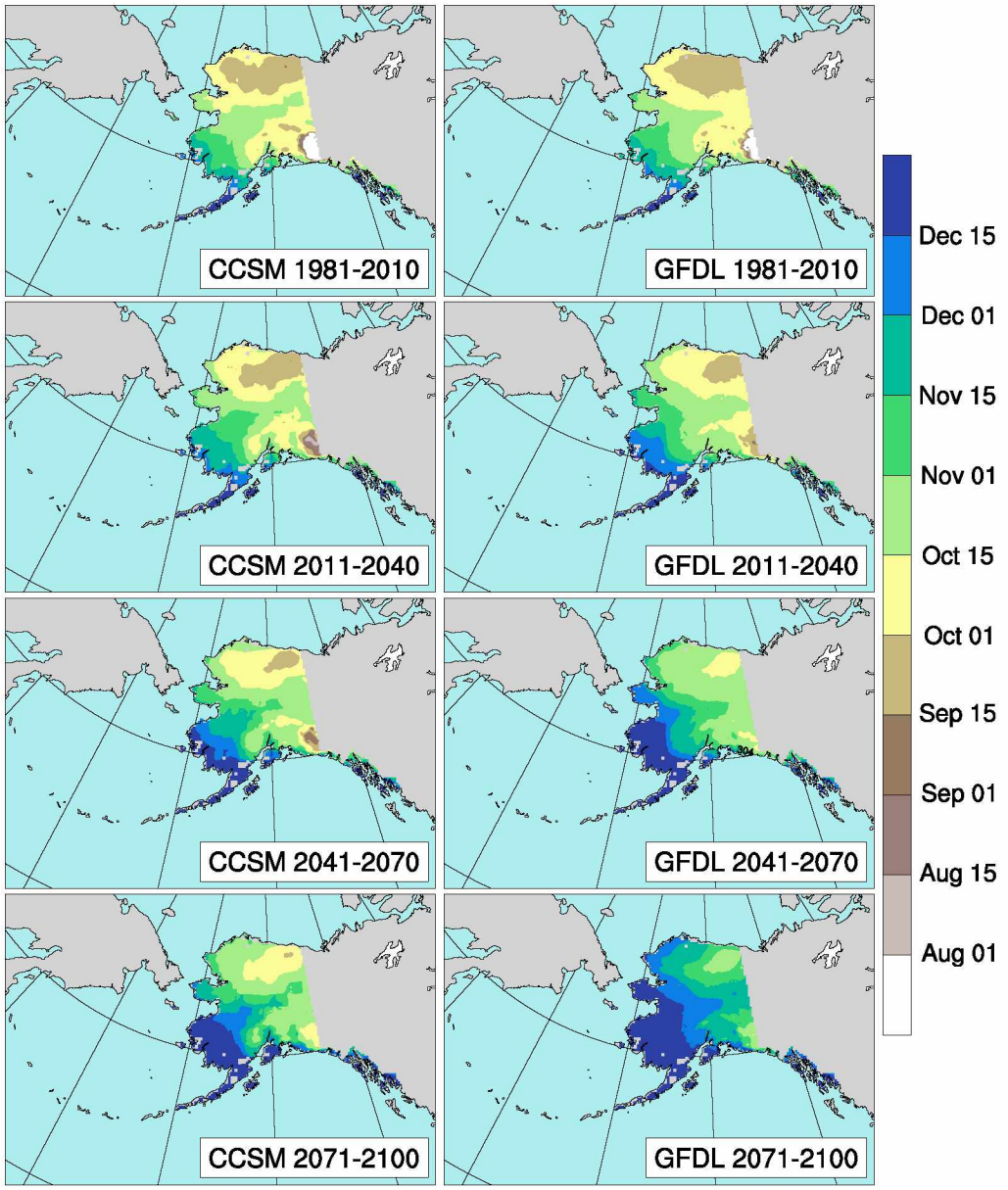

Figure 4.7 Onset of snow date (SWE continuously ≥ 2 mm) averaged for downscaled CCSM (left) and GFDL (right) over the indicated 30-year periods across Alaska.

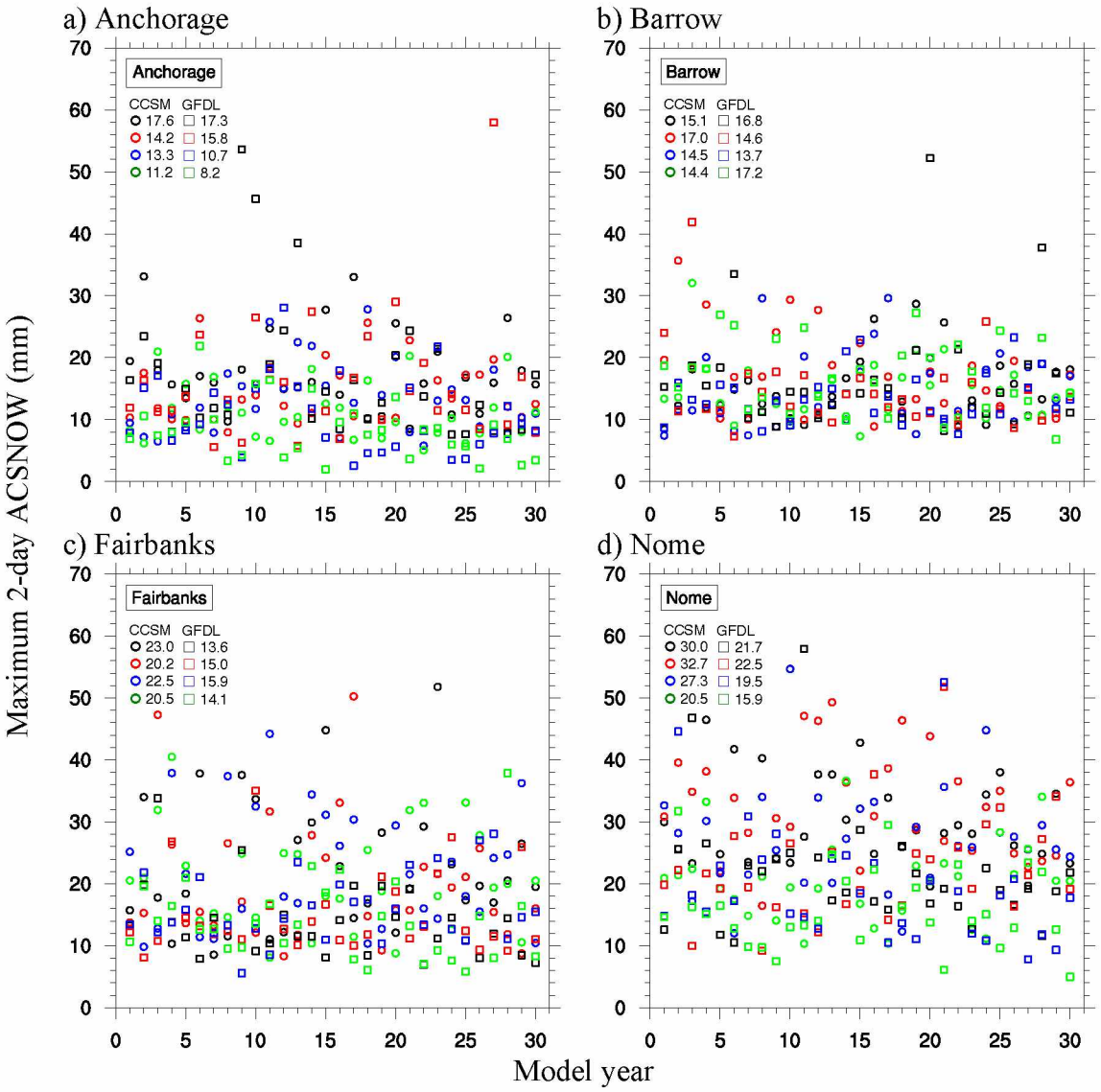

Figure 4.8 Annual 2-day maxima of water equivalent of accumulated snow depth (ACSNOW; mm) for the nearest downscaled grid cells to a) Anchorage, b) Barrow, c) Fairbanks, and d) Nome. Time series represent the downscaled CCSM (circles) and GFDL (squares) for 30-year periods across Alaska. These include: 1981-2010 (black), 2011-2040 (red), 2041-2070 (blue), and 2071-2100 (green). The 30-year average for each times series is provided in the upper left of each panel.

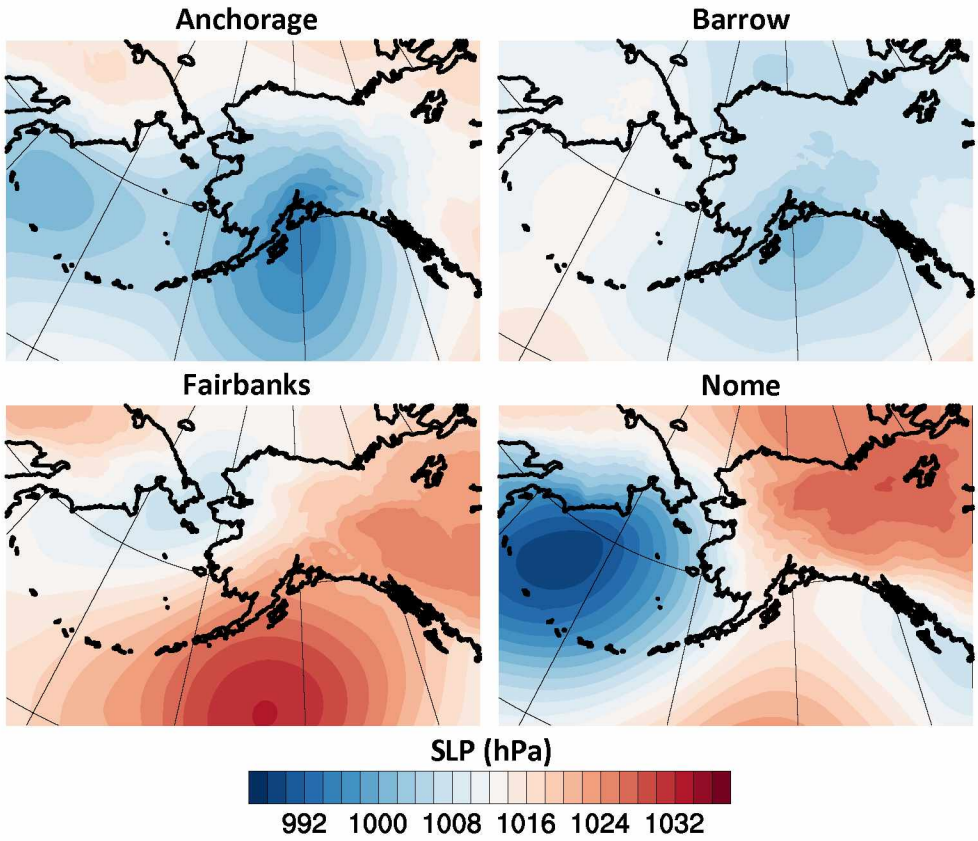

Figure 4.9 Historical (1981-2010) ERA-Interim sea level pressure (SLP; hPa) composites of the top ten annual snowfall maxima for Anchorage, Barrow, Fairbanks and Nome as indicated. Extreme snowfall events are selected from airport observations at each station.

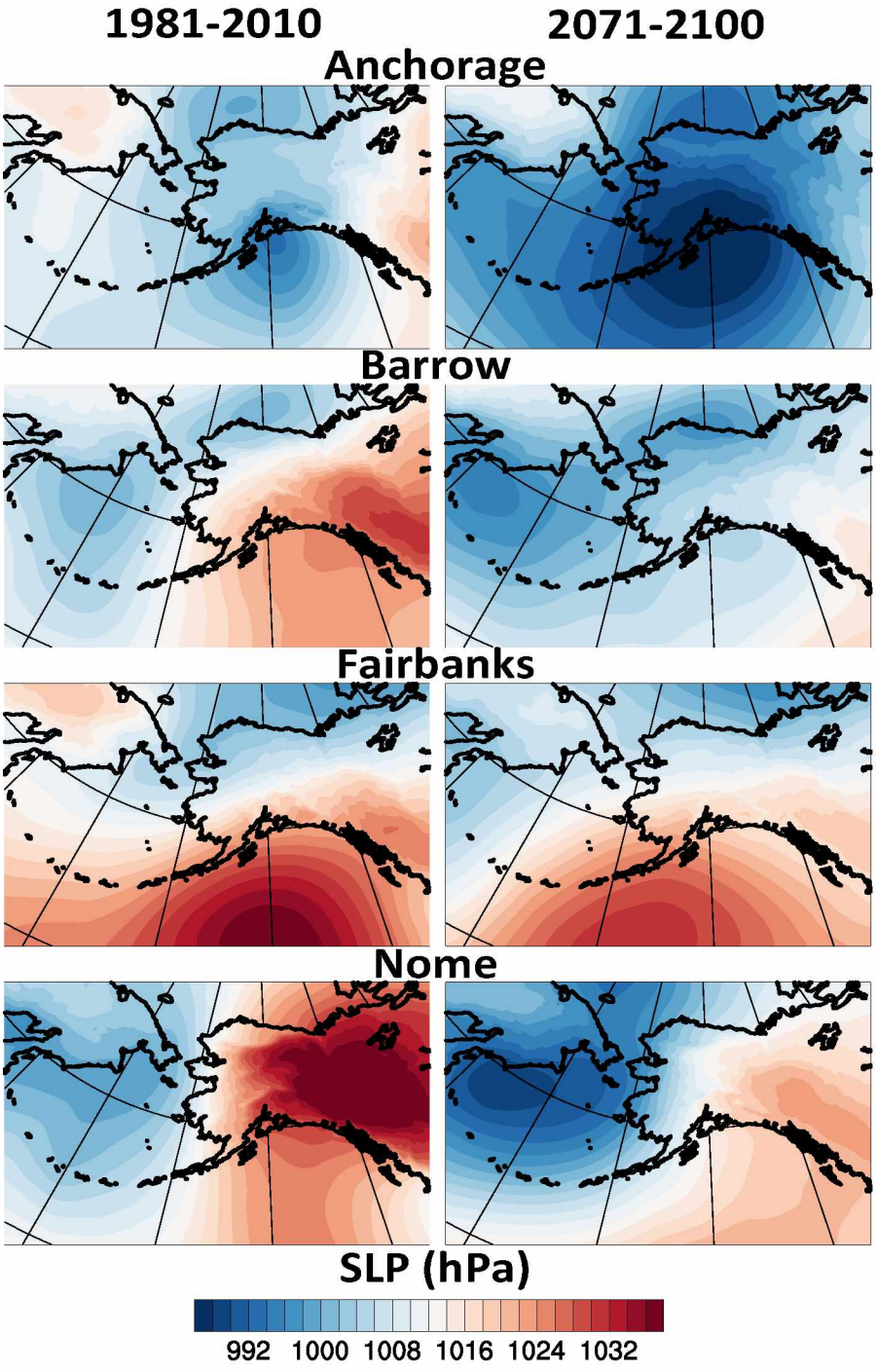

Figure 4.10 Historical (1981-2010; left) and late-century (2071-2100; right) sea level pressure (SLP; hPa) composites of the top ten annual snowfall maxima for the nearest downscaled CCSM4 grid cells to Anchorage, Barrow, Fairbanks and Nome.

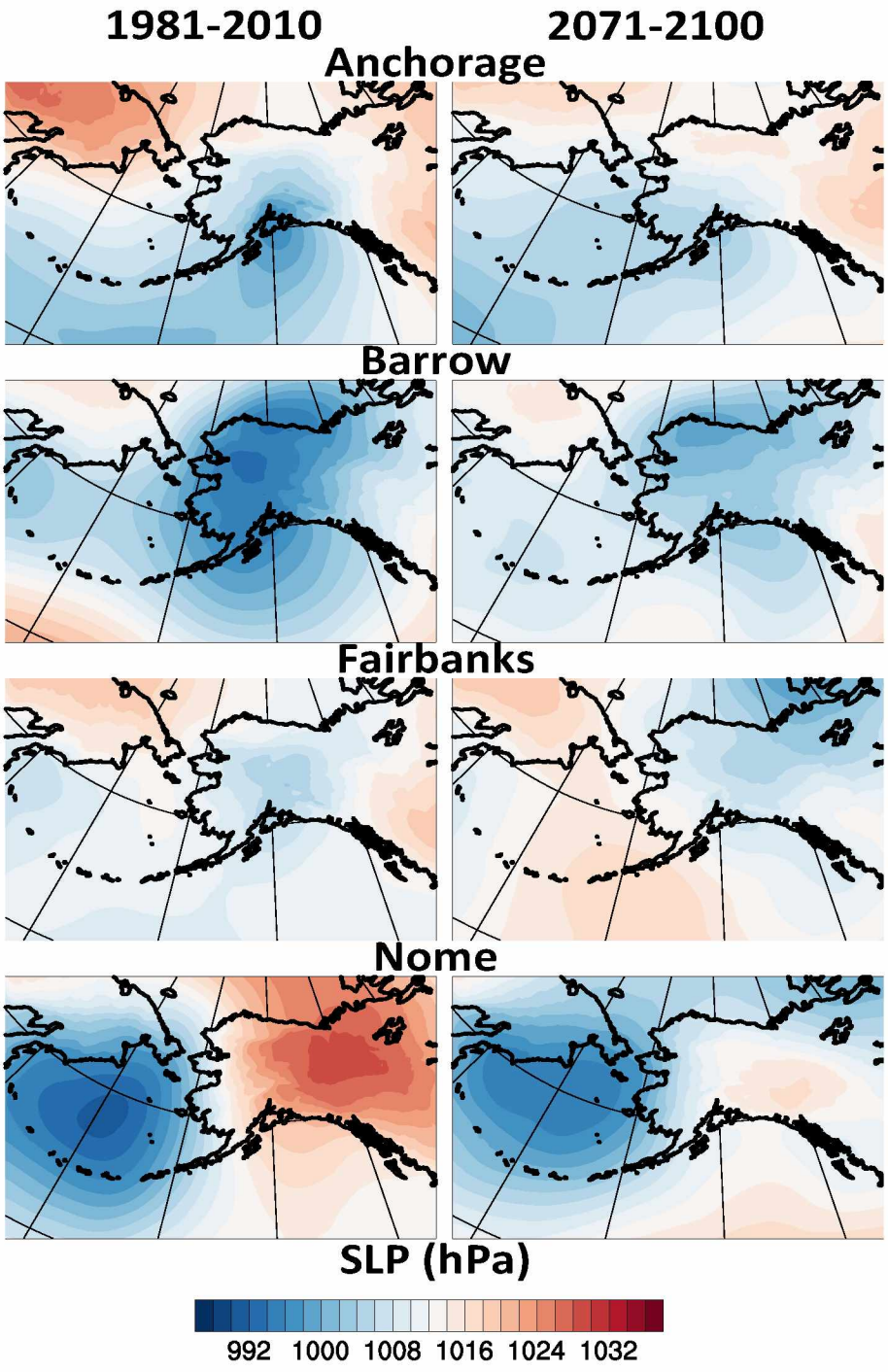

Figure 4.11 Historical (1981-2010; left) and late-century (2071-2100; right) sea level pressure (SLP; hPa) composites of the top ten annual snowfall maxima for the nearest downscaled GFDL-CM3 grid cells to Anchorage, Barrow, Fairbanks and Nome.

4.9 Tables

Table 4.1 Station information and annual cold season (i.e., all months excluding May-September) mean ($\bar{x}$), standard deviation (s) and linear regression coefficient (rc; per decade) of precipitation (PCPT; mm) and snowfall (SNOW; cm) from 1981-2010. Trend significance ($p < 0.05$; student's t-test) is shown in bold.

Num.	Station name	Lat. (°N)	Lon. (°W)	Elev. (m)	PCPT			SNOW		
					$\bar{x}$	s	rc	$\bar{x}$	s	rc
1	Cannery Creek	61.0	147.5	26	1739	319	-38	353	110	19
2	North Pole	64.8	147.3	145	113	80	-18	124	54	-14
3	Alyeska	61.0	149.1	83	1251	309	36	547	168	**106**
4	Auke Bay	58.4	134.7	13	849	194	-25	201	102	16
5	Anchorage	61.2	150.0	37	170	40	-5	190	53	**22**
6	Eagle	64.8	141.2	259	102	23	4	152	38	-5
7	College	64.9	147.9	182	107	41	-12	158	68	-25
8	Kodiak	57.8	152.5	24	1266	257	38	190	80	26
9	Bettles	66.9	151.5	196	145	52	20	221	70	7
10	St. Paul Island	57.2	170.2	11	343	71	-8	147	68	**34**
11	Cold Bay	55.2	162.7	24	646	203	60	184	65	5
12	King Salmon	58.7	156.7	20	211	57	-8	124	47	11
13	Annette	55.0	131.6	33	1771	257	29	84	52	**24**
14	McGrath	63.0	155.6	102	196	67	-11	241	82	-19
15	Juneau	58.4	134.6	5	928	228	75	220	113	28
16	Fairbanks	64.8	147.9	132	95	34	**-14**	157	64	-24
17	Bethel	60.8	161.8	31	186	54	17	152	53	**36**
18	Yakutat	59.5	139.7	10	2475	688	**-305**	399	157	12
19	Barrow	71.3	156.8	9	33	13	**7**	74	35	**34**
20	Nome	64.5	165.4	4	182	46	-2	187	55	**33**
21	Kotzebue	66.9	162.6	9	123	42	13	152	53	**35**

4.10 References

Adam, J. C., and D. P. Lettenmaier, 2003: Adjustment of global gridded precipitation for systematic bias. *J. Geophys. Res.*, **108**, D9, 4257, doi:10.1029/2002/JD002499.

AMAP, 2017: Snow, water, ice and permafrost summary. Summary for policy-makers. Arctic Monitoring and Assessment Programme (AMAP), Oslo, Norway. 20 pp.

Bieniek, P. A., U. S. Bhatt, L. A. Rundquist, S. D. Lindsey, X. Zhang, and R. L. Thoman, 2011: Large-scale climate controls of Interior Alaska river ice breakup. *J. Climate*, **24**, 286-297, doi:10.1175/2010JCLI3809.1.

Bieniek, P. A., and Coauthors, 2012: Climate divisions for Alaska based on objective methods. *J. Appl. Meteor. Climatol.*, **51**, 1276-1289, doi:10.1175/JAMC-D-11-0168.1.

Bieniek, P. A., U. S. Bhatt, J. E. Walsh, T. S. Rupp, J. Zhang, J. R. Krieger, and R. Lader, 2016: Dynamical downscaling of ERA-Interim temperature and precipitation for Alaska. *J. Appl. Meteor. Climatol.*, **55**, 635-654, doi:10.1175/JAMC-D-15-0153.1.

Bieniek, P. A., U. S. Bhatt, J. E. Walsh, R. Lader, B. Griffith, J. K. Roach, and R. L. Thoman, 2018: Assessment of Alaska rain-on-snow events using dynamical downscaling. *J. Appl. Meteor. Climatol.*, doi:10.1175/JAMC-D-17-0276.1, in press..

Brown, J, and V. E. Romanovsky, 2008: Report from the International Permafrost Association: State of permafrost in the first decade of the 21st century. *Permafrost and Periglac. Process.*, **19**, 255-260, doi:10.1002/ppp.618.

Brown, R. D., and D. A. Robinson, 2011: Northern Hemisphere spring snow cover variability and change over 1922-2010 including an assessment of uncertainty. *The Cryosphere*, **5**, 219-229, doi:10.5194/tc-5-219-2011.

Clilverd, H. M., D. M. White, A. C. Tidwell, and M. A. Rawlins, 2011: The sensitivity of northern groundwater recharge to climate change: A case study of Northwest Alaska. *J. Am. Water Resour. As.*, **47**, 1228-1240, doi:10.1111/j.1752-1688.2011.00569.x.

Cohen, J. L., J. C. Furtado, M. A. Barlow, V. A. Alexeev, and J. E. Cherry, 2012: Arctic warming, increasing snow cover and widespread boreal winter cooling. *Environ. Res. Lett.*, **7**, 014007, doi:10.1088/1748-9326/7/1/014007.

Cox, C. J., and Coauthors, 2017: Drivers and environmental responses to the changing annual snow cycle of northern Alaska. *Bull. Amer. Meteor. Soc.*, **98**, 2559-2577, doi: 10.1175/BAMS-D-16-0201.1.

Danco, J. F., A. M. DeAngelis, B. K. Raney, and A. J. Broccoli, 2016: Effects of a warming climate on daily snowfall events in the Northern Hemisphere. *J. Climate*, **29**, 6295-6318, doi:10.1175/JCLI-D-15-0687.1.

Dee, D. P., and Coauthors, 2011: The ERA-Interim reanalysis: Configuration and performance of the data assimilation system. *Quart. J. Roy. Meteor. Soc.*, **137**, 553-597, doi:10.1002/qj.828.

Derksen, C., R. Brown, L. Mudryk, and K. Luojus, 2016: Terrestrial Snow Cover [in Arctic Report Card 2016], http://www.arctic.noaa.gov/Report-Card.

Donner, L. J., and Coauthors, 2011: The dynamical core, physical parameterizations, and basic simulation characteristics of the atmosphere component AM3 of the GFDL global coupled model CM3. *J. Climate*, **24**, 3484-3519, doi:10.1175/2011JCLI3955.1.

Drusch, M. D., D. Vasiljevic, and P. Viterbo, 2004: ECMWF's Global Snow Analysis: Assessment and Revision Based on Satellite Observations. *J. Appl. Meteor.*, **43**, 1282-1294, doi:10.1175/1520-0450(2004)043<1282:EGSAAA>2.0.CO;2.

ESA, 2014: The third GlobSnow-2 newsletter gives an overview of the GlobSnow-2 SE and SWE v2.0 datasets released mid-December 2013, http://www.globsnow.info/index.php?page=Newsletters.

Estilow, T. W., A. H. Young, and D. A. Robinson, 2015: A long-term Northern Hemisphere snow cover extent data record for climate studies and monitoring. *Earth Sys. Sci. Data*, **7**, 137-142, doi:10.5194/essd-7-137-2015.

Frei, P., S. Kotlarski, M. A. Liniger, and C. Schär, 2017: Future snowfall in the Alps: projections based on the EURO-CORDEX regional climate models. *The Cryosphere*, **12**, 1-24, doi:10.5194/tc-12-1-2018.

Hall, A., 2004: The role of surface albedo feedback in climate. *J. Climate*, **17**, 1550-1568, doi:10.1175/1520-0442(2004)017<1550:TROSAF>2.0.CO;2.

Hinzman, L. D., and Coauthors, 2005: Evidence and implications of recent climate change in northern Alaska and other arctic regions. *Climatic Change,* **72**, 251-298, doi:10.1007/s10584-005-5352-2.

IPCC, 2013: *Climate Change 2013: The Physical Science Basis. Contribution of Working Group I to the Fifth Assessment Report of the Intergovernmental Panel on Climate Change* [Stocker, T.F., D. Qin, G.-K. Plattner, M. Tignor, S.K. Allen, J. Boschung, A. Nauels, Y. Xia, V. Bex and P.M. Midgley (eds.)]. Cambridge University Press, Cambridge, United Kingdom and New York, NY, USA, 1535 pp, doi:10.1017/CBO9781107415324.

Jeong, D. I., L. Sushama, and M. N. Khaliq, 2017: Attribution of spring snow water equivalent (SWE) changes over the northern hemisphere to anthropogenic effects. *Clim. Dynam.*, **48**, 3645-3658, doi:10.1007/s00382-016-3291-4.

Kotlarski, S., T. Bosshard, D. Lüthi, P Pall, and C. Schär, 2012: Elevation gradients of European climate change in the regional climate model COMSO-CLM. *Climatic Change*, **112**, 189-215, doi:10.1007/s10584-011-0195-5.

Krasting, J. P., A. J. Broccoli, K. W. Dixon, and J. R. Lanzante, 2013: Future changes in Northern Hemisphere snowfall. *J. Climate*, **26**, 7813-7828, doi:10.1175/JCLI-D-12-00832.1.

Kunreuther H., and Coauthors, 2014: Integrated Risk and Uncertainty Assessment of Climate Change Response Policies. In: *Climate Change 2014: Mitigation of Climate Change. Contribution of Working Group III to the Fifth Assessment Report of the Intergovernmental Panel on Climate Change* [Edenhofer, O., R. Pichs-Madruga, Y. Sokona, E. Farahani, S. Kadner, K. Seyboth, A. Adler, I. Baum, S. Brunner, P. Eickemeier, B. Kriemann, J. Savolainen, S. Schlömer, C. von Stechow, T. Zwickel and J.C. Minx (eds.)]. Cambridge University Press, Cambridge, United Kingdom and New York, NY, USA.

Lader, R., U. S. Bhatt, J. E. Walsh, and T. S. Rupp, 2016: Two-meter temperature and precipitation from atmospheric reanalysis evaluated for Alaska. *J. Appl. Meteor. Climatol.*, **55**, 901-922, doi:10.1175/JAMC-D-15-0162.1.

Lader, R., J. E. Walsh, U. S. Bhatt, and P. A. Bieniek, 2017: Projections of twenty-first-century climate extremes for Alaska via dynamical downscaling and quantile mapping. *J. Appl. Climatol. Meteorol.*, **56**, 2393-2409, doi:10.1175/JAMC-D-16-0415.1.

Lawrence, D. M., and A. G. Slater, 2010: The contribution of snow condition trends to future ground climate. *Clim. Dynam.*, **34**, 969-981, doi:10.1007/s00382-009-0537-4.

Lawrence, D. M., A. G. Slater, and S. C. Swenson, 2012: Simulation of present-day and future permafrost and seasonally frozen ground conditions in CCSM4. *J. Climate*, **25**, 2207-2225, doi:10.1175/JCLI-D-11-00334.1.

Lesack, L. F. W., P. Marsh, F. E. Hicks, and D. L. Forbes, 2014: Local spring warming drives earlier river-ice breakup in a large Arctic delta. *Geophys. Res. Lett.*, **41**, 1560-1567, doi:10.1002/2013GL058761.

Lindsay, R., M. Wensnahan, A. Schweiger, and J. Zhang, 2014: Evaluation of seven different atmospheric reanalysis products in the Arctic. *J. Climate*, **27**, 2588-2606, doi:10.1175/JCLI-D-13-00014.1.

Liston, G. E., and C. A. Hiemstra, 2011: The changing cryosphere: Pan-Arctic snow trends (1979-2009). *J. Climate*, **24**, 5691-5712, doi:10.1175/JCLI-D-11-00081.1.

McAfee, S. A., J. Walsh, and T. S. Rupp, 2013: Statistically downscaled projections of snow/rain partitioning for Alaska. *Hydrol. Process.*, **28**, 3930-3946, doi:10.1002/hyp .9934.

Melvin, A. M., and Coauthors, 2016: Climate change damages to Alaska public infrastructure and the economics of proactive adaptation. *Proc. Natl. Acad. Sci.*, **114 (2)**, E122-E131, doi:10.1073/pnas.1611056113.

Menne, M. J., I. Durre, R. S. Vose, B. E. Gleason, and T. G. Houston, 2012: An overview of the Global Historical Climatology Network-Daily Database. *J. Atmos. Ocean Tech.*, **29**, 897-910, doi:10.1175/JTECH-D-11-00103.1.

NOAA National Centers for Environmental Information, 2018: Climate at a Glance: City Time Series, published April 2018, retrieved on April 23, 2018 from http://www.ncd c.noaa.gov/cag/.

O'Gorman, P., 2014: Contrasting responses of mean and extreme snowfall to climate change. *Nature*, **512**, 416-418, doi:10.1038/nature13625.

Overland, J. E., E. Hanna, I. Hanssen-Bauer, S. –J Kim, J. E. Walsh, M. Wang, U. S. Bhatt, and R. L. Thoman, 2016: Surface Air Temperature [in Arctic Report Card 2016], http://www.arctic.noaa.gov/Report-Card.

Pastick, N. J., M. T. Jorgenson, B. K. Wylie, S. J. Nield, K. D. Johnson, and A. O. Finley, 2015: Distribution of near-surface permafrost in Alaska: Estimates of present and future conditions. *Remote Sens. Environ.*, **168**, 301-315, doi:10.1016/j.rse.2015.07.0 19.

Peng, X., and Coauthors, 2018: Spatiotemporal changes in active layer thickness under contemporary and projected climate in the Northern Hemisphere. *J. Climate*, **31**, 251-266, doi:10.1175/JCLI-D-16.0721.1.

Peters, G. P., and Coauthors, 2013: The challenge to keep global warming below 2°C. *Nature Clim. Change*, **3 (1)**, 4-6.

Rennert, K. J., 2009: Soil thermal and ecological impacts of rain on snow events in the circumpolar Arctic. *J. Climate*, **22**, 2302-2315, doi:10.1175/2008JCLI2117.1.

Riahi, K., S. Rao, V. Krey, C. Cho, V. Chirkov, G. Fischer, G. Kindermann, N. Nakicenovic, and P. Rafaj, 2011: RCP 8.5—A scenario of comparatively high greenhouse gas emissions. *Clim. Change.*, **109**, 33-57, doi:10.1007/s10584-011-0149-y.

Skamarock, W. C., and Coauthors, 2008: A description of the Advanced Research WRF version 3. NCAR Tech. Note NCAR/TN-475+STR, 113 pp., doi:10.1056/D68S4MVH.

Taylor, K. E., R. J. Stouffer, and G. A. Meehl, 2012: An overview of CMIP5 and the experiment design. *Bull. Amer. Meteor. Soc.*, **93**, 485-498, doi:10.1175/BAMS-D-11-00094.1.

Walsh, J. E., W. L. Chapman, V. Romanovsky, J. H. Christensen, and M. Stendel, 2008: Global climate model performance over Alaska and Greenland. *J. Climate*, **21**, 6156-6174, doi:10.1175/2008JCLI2163.1.

Wendler, G., and M. Shulski, 2009: A century of climate change for Fairbanks, Alaska. *Arctic*, **62**, 295-300.

Yang, D., B. E. Goodison, J. R. Metcalfe, V. S. Golubev, R. Bates, T. Pangburn, and C. L. Hanson, 1998: Accuracy of NWS 8" Standard Nonrecording Precipitation Gauge: Results and Application of WMO Intercomparison. *J. Atmos. Oceanic Technol.*, **15**, 54-68, doi:10.1175/1520-0426(1998)015<0054:AONSNP>2.0.CO;2.

Young-Robertson, J. M., W. R. Bolton, U. S. Bhatt, J. Cristóbal, and R. Thoman, 2016: Deciduous trees are a large and overlooked sink for snowmelt water in the boreal forest. *Sci. Rep.* **6**, 29504, doi:10.1038/srep29504.

Zhang, X., J. He, J. Zhang, I. Polyakov, R. Gerdes, J. Inuoe, and P. Wu, 2012: Enhanced poleward moisture transport and amplified northern high-latitude wetting trend. *Nat. Clim. Change*, **3**, 47-51, doi:10.1038/nclimate1631.

5 CONCLUSIONS

5.1 Projected extremes with an emphasis on climate model downscaling

This dissertation investigated observed and projected changes to extreme climate events in Alaska from 1981-2100 using a combination of observations, and downscaled reanalysis and climate model simulations. The analysis in each of the main chapters is arranged into 30-year periods: one historical (1981-2010) and three projected (2011-2040, 2041-2070, 2071-2100), with the projected from the RCP8.5 emissions scenario (Riahi et al. 2011). These extreme events, from a climate perspective, relate to threshold exceedances of specific points in the distributions of temperature and precipitation. In Alaska, they contribute to natural hazards that include: rapid sea ice and glacier loss, permafrost thaw, wildfire, changes to ocean chemistry, and coastal erosion (Chapin et al. 2014). It is estimated that unmitigated climate-related damages during the remainder of the 21st century will cost $5.5 billion in Alaska, primarily due to flooding and permafrost-related subsidence of the land surface (Melvin et al. 2016).

The ERA-Interim reanalysis (Dee et al. 2011) was downscaled to a 20-km spatial resolution to provide a gridded set of historical data that is often used as a proxy for observations. Compared to other reanalyses, the ERA-Interim frequently exhibits the lowest root-mean-square error (RMSE) with respect to observations of temperature and precipitation in Alaska (Lader et al. 2016). The downscaled ERA-Interim products display further improvements when compared to the coarser forcing data, primarily due to a better representation of topography (Bieniek et al. 2016; Lader et al. 2017). The two CMIP5 models that were downscaled and used in this research, GFDL-CM3 and CCSM4, ranked third and sixth out of 21 models, respectively, in terms of RMSE of

surface temperature, precipitation, and sea-level pressure for the Alaska domain (Walsh et al. 2018).

In Chapter 2, the climate extremes indices developed by the ETCCDI are calculated for Alaska using this high-resolution gridded climate data. Using a quantile-delta mapping methodology (Cannon et al. 2015) to bias-correct the downscaled output, it is found that unprecedented heat and precipitation are anticipated to occur during the remainder of the 21st century. Maximum 1-day and consecutive 5-day precipitation amounts are expected to increase by 53% and 50%, respectively, and the number of hot summer days per year (T_{max} > 25˚C) increases from a statewide average of 1.5 during 1981-2010 to 29.7 during 2071-2100. These results corroborate those from a global analysis that used 31 GCMs from CMIP5 (Sillmann et al. 2013a, b); however, the increases to temperature and precipitation are generally higher. This is likely due to an improved representation of topography, which would tend to reduce smoothing between disparate land surface types.

Chapters 3 and 4 explore how the shifting distributions of temperature and snowfall affect important parameters such as season length and associated start and end dates. Growing season length (Chapter 3) and snow season length (Chapter 4) are particularly susceptible to change because the statewide average temperature is below freezing currently, but exhibits a warming trend. Slight warming can have major ramifications. Following bias-correction using ERA-Interim, growing season length extends by 48-87 days by 2071-2100 with the largest changes in northern Alaska. In contrast, projections of snow season length are reduced such that many locations in southwest Alaska no

longer have continuous snow cover in the winter and all locations display substantial decreases.

While the models used in this dissertation are consistent, the bias correction methodologies are not. The downscaled climate model temperature and precipitation distributions in Chapter 2 are quantile-delta mapped according to the ERA-Interim (1981-2010). This is done for each 30-year future period (10950 days) and at each grid cell (n = 68,644). A similar approach is used in Chapter 3, but the quantile mapping is performed following the calculation of the various agro-climate indices. For example, after calculation, the historical CCSM4 growing season length distribution is subtracted from the same CCSM index from 2041-2070, and added to the ERA-Interim growing season length. Here n = 30 model years, which makes this less computationally expensive. However, the projected changes to important snow season characteristics in Chapter 4 are not bias-corrected with the ERA-Interim. The presented values are relative to each model's own climatology. The snow-water equivalent variable from the original ERA-Interim contains fixed parameterizations at high elevations (Drusch et al. 2004) and is not suitable for use as an observational proxy. More generally, snow products are sufficiently problematic that a suitable observational database for bias correction is unavailable. These issues, namely computational cost and inadequate gridded observations, demonstrate some of the continued limitations inherent to climate extremes studies for Alaska.

5.2 Implications

The largest projected shifts to the temperature distribution occur at the coldest temperatures and tend to occur for the late-century period (2071-2100). This is especially true for northern and western Alaska where sea ice is mostly absent during this time. These changes show a climate-warming signal emerging from the historical inter-annual variability for growing season length and snow season length. This indicates that every year during the late-century period and most years in the mid-century will have a longer (shorter) growing season (snow season) relative to present-day climatologies. For agricultural interests, in particular, this is a significant finding for long-term planning. Given increasing demand for food production and greater heat stress and drought in more southerly locations, Alaska could become more important in the global agricultural landscape.

The mid- and late-century periods are when the RCP scenarios diverge (Kunreuther et al. 2014), which indicates that planning decisions that are currently being made have the capacity to effect substantial future change. Melvin et al. (2016) note a projected $1.3 billion decrease in climate-related damages this century for Alaska if we follow RCP4.5, rather than RCP8.5. Furthermore, many adverse impacts to human health correlate with extreme events and hazards. As the frequency of severe wildfire, flooding, and habitat loss are projected to increase due to climate warming, so too are the dangerous health effects associated with accidents, poor air quality, and mental wellbeing (DHSS 2018). Alaska stands at the forefront of impacts due to changing climate extremes; this dissertation provides projections that can serve as guidance for informed decision-making that will help shape the state's future.

5.3 References

Bieniek, P. A., U. S. Bhatt, J. E. Walsh, T. S. Rupp, J. Zhang, J. R. Krieger, and R. Lader, 2016: Dynamical downscaling of ERA-Interim temperature and precipitation for Alaska. *J. Appl. Meteor. Climatol.*, **55**, 635-654, doi:10.1175/JAMC-D-15-0153.1.

Cannon, A. J., S. R. Sobie, and T. Q. Murdock, 2015: Bias correction of GCM precipitation by quantile mapping: How well do methods preserve changes in quantiles and extremes? *J. Climate*, **28**, 6938-6959.

Chapin, F. S., III, S. F. Trainor, P. Cochran, H. Huntington, C. Markon, M. McCammon, A. D. McGuire, and M. Serreze, 2014: Ch. 22: Alaska. *Climate Change Impacts in the United States: The Third National Climate Assessment*, J. M. Melillo, T. C. Richmond, and G. W. Yohe, Eds., U.S. Global Change Research Program, 514-536. [Available online at http://nca2014.globalchange.gov/system/files_force/downloads/high/NCA3_Full_Report_22_Alaska_HighRes.pdf?download=1.]

Dee, D. P., and Coauthors, 2011: The ERA-Interim reanalysis: Configuration and performance of the data assimilation system. *Quart. J. Roy. Meteor. Soc.*, **137**, 553-597, doi:10.1002/qj.828.

Dept. of Health and Social Services (DHHS), Division of Public Health, State of Alaska Epidemiology, 2018: *Assessment of the potential health impacts of climate change in Alaska*. Anchorage, AK: DHSS, 2018.

Donner, L. J., and Coauthors, 2011: The dynamical core, physical parameterizations, and basic simulation characteristics of the atmosphere component AM3 of the GFDL global coupled model CM3. *J. Climate*, **24**, 3484-3519, doi:10.1175/2011JCLI3955.1.

Drusch, M. D., D. Vasiljevic, and P. Viterbo, 2004: ECMWF's Global Snow Analysis: Assessment and Revision Based on Satellite Observations. *J. Appl. Meteor.*, **43**, 1282-1294, doi:10.1175/1520-0450(2004)043<1282:EGSAAA>2.0.CO;2.

Kunreuther H., and Coauthors, 2014: Integrated Risk and Uncertainty Assessment of Climate Change Response Policies. In: *Climate Change 2014: Mitigation of Climate Change. Contribution of Working Group III to the Fifth Assessment Report of the Intergovernmental Panel on Climate Change* [Edenhofer, O., R. Pichs-Madruga, Y. Sokona, E. Farahani, S. Kadner, K. Seyboth, A. Adler, I. Baum, S. Brunner, P. Eickemeier, B. Kriemann, J. Savolainen, S. Schlömer, C. von Stechow, T. Zwickel and J.C. Minx (eds.)]. Cambridge University Press, Cambridge, United Kingdom and New York, NY, USA.

Lader, R., U. S. Bhatt, J. E. Walsh, and T. S. Rupp, 2016: Two-meter temperature and precipitation from atmospheric reanalysis evaluated for Alaska. *J. Appl. Meteor. Climatol.*, **55**, 901-922, doi:10.1175/JAMC-D-15-0162.1.

Lader, R., J. E. Walsh, U. S. Bhatt, and P. A. Bieniek, 2017: Projections of twenty-first-century climate extremes for Alaska via dynamical downscaling and quantile mapping. *J. Appl. Climatol. Meteorol.*, **56**, 2393-2409, doi:10.1175/JAMC-D-16-0415.1.

Melvin, A. M., and Coauthors, 2016: Climate change damages to Alaska public infrastructure and the economics of proactive adaptation. *Proc. Natl. Acad. Sci.*, **114 (2)**, E122-E131, doi:10.1073/pnas.1611056113.

Riahi, K., S. Rao, V. Krey, C. Cho, V. Chirkov, G. Fischer, G. Kindermann, N. Nakicenovic, and P. Rafaj, 2011: RCP 8.5—A scenario of comparatively high greenhouse gas emissions. *Clim. Change.*, **109**, 33-57, doi:10.1007/s10584-011-0149-y.

Sillmann, J., V. V. Kharin, X. Zhang, F. W. Zwiers, and D. Bronaugh, 2013a: Climate extremes indices in the CMIP5 multimodel ensemble: Part 1. Model evaluation in the present climate. *J. Geophys. Res. Atmos.*, **118**, 1716-1733, doi:10.1002/jgrd.50203.

Sillmann, J., V. V. Kharin, F. W. Zwiers, X. Zhang, and D. Bronaugh, 2013b: Climate extremes indices in the CMIP5 multimodel ensemble: Part 2. Future climate projections. *J. Geophys. Res. Atmos.*, **118**, 2473-2493, doi:10.1002/jgrd.50188.

Walsh, J. E., and Coauthors, 2018: Downscaling of climate model output for Alaskan stakeholders. *Environ. Modeling and Software*, **2018**, 1-14, doi:10.1016/j.envsoft.2018.03.021.